ISSN 1997-308X
eISSN 2412-8767

ИЗВЕСТИЯ ВУЗОВ
ПОРОШКОВАЯ МЕТАЛЛУРГИЯ И ФУНКЦИОНАЛЬНЫЕ ПОКРЫТИЯ

POWDER METALLURGY AND FUNCTIONAL COATINGS

2024
Том 18 № 2
Vol. No.
powder.misis.ru

ISSN 1997-308X
eISSN 2412-8767

POWDER METALLURGY AND FUNCTIONAL COATINGS

Scientific and Technical Journal
Founded in 2007
Six issues per year

2024
Vol. 18 No. 2
Том 18 № 2

ИЗВЕСТИЯ ВУЗОВ ПОРОШКОВАЯ МЕТАЛЛУРГИЯ И ФУНКЦИОНАЛЬНЫЕ ПОКРЫТИЯ

Научно-технический журнал
Основан в 2007 г.
Выходит 6 раз в год

POWDER METALLURGY AND FUNCTIONAL COATINGS

ISSN 1997-308X
eISSN 2412-8767

Scientific and Technical Journal
Founded in 2007
Six issues per year

http://powder.misis.ru

Founder: MISIS University of Science and Technology

National University of Science and Technology "MISIS"
Address: 4 bld. 1 Leninskiy Prosp., Moscow 119049, Russian Federation
http://www.misis.ru

Journal is included into the List of peer-reviewed scientific publications recommended by the Highest Attestation Commission of the Ministry of Education and Science of the Russian Federation for publishing the results of doctoral and candidate dissertations.
Abstracting/Indexing: Scopus, Russian Science Citation Index (RSCI), Ulrich's Periodicals Directory, VINITI Database (Abstract Journal).

Certificate of registration **No. FS77-27955** (12.04.2007)
Re-registration **PI No. FS77-79230** (25.09.2020)

Signed print 20.04.2024. Format 60×90 1/8
Offset paper No. 1. Digital printing. Quires 8.75
Order 19530. Free price
Printed in the printing house of the MISIS Publish House
4 bld. 1 Leninskiy Prosp., Moscow, 119049 Russian Federation
Phone/fax: +7 (499) 236-76-17

ИЗВЕСТИЯ ВУЗОВ
ПОРОШКОВАЯ МЕТАЛЛУРГИЯ
И ФУНКЦИОНАЛЬНЫЕ ПОКРЫТИЯ

НАУЧНО-ТЕХНИЧЕСКИЙ ЖУРНАЛ
ОСНОВАН В 2007 Г.
ВЫХОДИТ 6 РАЗ В ГОД

http://powder.misis.ru

ISSN 1997-308X
eISSN 2412-8767

Учредитель:

ФГАОУ ВО Национальный исследовательский технологический университет «МИСИС»
Адрес: 119049, Москва, Ленинский пр-т, 4, стр. 1
https://www.misis.ru

Журнал включен в Перечень рецензируемых научных изданий, рекомендованных ВАК Минобрнауки РФ для публикации результатов диссертаций на соискание ученых степеней.
Журнал включен в базы данных: Scopus, Russian Science Citation Index (RSCI), Ulrich's Periodicals Directory, РИНЦ, БД/РЖ ВИНИТИ.

Редакция журнала

Адрес: 119049, Москва,
Ленинский пр-т, 4, стр. 1. НИТУ МИСИС

Тел.: +7 (495) 638-45-35. ***Эл. почта:*** izv.vuz@misis.ru

Свидетельство о регистрации № **ФС77-27955** от 12.04.2007 г.
Перерегистрация 25.09.2020 г. **ПИ № ФС77-79230**

Ведущий редактор: О.В. Соснина
Выпускающий редактор: А.А. Кудинова
Дизайн и верстка: В.В. Расенець

Подписано в печать 20.04.2024. Формат 60×90 $^1/_8$
Бум. офсетная № 1. Печать цифровая. Усл. печ. л. 8,75
Заказ 19530. Цена свободная
Отпечатано в типографии Издательского Дома МИСИС
119049, г. Москва, Ленинский пр-т, 4, стр. 1
Тел./факс: +7 (499) 236-76-17

Contents

Содержание

Theory and Processes of Formation and Sintering of Powder Materials
Теория и процессы формования и спекания порошковых материалов

UDC 621.762
https://doi.org/10.17073/1997-308X-2024-2-5-13

Research article
Научная статья

Influence of copper salts on the physical and mechanical properties of copper–graphite composite materials

N. D. Ogleznev, I. I. Yakubaev, S. A. Oglezneva, S. E. Porozova

Perm National Research Polytechnic University
29 Komsomolsky Prosp., Perm 614990, Russia

ogleznevasa@pstu.ru

Abstract. We investigated composite materials based on electrolytic copper powder containing 1 and 5 wt. % powder of colloidal graphite the addition of trace amounts of copper sulfate and acetate. The materials were obtained through double cold pressing in a mold at a pressure of 600 MPa, intermediate sintering (annealing) in hydrogen at a temperature of 870 °C, and final sintering in vacuum at the copper premelting temperature. To analyze the influence of copper salts on the density, porosity, electrical resistivity, and strength of copper–graphite composite materials, we employed *X*-ray phase analysis, scanning electron microscopy, conducted strength tests in three-point bending, and determined electrical resistivity. We established that higher graphite content results in increased porosity and electrical resistivity of composite materials, along with decreased strength. In the materials containing copper sulfate, copper is reduced from the salt in the form of nanodispersed particles on the surfaces and inside graphite flakes, leading to a decrease in electrical resistivity compared to copper–graphite composites without salt additives. When copper acetate was added to the composite material, copper is reduced from the salt mainly on the surfaces of graphite particles in the form of microdispersed particles and their aggregations, as the copper acetate solution does not wet the graphite. In this case, the electrical resistivity was somewhat higher than that of the composite with sulfate but lower than that of the material without salts. The bending strength of the studied materials decreased as salts were introduced due to increased porosity and emerging defects in the crystal structure of graphite during its intercalation with copper.

Keywords: composite material (CM), copper, graphite, copper sulfate, copper acetate, electrical resistivity, porosity, strength, intercalation

For citation: Ogleznev N.D., Yakubaev I.I., Oglezneva S.A., Porozova S.E. Influence of copper salts on the physical and mechanical properties of copper–graphite composite materials. *Powder Metallurgy and Functional Coatings*. 2024;18(2):5–13. https://doi.org/10.17073/1997-308X-2024-2-5-13

Влияние солей меди на физико-механические свойства композиционных материалов медь–графит

Н. Д. Оглезнев, И. И. Якубаев, С. А. Оглезнева, С. Е. Порозова

Пермский национальный исследовательский политехнический университет
Россия, 614990, г. Пермь, Комсомольский пр-т, 29

ogleznevasa@pstu.ru

Аннотация. Исследованы композиционные материалы на основе электролитического порошка меди, содержащие 1 и 5 мас. % порошка коллоидного графита, с добавлением в микроколичествах сульфата и ацетата меди. Материалы получали методами двойного холодного прессования в пресс-форме при давлении 600 МПа, промежуточного спекания (отжига) в водороде при температуре 870 °С и окончательного спекания в вакууме при предплавильной температуре меди. Методами рентгенофазового анализа, сканирующей электронной микроскопии, испытаний на прочность при трехточечном изгибе и определения электросопротивления исследовано влияние солей меди на плотность, пористость, удельное электросопротивление и проч-

ность композиционных материалов медь–графит. Установлено, что с увеличением содержания графита повышаются пористость и удельное электросопротивление композиционных материалов, а прочность снижается. В материалах, содержащих сульфат меди, происходит восстановление меди из соли в виде нанодисперсных частиц на поверхностях и внутри графитовых чешуек, что способствует снижению удельного электросопротивления по сравнению с композитами медь–графит без добавок солей. При добавлении ацетата меди в композиционный материал восстановление меди из соли происходит преимущественно на поверхностях частиц графита в виде микродисперсных частиц и их сростков, так как раствор ацетата меди не смачивает графит. Удельное электросопротивление при этом было несколько больше, чем у композита с сульфатом, но меньше, чем у материала без солей. Прочность на изгиб исследованных материалов при введении солей понижалась за счет повышения пористости и появления дефектов кристаллического строения графита при его интеркалировании медью.

Ключевые слова: композиционный материал (КМ), медь, графит, сульфат меди, ацетат меди, удельное электросопротивление, пористость, прочность, интеркалирование

Для цитирования: Оглезнев Н.Д., Якубаев И.И., Оглезнева С.А., Порозова С.Е. Влияние солей меди на физико-механические свойства композиционных материалов медь–графит. *Известия вузов. Порошковая металлургия и функциональные покрытия*. 2024;18(2):5–13. https://doi.org/10.17073/1997-308X-2024-2-5-13

Introduction

Copper–carbon composites combine the high thermal and electrical conductivity of copper alongside the low thermal expansion coefficient, specific mass, and high melting point of carbon [1]. Consequently, they find extensive application in electrical devices and the semiconductor industry, serving as materials for thermally conductive bases in the housings of high-power rectifying and laser diodes, microwave transistors, power amplifiers [2; 3], as well as in electro-erosion machining of metals, heavy-duty power modules, and optoelectronic devices such as pantograph sliders, brushes in electric motors, and other machinery components [4]. However, the electrical resistivity of graphite is two orders of magnitude greater than that of copper, leading to a decrease in the overall electrical conductivity of the composite material (CM) when graphite is added in large quantities.

Intercalation with metal ions, including the formation of superconducting structures, can enhance the graphite conductive properties. For example, graphite intercalated with calcium exhibits superconductivity [5], while iron enhances the thermal and electrical conductivity of carbon materials [6]. Copper intercalation into graphite [7; 8] and carbon nanotubes (CNTs) [9] has also been reported. However, the lack of physicochemical interaction between the components, including the high surface tension of the metal melt, poses challenges to the manufacturing technologies for copper–graphite and copper–CNT systems [10]. Metal ions are introduced into graphite, CNTs, and fullerenes using salt solutions. For instance, in [9], CNT powder was mixed with copper acetate hydrate, and quantum copper wires up to 50 nm long were obtained after thermal treatment inside CNTs. The authors in [7; 8] utilized copper chloride for graphite intercalation to produce superconducting materials [11].

Due to the significant difference in thermal expansion coefficients, conventional preparation methods struggle to achieve effective interfacial adhesion between the copper matrix and carbon. Even rolling at different temperatures with high degrees of deformation [13] fails to strengthen the phase interface and reduce electrical resistivity.

Since graphite lacks physicochemical interaction with the copper matrix, carbide-forming elements such as boron, chromium, etc. [14] are added to the CM to enhance bonding between copper and carbon at the phase interface. Additionally, the carbon surface is oxidized with acids [15] and salts, resulting in the introduction of ultra-dispersed copper into the material pores. This process leads to reduced friction coefficient and wear, while improving electrical conductivity and mechanical properties [16]. In [17], preliminary chemical copper-plating of natural flake graphite is utilized to enhance the adhesion of graphite to the copper matrix, albeit complicating the technological process and increasing costs.

There are documented instances of obtaining intercalated structures of graphite without special processing. In [18], graphite was introduced into a copper melt at 1200–1250 °C, yielding a copper alloy with lower electrical resistivity and higher tensile strength compared to existing ones. Authors in [19] conducted intercalation by incubating samples of highly oriented pyrolytic graphite (HOPG) for 20 min in a 99.99 % pure copper melt at 1473 K in vacuum. Analysis of the diffraction pattern of graphite containing copper atoms revealed planes with atoms displaced from their initial positions within its structure. The authors explain these results by the formation of intermediate complexes with copper ions in graphite. If the metal atom leaves a pair of rings in the plane of the graphite grid, the latter instantly establishes “diamond” bonds with molecular networks corrugating in the area where the metal was located.

The powder metallurgical technique enables to control the properties of composite materials by adjusting compositions and manufacturing methods across a wide range of options. In [20], a copper–graphite composite material was fabricated through sintering at a pre-melting copper temperature. Additional reflections identified via *X*-ray phase analysis of the sintered CM of copper and colloidal graphite corresponded to those described in [21]. The resulting materials exhibited low electrical resistivity and were evaluated as electrodes-tools for electro-erosion machining, benefitting from their high electrical and thermal conductivity properties.

Considering the method of pretreating graphite with acids and subjecting it to high pressure of copper vapor, the formation of intercalated compounds with copper appears quite feasible [21; 22].

The objective of the current study is to investigate the impact of treating graphite with copper salts on the physical and mechanical properties of copper–graphite CMs.

Experimental and research techniques

To produce copper–graphite samples, we utilized PMS-1 copper powder (according to GOST 4960-75), S-1 colloidal graphite (per TS 113-08-48-63-90), $CuSO_4$ (according to GOST 19347–2014), or $(CH_3COO)_2Cu$ salt, which was prepared from copper powder and glacial acetic acid. The surface of compacted graphite powder was moistened with 7 %-aqueous solutions of salts using the sessile drop method, with the wetting angle being determined based on photographs. In some instances, non-ionogenic surfactants were added to the salt solutions.

We mixed S-1 graphite powder with copper salts in amounts sufficient to achieve 10 % copper content after reduction. Distilled water with or without the required amounts of salts and surfactants was added, and the powder was dispersed in an ultrasonic bath (USB) ST-400S (Russia), then dried at room temperature and subsequently reduced in hydrogen at temperatures ranging from 750 to 1000 °C. For the production of composite materials (CMs), copper and graphite powders were mixed in proportions of 1 or 5 wt. % with a non-ionogenic surfactant (with salts added in some cases). The mixtures were dispersed in the USB (ST-400S) with ethyl alcohol and dried. The resulting powders were pressed at a pressure of 600 MPa using the P-125 press (manufactured in Russia) and annealed in the SGV furnace (manufactured in Russia) in a hydrogen atmosphere at 870 °C for 1 h. After annealing, samples were additionally compacted in the mold at a pressure of 600 MPa. Finally, the samples were sintered in a vacuum at temperatures ranging from 1070 to 1080 °C for 2 h using the SNVE-1.3.1/16 furnace (Russia).

The *X*-ray phase analysis was conducted using the XRD-6000 diffractometer (Shimadzu, Japan) with CuK_α-radiation. The phase composition was identified using the International Center for Diffractographic Measurements files, and Crystallographica Search-Match Version 2.0.3.1 (Oxford Cryosystems Ltd), was employed for data processing. The shooting parameters included an angle range from 10 to 110° with a step of 0.02°. The structure of copper–graphite CM samples was examined using a Tescan Vega 3 scanning electron microscope equipped with an EDX-analyzer (Czech Republic).

The properties were tested on 3–10 samples per point. The density and porosity of composite materials were determined using the calculation method according to the standard technique (GOST 18898–89). The electrical resistivity of the CM was calculated from the sample resistance determined by the GOM-802 device (Russia), using a method based on measuring the potential difference across the conductor section. The strength at three-point bending of samples without cracks was tested using the FP 10/1 machine (Germany), following the procedures outlined in GOST 18227–85, with a loading speed of 2 mm/min and a distance of 40 mm between the supports.

Results and discussion

The contact angle of wetting the graphite surface with copper sulfate solution was significantly smaller than that of wetting it with copper acetate solution (Fig. 1, *a*, *b*). Upon addition of a non-ionogenic surfactant to the aqueous solutions of both salts, these values decreased further: from 70 to 34° for copper sulfate (Fig. 1, *c*), indicating wetting according to the well-known Thomas Young formula, suggesting that the solution with surfactant is close to spreading on graphite. However, for copper acetate, the contact angle decreased only insignificantly, from 110 to 98°, implying nonwettability (Fig. 1, *d*).

It is noteworthy that even after several minutes, drops of salt solutions continued to spread on the graphite surface, indicating its interaction with the salts. The experiment involving the reduction of graphite powder treated with salt solutions allowed us to simulate the mechanism of forming the structure of copper–graphite composite material during sintering.

We examined the phase composition after the reduction of copper salts in mixtures with graphite in hydrogen (Table 1). It was observed that copper acetate is

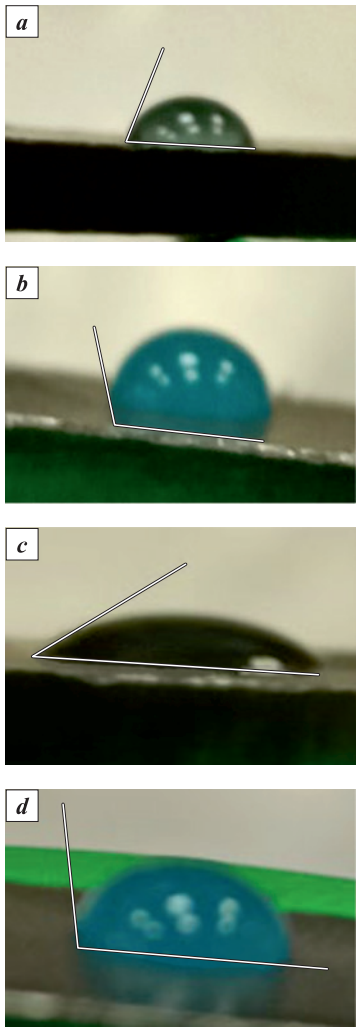

Fig. 1. Determination of the contact angle of wetting with aqueous solutions of $(CH_3COO)_2Cu$ and $CuSO_4$ salts on the surface of pressed graphite powder

a – solution $CuSO_4$ without surfactant (θ = 70°)
b – solution $(CH_3COO)_2Cu$ without surfactant (θ = 110°)
c – solution $CuSO_4$ with surfactant (θ = 34°)
d – solution $(CH_3COO)_2Cu$ with surfactant (θ = 98°)

Рис. 1. Определение краевого угла смачивания водными растворами солей $(CH_3COO)_2Cu$ и $CuSO_4$ на поверхности прессованного порошка графита

a – р-р $CuSO_4$ без ПАВ (θ = 70°)
b – р-р $(CH_3COO)_2Cu$ без ПАВ (θ = 110°)
c – р-р $CuSO_4$ с добавкой ПАВ (θ = 34°)
d – р-р $(CH_3COO)_2Cu$ с добавкой ПАВ (θ = 98°)

reduced to pure copper even at a temperature of 750 °C, with a small amount of Cu_2O oxidized copper formed (Table 1). As the temperature increases to 1000 °C, copper oxide is no longer detected, which is consistent with previous data on copper reduction in hydrogen at temperatures ranging from 200 to 400 °C [23]. At 750 °C, copper sulfate transforms into copper sulfide, and as the temperature rises to 1000 °C, the sulfide is reduced to copper, in accordance with thermodynamic calculations [24].

SEM images of graphite mixtures after reduction with copper salts reveal that in the sample treated with copper sulfate, copper particles are distributed both on the surfaces and inside the graphite particles and the distribution is quite uniform (Fig. 2, *a*, *b*). Surface particles account for approximately 20 %, with a maximum of 50 % (Fig. 2, *a*, Table 1). The copper particles reduced from sulfate measure between 0.2 and 1.0 μm in size (Fig. 2, *b*, Table 1).

In the graphite sample treated with an aqueous copper acetate solution and impregnated to a shallow depth, the reduced copper particles are predominantly located on the surfaces of graphite particles (Fig. 2, *c*, *d*) in the form of large crystals, with a concentration on the surface reaching 60 % (78 % maximum, Table 1). The particles of copper reduced from acetate range from 0.1 to 3.0 μm in size. Given that the average copper content in both samples was approximately 10 wt. % relative to the graphite mass, it is evident that the majority of copper reduced from acetate is concentrated on the surfaces of graphite particles, while in the sample treated with copper sulfate, copper particles are mostly situated in the interlayer spaces of graphite flakes. These results suggest a similar reduction of copper from salts during CM sintering after their addition.

After the final sintering of composite materials containing 99–95 % of PMS-1 copper powder and 1–5 % of colloidal graphite powder (with and without addition of salts), SEM images reveal that copper, in the form of spheres of varying diameters, is uniformly distributed within graphite inclusions (Fig. 3–5).

Table 1. **Phase composition of graphite impregnated with salt after reduction**

Таблица 1. **Фазовый состав графита, пропитанного солью, после восстановления**

Phase composition			Copper concentration, wt. %		Copper particle size, μm
before reduction	after reduction		average in the mixture (XRF)	on the graphite surface average/maximum (EDX analysis)	
	750 °C	1000 °C			
Powder mix C + $(CH_3COO)_2Cu$	C, Cu, Cu_2O	Cu, C	~10	60/78	0.1–3.0
Powder mix C + $CuSO_4$	C, Cu, Cu_2O, Cu_2S	Cu, C	~10	20/50	0.2–1.0

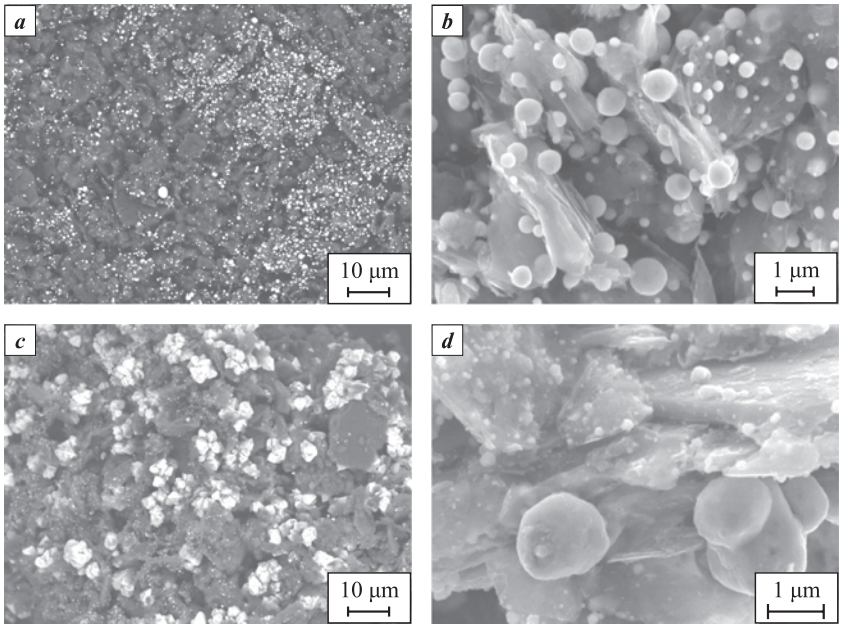

Fig. 2. SEM image of S-1 graphite powder after impregnation with aqueous salt solutions and reduction
a – $CuSO_4$, size of research area S = 100 μm, ***b*** – $CuSO_4$, S = 11 μm, ***c*** – $(CH_3COO)_2Cu$, S = 80 μm, ***d*** – $(CH_3COO)_2Cu$, S = 7 μm

Рис. 2. СЭМ-изображения порошка графита С-1 после пропитки водными растворами солей и восстановления
a – $CuSO_4$, размер области исследования S = 100 мкм, ***b*** – $CuSO_4$, S = 11 мкм, ***c*** – $(CH_3COO)_2Cu$, S = 80 мкм, ***d*** – $(CH_3COO)_2Cu$, S = 7 мкм

On the fracture surface of the sintered CM sample with 5 % graphite without the addition of salts (Fig. 3, *a*), dispersed copper particles ranging in size from 0.1 to 0.5 μm are observed in small concentrations. These particles are located both inside and on the surfaces of graphite particles (Fig. 3, *b*).

In the SEM images of the sintered sample containing 1 % graphite with the addition of copper sulfate (Fig. 4), copper particles measuring 5–10 μm in size are uniformly distributed in large quantities, appearing on both the surfaces of graphite flakes and between the layers of particles (Fig. 4, *b*).

Since the copper acetate solution fails to wet the graphite and does not penetrate deeply, the copper particles in Fig. 5, *a* appear as clusters and aggregates on the surfaces of graphite particles, with limited presence between the layers (Fig. 5, *b*). These copper particles on graphite flakes measure about 10–20 μm in size, notably larger than those observed in materials without salts and after treatment with copper sulfate.

Samples containing 1 % graphite exhibit lower porosity (*П*) and consequently, lower electrical resistivity (ρ), while their bending strength (σ_{bend}) surpasses that of CM with 5 % graphite (Table 2). Evidently, achieving high density and strength is challenging due to the elastic nature of graphite and its limited interaction with copper; indeed, some samples with high graphite content experienced destruction during pressing or after sintering.

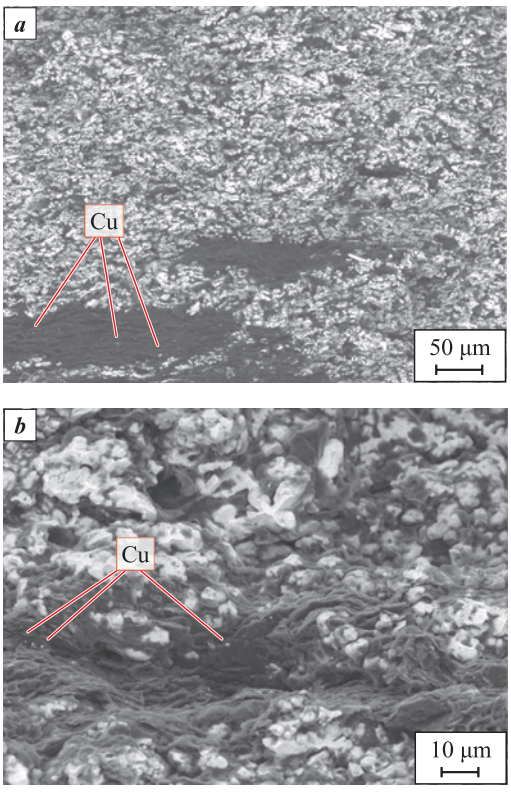

Fig. 3. SEM images of a copper-based CM sample with 5 % graphite without salts
a – CM fracture, ***b*** – graphite phase in CM

Рис. 3. СЭМ-изображения образца КМ на основе меди с 5 % графита без добавки солей
a – излом КМ, ***b*** – фаза графита в КМ

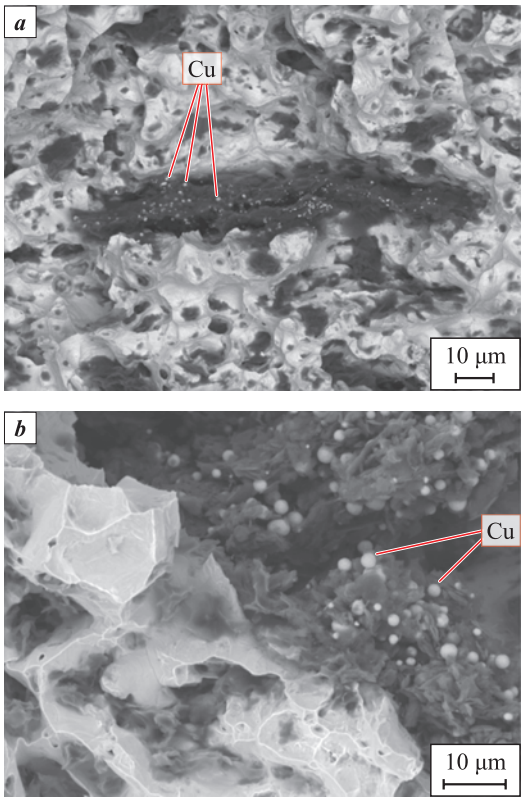

Fig. 4. SEM images of a copper-based CM sample with 1 % graphite and addition of copper sulfate
a – CM fracture, ***b*** – graphite phase in CM

Рис. 4. СЭМ-изображение образца КМ на основе меди с 1 % графита и добавлением сульфата меди
a – излом КМ, ***b*** – фаза графита в КМ

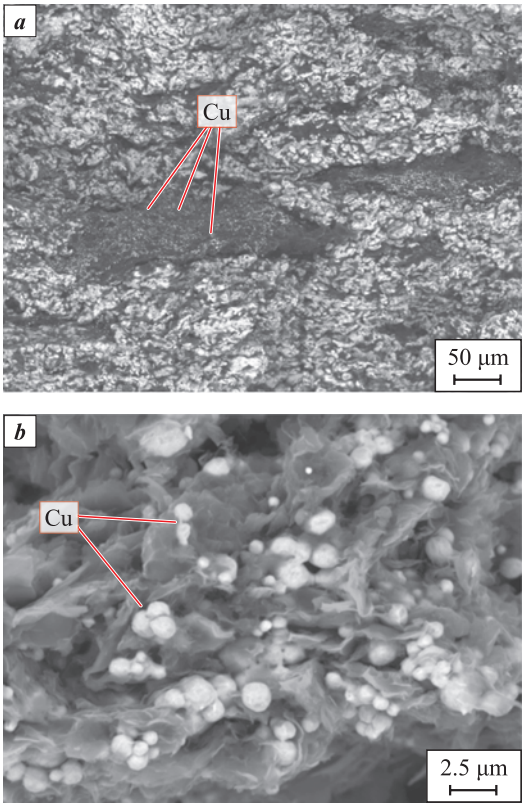

Fig. 5. SEM images of a copper-based CM sample with 5 % graphite and addition of copper acetate
a – CM fracture, ***b*** – graphite phase in CM

Рис. 5. СЭМ-изображение образца КМ на основе меди с 5 % графита и добавлением ацетата меди
a – излом КМ, ***b*** – фаза графита в КМ

The treatment of graphite with copper salts significantly influences the structure, as well as the physical and mechanical properties, of the investigated composite materials, a trend clearly observable in samples with 1 % graphite. In materials where graphite remains untreated, nanodispersed copper particles form in low concentrations, resulting in minimal disruption to the graphite crystal structure and yielding the strongest CM samples.

Table 2. **Physical and mechanical properties of copper–graphite composite materials**

Таблица 2. **Физико-механические свойства композиционных материалов медь–графит**

Graphite content, wt. %	Salt added	*П*, %	$\rho \cdot 10^{-8}$, mΩ·mm	σ_{bend}, MPa
1	–	2	1.94 ± 0.15	270 ± 19
5	–	8	3.48 ± 0.23	90 ± 11
1	Copper acetate	2	1.71 ± 0.13	230 ± 20
5	Copper acetate	8	3.30 ± 0.20	75 ± 9
1	Copper sulfate	7	1.69 ± 0.13	200 ± 22

In the structure of graphite treated with copper sulfate, the reduced copper particles are larger and their concentration in the interlayer spaces of graphite flakes is greater higher. Furthermore, after the final sintering, there is a slight increase in porosity, indicating the thermal expansion of the graphite [24; 25]. This may also suggest the completion of copper reduction from sulfate. Consequently, in this material, the bonds in the graphite crystalline lattice are disrupted, defects are formed, and interplanar distances increase. Such structural changes naturally result in increased porosity and decreased strength compared to CM without salts. However, the same material with the highest porosity exhibits lower electrical resistivity than pure copper ($\rho = (1.75 \div 1.80) \cdot 10^{-8}$ mΩм·mm) due to the high concentration of conductive copper particles inside the graphite particles.

After treatment with copper acetate, the amount of reduced copper particles inside the graphite particles is lower than that after sulfate treatment, leading

to slightly higher electrical resistivity and strength. However, compared to the material containing untreated graphite the specific resistance of the copper acetate-modified graphite is lower at equal porosity. This is attributed to the presence of copper particles inside the graphite. Additionally, the lower strength value of these samples is a consequence of some disruption of the crystalline structure of the graphite.

Conclusions

The following conclusions were drawn from the experimental research results.

1. An increase in the graphite content from 1 to 5 % in copper-based composites, both with and without salts, leads to higher porosity.

2. Copper acetate undergoes reduction at a temperature of 750 °C during heat treatment in hydrogen, while copper sulfate is reduced at 1000 °C.

3. The copper reduced from copper acetate salt, in the form of large particles, is predominantly observed on the surfaces of graphite flakes.

4. During the sintering of CM, even without graphite treatment with copper salts, copper vaporizes and penetrates inside graphite particles.

5. The samples treated with copper salts, after sintering, exhibit slightly lower strength and reduced electrical resistivity compared to CMs without salts. The decrease in electrical resistivity may be attributed to possible graphite intercalation with copper, while the reduction in strength may be due to emerging defects in the graphite structure.

References / Список литературы

1. Allabergenov B., Kim S. Investigation of electrophysical and mechanical characteristics of porous copper-carbon composite materials prepared by spark plasma sintering. *International Journal of Precision Engineering and Manufacturing*. 2013;14(7):1177–1183. https://doi.org/10.1007/s12541-013-0160-5
2. Bodnar' D.M. Metallic and composite thermal conductive materials for powerful semiconductor packages. *Komponenty i tehnologii*. 2014;12:155–160. (In Russ.).

   Боднарь Д.М. Металлические и композитные теплопроводящие материалы для мощных полупроводниковых корпусов. *Компоненты и технологии*. 2014;12:155–160.
3. Nanoparticles, nanosystems and their application. Pt. II. Carbon and related layered materials for modern nanoelectronics: Textbook in 2 parts (eds. V.A. Moshnikova, O.A. Alexandrova). Ufa: Ajeterna, 2016. 330 p. (In Russ.).

   Наночастицы, наносистемы и их применение. Ч. II. Углеродные и родственные слоистые материалы для современной наноэлектроники: Учеб. пос. в 2 ч. Под ред. В.А. Мошникова, О.А. Александровой. Уфа: Аэтерна, 2016. 330 с.
4. Savich V.V., Oglezneva S.A. Powder metallurgy: Current state and development prospects: monograph. Perm: Publishing house PNIPU, 2021. 695 p. (In Russ.).

   Савич В.В., Оглезнева С.А. Порошковая металлургия: современное состояние и перспективы развития: Монография. Пермь: Изд-во ПНИПУ, 2021. 695 с.
5. Emery N., Hérold C., d'Astuto M., Garcia V., Bellin Ch., Marêché J. F., Lagrange P., Loupias G. Superconductivity of Bulk CaC_6. *Physical Review Letters*. 2005.95(8): 087003. https://doi.org/10.1103/PhysRevLett.95.087003
6. Dunaev A.V., Arkhangelsky I.V., Zubavichus Ya.V., Avdeev V.V. Preparation, structure and reduction of graphite intercalation compounds with hexachloroplatinic acid. *Carbon*. 2008;46(5):788–795. https://doi.org/10.1016/j.carbon.2008.02.003
7. Kyle Kalbus. Copper intercalation into graphite: Theses and Dissertations. Milwaukee (USA), University of Wisconsin Milwaukee, 2012. 34 p. https://dc.uwm.edu/etd/34.
8. Bin X., Chen Jiazang, Cao Hong, Ma Enbao, Wang Xuehua, Yuan Jizhu. Preparation and structural investigation of $CuCl_2$ graphite intercalation compounds. *Acta Geologica Sinica: English Edition*. 2008.82(5):1056–1060. https://doi.org/10.1111/j.1755-6724.2008.tb00663.x
9. Mishhenko S.V., Tkachev A.G. Carbon nanomaterials. Production, properties, application: scientific. Moscow: Mashinostroenie, 2008. 320 p. (In Russ.).

   Мищенко С.В., Ткачев А.Г. Углеродные наноматериалы. Производство, свойства, применение. М.: Машиностроение, 2008. 320 с.
10. Kozlov V.V., Kozhitov L.V., Krapukhin V.V., Karpacheva G.P., Pavlov S.A. Highly selective low-temperature nanocomposite Cu/C catalyst for methanol oxidation reaction *Izvestiya vysshikh uchebnykh zavedenii. Materialy elektronnoi tekhniki*. 2006;3:73–76. (In Russ.).

    Козлов В.В., Кожитов Л.В., Крапухин В.В., Карпачева Г.П., Павлов С.А. Высокоселективный низкотемпературный нанокомпозитный катализатор Cu/C реакции окисления метанола. *Известия высших учебных заведений. Материалы электронной техники*. 2006;3:73–76.
11. Brandt N.B., Kulbachinsky V.A., Nikitina O.M., Avdeev V.V., Akim V.Ya., Ionov S.G. Supermetallic conductivity and energy spectrum of the third-stage copper chloride intercalation compound in graphite. *Pis'ma v ZhTF*. 1987;13(5):302–305. (In Russ.).

    Брандт Н.Б., Кульбачинский В.А., Никитина О.М., Авдеев В.В., Аким В.Я., Ионов С.Г. Суперметаллическая проводимость и энергетический спектр у соединения внедрения в графит хлорида меди третьей ступени. *Письма в ЖТФ*. 1987;13(5):302–305.
12. Wang Z., Xu L., Peng J., Tang Z., Han Z., Liu J.. Effect of the microstructure and properties of graphite/copper composites fabricated by microwave sintering. *Journal of Materials Science*. 2021;56(15):9183–9195. https://doi.org/10.1007/s10853-021-05891-5
13. Oganyan R.A., Zharikov O.V., Oganyan Ya.N., Osip'yan Yu.A. Sintered composite material: Patent 2087575C1 (RF), 1997. (In Russ.).

Оганян Р.А., Жариков О.В., Оганян Я.Н., Осипьян Ю.А. Спеченный композиционный материал: Патент 2087575С1 (РФ), 1997.

14. Jia S.Q., Yang F. High thermal conductive copper/diamond composites: State of the art. *Journal of Materials Science*. 2021;56(3):2241–2274. https://doi.org/10.1007/s10853-020-05443-3

15. Wang J., Ding X., Zhang J., Zhang H., Zhang F., Liu Y., Fan T. Synthesis and properties of surface-modified carbon nanotube/copper composites. *Metallurgical and Materials Transactions A*. 2019;50(3):1448–1459. https://doi.org/10.1007/s11661-018-05105-9

16. Eroshenko V.D., Ovchinnikov A.N. Improving the tribological and electrical properties of products from a carbon composite material by impregnation with aqueous solutions of copper salts. *Izvestija vysshih uchebnyh zavedenij. Severo-Kavkazskij Region. Serija: Tehnicheskie nauki*. 2017;2(194):122–126. (In Russ.).

Ерошенко В.Д., Овчинников А.Н. Повышение трибологических и электротехнических свойств изделий из углеродного композиционного материала путем пропитки водными растворами солей меди. *Известия высших учебных заведений. Северо-Кавказский Регион. Серия: Технические науки*. 2017;2(194):122–126.

17. Wenhui Zh. Copper-plating graphite composite material and preparation method thereof: Patent CN 101230456 (China). 2008.

18. Yoshihito I., Kenichi O. Copper alloy and method for obtaining a copper alloy: Patent 2510420 (RF). 2010. (In Russ.).

Йосихито И., Кенити О. Медный сплав и способ получения медного сплава: Патент 2510420 (РФ). 2010.

19. Andreeva V.D., Stepanova T.R. The effect of copper atoms on the graphite structure. *Technical Physics Letters*. 2002;28(9):759–761. https://doi.org/10.1134/1.1511776

Андреева В. Д., Степанова Т. Р. Влияние атомов меди на структуру графита. *Письма в ЖТФ*. 2002;28(18):18–23.

20. Oglezneva S.A., Ogleznev N.D., Sirotenko L.D. Study of the relationship between structure and properties of electrodes for EDM tools cutting systems “copper – metal” and “copper – graphite”. *Vestnik Uzhno-Ural'skogo gosudarstvennogo universiteta. Seriya “Mashinostroenie”*. 2016;16(1):63–71. (In Russ.). https://doi.org/10.14529/engin160105

Оглезнева С.А., Оглезнев Н.Д., Сиротенко Л.Д. Исследование взаимосвязи между структурой и свойствами электродов-инструментов для электроэрозионной резки систем «медь – металл» и «медь – графит». *Вестник ЮУРГУ. Серия «Машиностроение»*. 2016;16(1):63–71. https://doi.org/10.14529/engin160105

21. Oglezneva S.A., Porozova S.E., Ogleznev N.D., Gilev V.G., Torsunov M.F. Investigation of the interaction in powder materials of the “copper–carbon phases” system for electrodetools. *Metalloobrabotka*. 2015;3(87):35–45. (In Russ.).

Оглезнева С.А., Порозова С.Е., Оглезнев Н.Д., Гилев В.Г., Торсунов М.Ф. Исследование взаимодействия в порошковых материалах системы «медь–углеродные фазы» для электродов–инструментов. *Металлообработка*. 2015;3(87):35–45.

22. Oglezneva S.A., Porozova S.E., Ogleznev N.D., Kachenyuk M.N. Interaction between copper and thermally expanded graphite during mechanical alloying and spark plasma sintering. *Tsvetnye Metally*. 2021;(10):86–93. (In Russ.). https://doi.org/10.17580/tsm.2021.10.12

Оглезнева С.А., Порозова С.Е., Оглезнев Н.Д., Качанюк М.Н. Взаимодействие меди и терморасширенного графита при механическом легировании и искровом плазменном спекании. *Цветные металлы*. 2021;(10):86–93. https://doi.org/10.17580/tsm.2021.10.12

23. Evstifeev E.N., Novikova A.A. Obtaining copper nanoparticles by thermal decomposition of copper formate complex with triethylamine. *Mezhdunarodnyi zhurnal prikladnykh i fundamental'nykh issledovaniy*. 2017;9:135–139. (In Russ.).

Евстифеев Е.Н., Новикова А.А. Получение наночастиц меди термическим разложением комплекса формиата меди с триэтиламином. *Международный журнал прикладных и фундаментальных исследований*. 2017;9:135–139.

24. Sorokina N.E., Avdeev V.V., Tikhomirov A.S., Lutfullin M.A., Saidaminov M.I. Composite nanomaterials based on intercalated graphite: a textbook. Moscow: MGU, 2010. 50 p. (In Russ.).

Сорокина Н.Е, Авдеев В.В., Тихомиров А.С., Лутфуллин М.А., Саидаминов М.И. Композиционные наноматериалы на основе интеркалированного графита: Учеб. пос. М.: МГУ, 2010. 50 с.

25. Belova M.Yu. From black chalk to TRG seals. *Armaturostroenie*. 2008;1(52):36–43. (In Russ.).

Белова М.Ю. От «черного мела» к уплотнениям из ТРГ. *Арматуростроение*. 2008;1(52):36–43.

Information about the Authors

Nikita D. Ogleznev – Cand. Sci. (Eng.), Engineer at the Department of Mine Survey, Geodesy, and Geoinformation Systems, Perm National Research Polytechnic University (PNRPU)
ORCID: 0000-0002-9785-5405
E-mail: fastrex@mail.ru

Il'ya I. Yakubaev – Graduate Student at the Department of Mechanics of Composite Materials and Structures, PNRPU
ORCID: 0009-0008-7078-6420
E-mail: iakubaev.ilya@gmail.com

Сведения об авторах

Никита Дмитриевич Оглезнев – к.т.н., вед. инженер кафедры маркшейдерского дела, геодезии и геоинформационных систем, Пермский национальный исследовательский политехнический университет (ПНИПУ)
ORCID: 0000-0002-9785-5405
E-mail: fastrex@mail.ru

Илья Иванович Якубаев – аспирант кафедры механики композиционных материалов и конструкций, ПНИПУ
ORCID: 0009-0008-7078-6420
E-mail: iakubaev.ilya@gmail.com

Svetlana A. Oglezneva – Dr. Sci. (Eng.), Professor at the Department of Mechanics of Composite Materials and Structures, PNRPU
ORCID: 0000-0002-5529-4259
E-mail: ogleznevasa@pstu.ru

Svetlana E. Porozova – Dr. Sci. (Eng.), Professor at the Department of Mechanics of Composite Materials and Structures, PNRPU
ORCID: 0000-0001-5835-9727
E-mail: porozovase@pstu.ru

Светлана Аркадьевна Оглезнева – д.т.н., профессор кафедры механики композиционных материалов и конструкций, ПНИПУ
ORCID: 0000-0002-5529-4259
E-mail: ogleznevasa@pstu.ru

Светлана Евгеньевна Порозова – д.т.н., профессор кафедры механики композиционных материалов и конструкций, ПНИПУ
ORCID: 0000-0001-5835-9727
E-mail: porozovase@pstu.ru

Contribution of the Authors

N. D. Ogleznev – determining the purpose of the work, conducting experiments to define the properties, and writing the article.
I. I. Yakubaev – preparing the mixture and initial samples, participating in the discussion of the results.
S. A. Oglezneva – conducting experiments to investigate the structure, participating in the discussions of the results.
S. E. Porozova – conducting wetting experiments, participating in the discussions of the results.

Вклад авторов

Н. Д. Оглезнев – определение цели работы, проведение экспериментов по определению свойств, написание текста статьи.
И. И. Якубаев – подготовка смеси композиционных материалов и исходных образцов, участие в обсуждении результатов.
С. А. Оглезнева – проведение экспериментов по исследованию структуры, участие в обсуждении результатов.
С. Е. Порозова – проведение экспериментов по смачиваемости, участие в обсуждении результатов.

Received 04.09.2023
Revised 14.11.2023
Accepted 16.11.2023

Статья поступила 04.09.2023 г.
Доработана 14.11.2023 г.
Принята к публикации 16.11.2023 г.

Refractory, Ceramic, and Composite Materials
Тугоплавкие, керамические и композиционные материалы

UDC 621.762

https://doi.org/10.17073/1997-308X-2024-2-14-22

Research article
Научная статья

Establishing theoretical foundations for predicting the structural and morphological characteristics of diffusion-welded joints of the beryllium–copper composite

B. V. Syrnev, O. I. Maslennikov, O. V. Semilutskaya

East Kazakhstan Technical University named after D. Serikbayev
19 Serikbaev Str., Ust-Kamenogorsk 070004, Kazakhstan

izusan@mail.ru

Abstract. The paper presents the results of theoretical and experimental studies regarding the quality of diffusion welding of the beryllium–copper composite. Numerical investigations of the parameters of heterodiffusion of diffusants and the thickness of the Be–Cu pair welded joint under varying temperature-time conditions were conducted. The analytical examinations revealed that the thickness of the diffusion weld at the Be–Cu joint varies between 26 and 345 μm, with the temperature increasing from 800 to 1000 °C and the holding time ranging from 20 to 120 min. The calculated layer thickness during the diffusion welding of a Be–Cu pair at 800 °C for 2 h is 65 μm, with 15 μm on the beryllium side and 50 μm on the copper side. Notably, a $CuBe_3$ intermetallic compound zone can form in the diffusion weld, which should be considered an adverse factor that reduces the mechanical properties. To theoretically substantiate the modification of the structure and properties of the diffusion zone, a numerical study of welding was carried out using a 10 μm thick nickel foil spacer, which is readily soluble in beryllium. It was demonstrated that after exposure to temperature-time conditions at 900 °C for 20 min, a 50 μm wide diffusion-bonded joint is formed. Its structure includes two single-phase zones of solid solutions based on copper and beryllium, as well as two two-phase regions consisting of solid solutions hardened with intermetallic compounds. Since the weld lacks structural zones consisting solely of intermetallic compounds (unlike when welding the Be–Cu diffusion pair), there are grounds to anticipate a reduction in the embrittling effect on the weld. The results obtained from the analytical studies can serve as the foundation for a theoretical prediction method for assessing the quality of diffusion welding of the beryllium–copper composite.

Keywords: beryllium, copper, iron, diffusion welding, heterodiffusion, diffusion rate, composite, temperature, time, phase composition, mechanical properties, microstructure

For citation: Syrnev B.V., Maslennikov O.I., Semilutskaya O.V. Establishing theoretical foundations for predicting the structural and morphological characteristics of diffusion-welded joints of the beryllium–copper composite. *Powder Metallurgy and Functional Coatings*. 2024;18(2):14–22. https://doi.org/10.17073/1997-308X-2024-2-14-22

Отработка теоретических основ прогнозирования структурно-морфологических характеристик диффузионно-сварных швов композита бериллий–медь

Б. В. Сырнев, О. И. Масленников, О. В. Семилуцкая

Восточно-Казахстанский технический университет им. Д. Серикбаева
Казахстан, 070004, г. Усть-Каменогорск, ул. Серикбаева, 19

izusan@mail.ru

Аннотация. Представлены результаты теоретических и экспериментальных исследований качества диффузионной сварки композита бериллий–медь. Проведены численные исследования параметров гетеродиффузии диффузантов и толщины сварного шва пары Be–Cu в зависимости от температурно-временных режимов. В результате аналитических исследований было установлено, что толщина диффузионного шва в стыке Be–Cu изменяется от 26 до 345 мкм при увеличении температуры с 800 до 1000 °C и времени выдержки – от 20 до 120 мин. Расчетная толщина слоя при диффузионной сварке пары Be–Cu при t = 800 °C в течение 2 ч составляет 65 мкм: 15 мкм со стороны бериллия и 50 мкм со стороны меди. Обращает на себя внимание вероятность образования в диффузионном шве зоны интерметаллидного соединения $CuBe_3$, что является неблагоприятным фактором, снижающим механические свойства. Для теоретического обоснования модификации структуры и свойств диффузионной зоны проведены численные исследования сварки с использованием фольговой прокладки толщиной 10 мкм из материала, хорошо растворимого в бериллии, – никеля. Показано, что после температурно-временной экспозиции при t = 900 °C в течение 20 мин формируется диффузионно-сварной шов шириной 50 мкм. Его структура состоит из 2 однофазных зон твердых растворов на основе меди и бериллия, а также двух двухфазных зон, представляющих собой упрочненные интерметаллидами твердые растворы. Отсутствие в шве структурных зон, состоящих только из интерметаллидов (как это имело место при сварке диффузионной пары Be–Cu), позволяет ожидать снижения охрупчивающего сварной шов эффекта. Полученные результаты аналитических исследований могут служить основой методики теоретического прогнозирования качества диффузионной сварки композита бериллий–медь.

Ключевые слова: бериллий, медь, железо, диффузионная сварка, гетеродиффузия, скорость диффузии, композит, температура, время, фазовый состав, механические свойства, микроструктура

Для цитирования: Сырнев Б.В., Масленников О.И., Семилуцкая О.В. Отработка теоретических основ прогнозирования структурно-морфологических характеристик диффузионно-сварных швов композита бериллий–медь. *Известия вузов. Порошковая металлургия и функциональные покрытия*. 2024;18(2):14–22. https://doi.org/10.17073/1997-308X-2024-2-14-22

Introduction

Energy issues have recently become more pressing. The steadily increasing energy consumption has led to a drastic surge in the prices of “carbon” fuels such as gas, oil, and coal. Meanwhile, aspirations for “green” technologies are constrained by limitations in hydro, wind, solar, and geothermal energy. Concurrently, scientists have linked global warming to the use of carbon-based fuels, making the introduction of a “carbon” tax a reasonable measure.

In light of these developments, scientists are redirecting their focus towards new sources of energy, particularly “hydrogen” and “helium”. Overcoming the apprehension surrounding radioactivity, they are also considering the application and further advancement of nuclear energy. One promising avenue in this regard is the development of the fusion energy industry, which offers several key advantages. The process is highly secure, as accidental power excursions in the power reactor are virtually impossible. Fuel reserves in the form of hydrogen isotopes are nearly limitless, and the energy processes are exceptionally eco-friendly compared to traditional thermal and nuclear power plants. International collaborative research groups are actively engaged in this field, notably in the “International Thermonuclear Experimental Reactor” project [1; 2].

The energy generated by thermonuclear reactions between hydrogen isotopes is released in the form of neutron energy (14.1 MeV) and helium ions, specifically alpha particles (3.5 MeV). This energy is absorbed by a specialized device surrounding the plasma called the “blanket” and subsequently removed by the primary coolant. The reactor employs deuterium and lithium as fuel, with tritium being produced during the fusion reaction through contact with lithium [3; 4].

In order to create a fusion reactor, an array of scientific and technical challenges must be addressed. Various components of the reactor are manufactured from materials with exceptional physical and mechanical properties across a wide range of temperatures and

loads. These materials must also exhibit erosion and corrosion resistance in diverse environments while remaining unaffected by electromagnetic and electric fields and radioactive radiation, among other factors. Certain grades of steel, heat-resistant alloys, non-ferrous metals like copper, aluminum, beryllium, and tungsten, along with super-hard alloys and ceramic-metal materials, meet these stringent requirements [5–10].

Notably, the inner wall of the toroidal working chamber, a critical component, is constructed using beryllium [11–20]. Physicists involved in the development determined the optimal design for the blanket, a three-layer composite consisting of beryllium, a copper alloy, and stainless steel with an internal channel system for water cooling (Fig. 1). The areas where the constituents of the "beryllium – copper alloy – stainless steel" composite solidify should exhibit high thermal strength and thermal conductivity. Significant progress has been achieved in bonding beryllium and copper through brazing technology [18–20]. Nevertheless, the diffusion welding technique offers certain advantages [21–24] and, according to the authors, holds potential for further enhancing the performance properties of these composites.

The research aimed to perform numerical studies of the diffusion interaction between composite components and to establish a theoretical framework for predicting the morphology, composition, and structure of diffusion-welded joints.

Experimental

The mathematical tools developed by the staff of the Moscow Engineering Physics Institute under the supervision of Dr. Sci. D. Skorov were used to perform diffusion calculations for the interaction between beryllium and impurities [25]. Principles for shaping the structure of contact zones in heterodiffusion [26] were applyed, and reference data on numerical patterns of diffusion mobility of the elements under investigation [27] were incorporated. Furthermore, corresponding state diagrams [28] were analyzed to formulate an engineering algorithm for both qualitative (structure) and quantitative (width of diffusion and structural zones) assessments of contact zones within a specific beryllium–copper–iron composite.

The experimental and analytical studies were conducted in two distinct stages:

1) analytical studies focused on heterodiffusion parameters (depth and concentration) of elements in the contact zone of diffusion pairs, with a particular emphasis on their variation under different temperature-time conditions;

2) the prediction of the phase composition and sizes of structural zones as a function of diffusion welding modes.

In the analytical study of element heterodiffusion, the concentration of the diffusing element $C(z)$ was calculated as a function of distance (x) from the initial boundary of contact between diffusion pairs and time (τ) using equation [25]

$$C(z) = C(0)\left\{\frac{\exp\left(-z^2\right) - \frac{\gamma}{\sqrt{\gamma^2+1}}\exp\left(-z^2\frac{\gamma^2+1}{\gamma^2}\right)}{1-\frac{\gamma}{\sqrt{\gamma^2+1}}} - \frac{\sqrt{\pi}z\left[\operatorname{erf}C(z) - \operatorname{erf}C\left(z\frac{\sqrt{\gamma^2+1}}{\gamma}\right)\right]}{1-\frac{\gamma}{\sqrt{\gamma^2+1}}}\right\}, \quad (1)$$

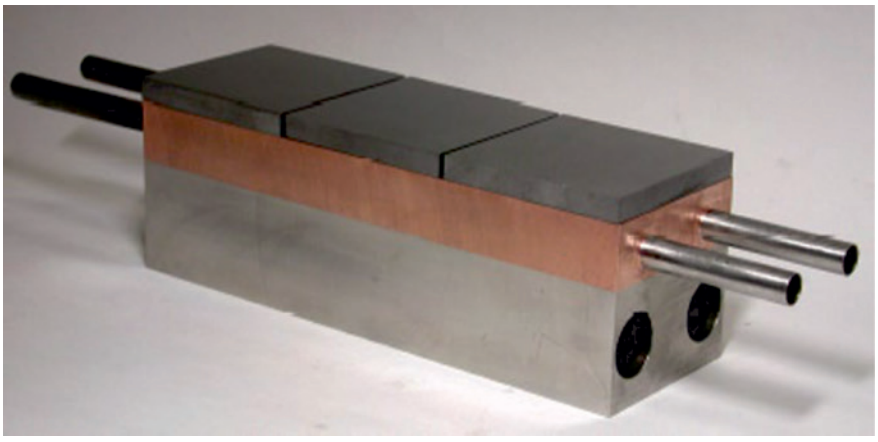

Fig. 1. Model of a fragment of the International Thermonuclear Experimental Reactor first wall

Рис. 1. Макет фрагмента первой стенки ИТЭР (International Thermonuclear Experimental Reactor)

where $z = \frac{x}{2}\sqrt{D\tau}$, $\gamma = \sqrt{\frac{\tau_2}{\tau_1}}$; τ_1 and τ_2 stand for interaction time at constant and instantaneous diffusion sources, respectively; $C(0)$ represents the concentration of the diffusant element at the contact boundary.

In order to determine the value of $C(0)$, the logic of contact zone formation during the sintering of dissimilar, mutually soluble materials was followed by the researchers [26]. The Be–Cu state diagram revealed that heterodiffusion at the junction of the diffusion pair at a temperature of 800 °C produced an intermediate γ-phase CuBe with a variable composition. This phase contained 11.3 wt. % of Be on the copper side and 86.7 wt. % of Cu on the beryllium side. The specified phase, along with its corresponding chemical composition, was considered as a constant source with concentration values $C(0)$ of the respective diffusant at the interphase under the studied temperature conditions.

The temperature-dependent variation of the diffusion coefficient is represented by the conventional equation [27]

$$D = D_0 \exp\left(-\frac{Q}{RT}\right),$$

where D_0 is a coefficient that varies depending on the nature of the element; Q represents the activation energy for the process, kJ; R is the gas constant; T denotes temperature, K.

The diffusion coefficients were calculated using the formulas [27]

$$\text{Be in Cu: } D = 0.66 \exp\left(\frac{-159.9\ \text{kJ}}{RT}\right), \quad (2)$$

$$\text{Cu in Be: } D = 0.084 \exp\left(\frac{-198.7\ \text{kJ}}{RT}\right). \quad (3)$$

The procedure for solving equation (1) is outlined in tabular form in [25] and was applied to compute the concentrations of diffusants as a function of temperature, time, and the distance from the point where the components of the composite initially make contact.

Results and discussion

The thickness of the diffusion zone, or weld, was determined as a result of heterodiffusion involving the elements of Be–Cu model pairs, in relation to temperature and welding time (Fig. 2). Analysis of the diagrams reveal that the thickness of the diffusion weld at the Be–Cu joint varies from 26 to 345 μm, with an increase in temperature from 800 to 1000 °C and an extension of the holding time from 20 to 120 min. Theoretical prediction of the phase composition during diffusion welding (Fig. 3) was determined by comparing the concentrations of the components (diffusant and matrix metal) calculated using formulas (1) to (3) with the Be–Cu state diagram.

The calculated layer thickness of the Be–Cu pair during diffusion welding at 800 °C for 2 h measures 65 μm: 15 and 50 μm on the beryllium and copper sides, respectively. It's worth noting that the formation of intermetallic compounds is possible in the diffusion weld. Under the specified welding conditions (800 °C for 2 h), the resulting diffusion weld exhibits a multiphase structure, as shown in Fig. 3. At its periphery, solid solutions based on beryllium (α_{Be}) and copper (α_{Cu}), are expected to form, while the $CuBe_3$ intermetallic compound zone and two-phase regions $\alpha_{Be} + CuBe_3$, $\beta_{Cu} + CuBe$, $\alpha_{Cu} + \beta_{Cu}$ should emerge closer to the initial contact boundary.

Cooling to 20 °C is expected to lead to a reduction in the number of phases. The β_{Cu} phase will disappear, and the regions containing copper- and beryllium-based solid solutions will contract. At room temperature, the 65-μm thick diffusion zone, which includes $CuBe_3$ and CuBe intermetallic compounds alongside solid solutions, will remain intact (see Fig. 3).

In order to assess the quality of diffusion bonding, an experimental validation was conducted. Cylindrical blanks, each 50 mm in height with a diameter of 100 mm, were fabricated using beryllium grade TGP-56 and M3 copper. After surface cleaning via etching, the Be–Cu cylindrical blocks were assembled. Diffusion welding [24] took place in a laboratory hot-pressing furnace under vacuum conditions (1.33 Pa) at temperatures ranging from 700 to 850 °C for 2 h, all while subject to uniaxial compression at a pres-

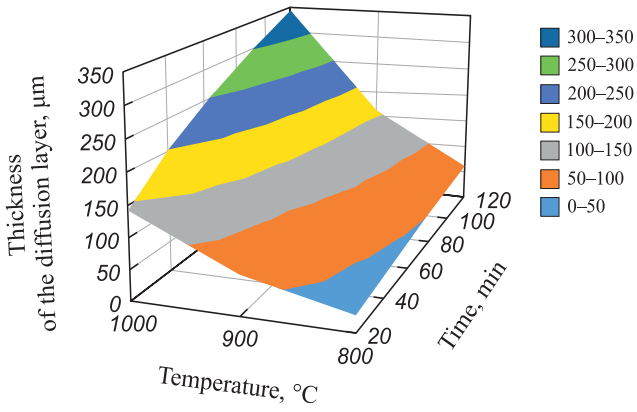

Fig. 2. Dependence of the thickness of the Be–Cu diffusion zone on temperature and time during diffusion welding (20–120 min)

Рис. 2. Зависимость толщины диффузионной зоны Be–Cu от температуры и времени (20–120 мин) диффузионной сварки

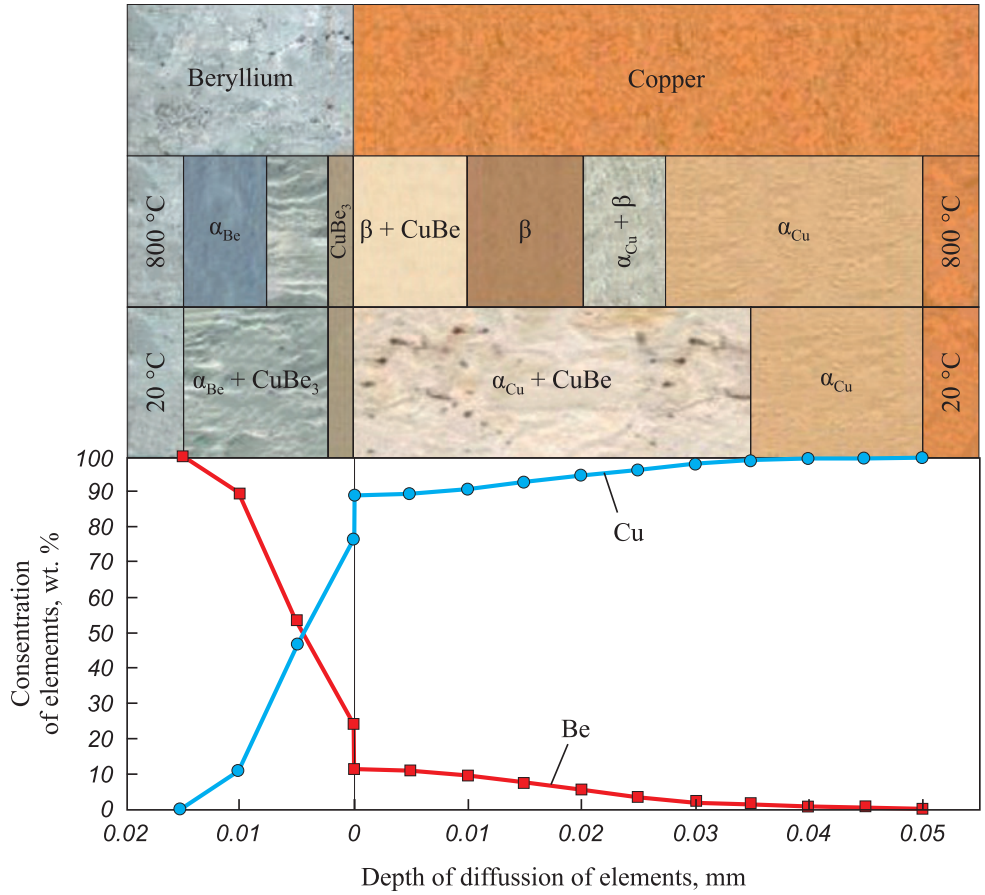

Fig. 3. Predicted quality parameters of Be–Cu diffusion welds at t = 20 and 800 °C, including diffusion depth, concentration of elements, phase composition, and dimensions of structural zones

Рис. 3. Прогнозируемые параметры качества диффузионно-сварных швов Be–Cu (глубина диффузии, концентрация элементов, фазовый состав и размеры структурных зон) при t = 20 и 800 °C

sure of 10 MPa. The integrity of each blank's joint was evaluated based on the outcomes of mechanical tensile tests performed on three samples (as depicted in Fig. 4). The results are provided in the Table below.

The analysis of the data obtained reveals that, in all cases, the samples were damaged at the juncture of the ingredients intended for welding, where the $CuBe_3$ embrittling intermetallic phase was formed during the diffusion interaction (Fig. 5). For this reason, the level of joint's mechanical properties did not surpass 50 % of the values for the matrix metal which is beryllium.

Fig. 4. Mechanical test samples

Рис. 4. Образцы для механических испытаний

Be–Cu diffusion-welded bimetal samples' mechanical test results

Результаты механических испытаний образцов из диффузионно-сварного биметаллла Be–Cu

Welding temperature, °C	Relative elongation, %	Tensile strength, MPa	Offset yield point, MPa
700	The samples were destroyed during manufacturing process		
750	0.6	185	172
800	–	120	–
850	The samples were destroyed during manufacturing process		

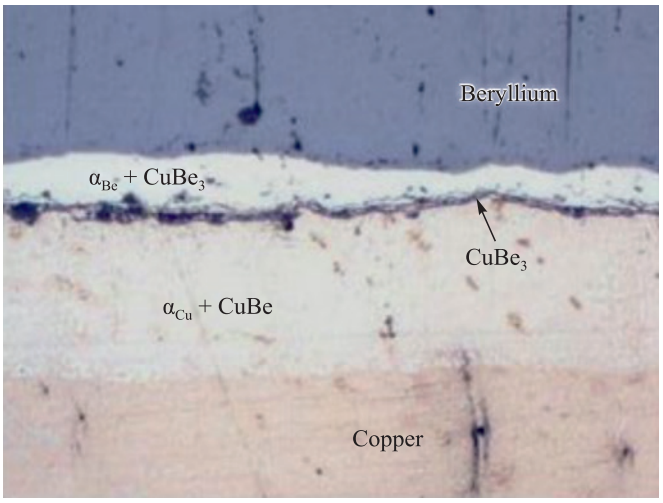

Fig. 5. Microstructure (×200) of Be–Cu weld after diffusion welding at t = 800 °C for 2 h

Рис. 5. Микроструктура (×200) сварного шва Be–Cu после диффузионной сварки при t = 800 °C, 2 ч

Therefore, the underlying issue with the designed composite lies in the fact that the Be–Cu zone, which emerges in the weld structure, comprises grains of the $CuBe_3$ intermetallic compound exclusively. This can result in the embrittlement of the welded joint and a subsequent reduction in its mechanical characteristics.

In order to address this structural flaw, further numerical studies were carried out with an aim to employ foil spacers made from metals that readily dissolve in the materials of the diffusion pair. These metals must have a melting point not lower than that of copper and should not form structural single-phase regions consisting solely of intermetallic compounds. The thickness of these spacers is also a critical factor. During the process of heterodiffusion, the spacer's material should dissolve within the major components (beryllium and copper).

Hence, the decision was made to employ a 10 μm thick nickel foil spacer, which was hypothetically positioned between the beryllium and copper materials. Subsequently, numerical studies were conducted based on the aforementioned algorithm. To calculate diffusion coefficients [27], using the relationships (2)–(7):

$$\text{Cu in Ni: } D = 7.0\exp\left(\frac{-238\ \text{kJ}}{RT}\right), \quad (4)$$

$$\text{Ni in Cu: } D = 1.95\exp\left(\frac{-236\ \text{kJ}}{RT}\right), \quad (5)$$

$$\text{Ni in Be: } D = 2.24\exp\left(\frac{-247\ \text{kJ}}{RT}\right), \quad (6)$$

$$\text{Be in Ni: } D = 0.02\exp\left(\frac{-193\ \text{kJ}}{RT}\right), \quad (7)$$

heterodiffusion parameters, including depth, concentration, and the thickness of diffusion zones formed during welding within the temperature range of 800–1000 °C for 20–120 min, were determined employing equation (1) (Fig. 6).

Analysis of the diagrams (refer to Fig. 4 and 6) reveals that a diffusion zone, similar in thickness to the one achieved by Be–Cu welding (at t = 800 °C for 2 h), can be attained by welding with a nickel spacer at t = 900 °C for 20 min. The predicted concentration of elements and the structure of the weld are presented in Fig. 7.

At a welding temperature of 900 °C, the diffusion layer encompasses two zones comprising solid

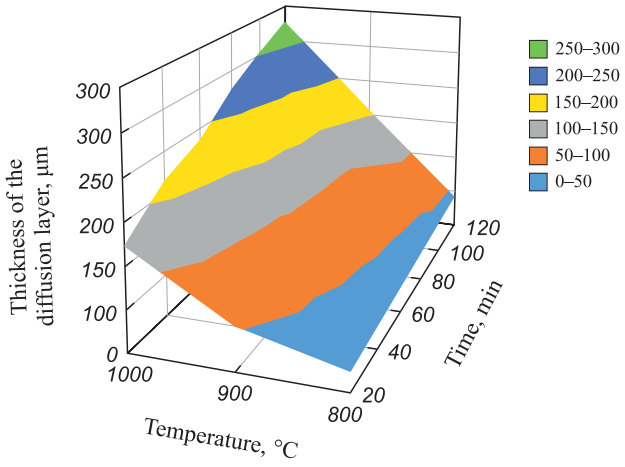

Fig. 6. Dependence of the thickness of the Be–Ni–Cu diffusion zone on temperature and time during diffusion welding (20–120 min)

Рис. 6. Зависимость толщины диффузионной зоны Be–Ni–Cu от температуры и времени (20–120 мин) диффузионной сварки

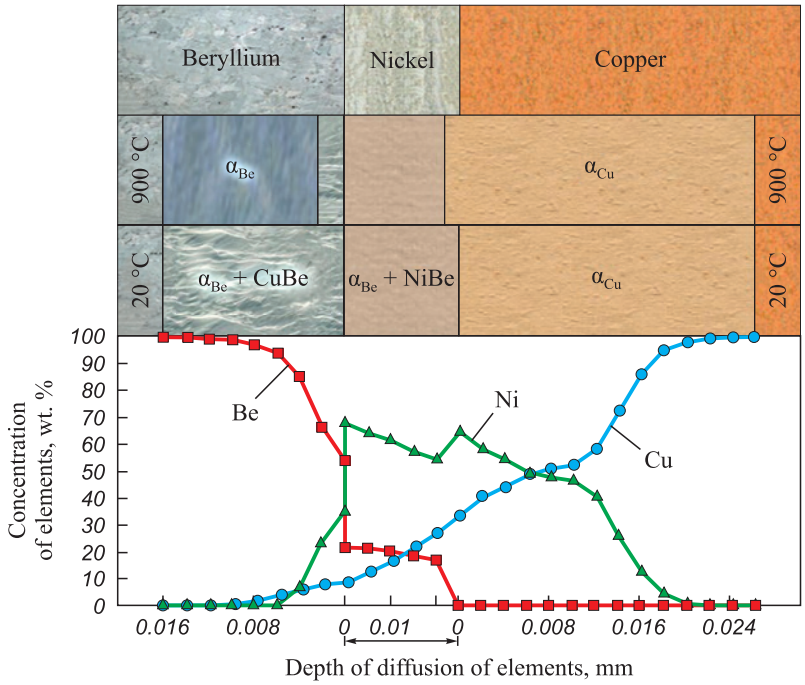

Fig. 7. Predicted quality parameters of Be–Ni–Cu diffusion welds at t = 20 and 900 °C, including diffusion depth, concentration of elements, phase composition, and dimensions of structural zones

Рис. 7. Прогнозируемые параметры качества диффузионно-сварных швов Be–Ni–Cu (глубина диффузии, концентрация элементов, фазовый состав и размеры структурных зон) при t = 20 и 900 °C

solutions based on copper α_{Cu} and beryllium α_{Be}. Additionally, there are two zones with structures reinforced by intermetallic compounds, specifically CuBe and NiBe. However, upon cooling to room temperature, the α_{Be} zone disappears, leaving three distinct structural zones: α_{Be} + CuBe, α_{Be} + NiBe and α_{Cu} (refer to Fig. 7).

Notably, what stands out is that the formation of single-phase regions consisting solely of intermetallic compounds is not anticipated in the structure of the diffusion-welded joint. This outcome should be considered a positive effect stemming from the utilization of a nickel spacer in Be–Cu diffusion welding.

Conclusions

Based on the numerical studies and theoretical prediction, the following conclusions can be drawn.

1. When diffusion welding the beryllium-copper model pair at 800 °C for 2 h, a diffusion solidification zone, 65 μm in width, is expected to form. This zone will consist of beryllium-based solid solutions α_{Be} and copper-based solid solutions α_{Cu}, two-phase regions α_{Be} + $CuBe_3$, α_{Cu} + CuBe, and a layer of $CuBe_3$ intermetallic compound.

2. The presence of a single-phase region composed of $CuBe_3$ intermetallic compound in the structure of diffusion-welded joint should be considered a detrimental factor that makes the weld brittle and reduces its overall quality.

3. The introduction of a 10 μm thick nickel spacer between the welded beryllium–copper elements allows for the modification of the studied joint by eliminating the single-phase intermetallic region from the weld structure.

4. Following additional experimental validation, the results obtained from the analytical studies can serve as the foundation for a method to theoretically predict the structural and morphological quality of beryllium-copper diffusion-welded joints. This prediction method encompasses phase composition and the size of structural zones within the diffusion welds.

References / Список литературы

1. Dorn C., Vidal E., Goods S. Beryllium materials for fusion reactor wall applications. *Proceedings of the 13th International Workshop on Beryllium Technology (BeWS-13)*. (Narita, Japan, 20–21 September, 2017).
2. ITER blanket, shield and material data base. International atomic energy agency. Iter documentation series. No. 29. Vienna, 1991, 264 p. https://inis.iaea.org/collection/NCLCollectionStore/_Public/23/003/23003898.pdf
3. Pitts R.A., Corpentier S., Escourbiac F., Hirai T., Komarov V., Kukushkin A.S., Lisgo S., Loarte A., Merola M., Mitteau R., Raffray A.R., Shimada M., Stangeby P.C. Physics basis and design of the ITER plasma-facing

components. *Journal Nuclear Material*. 2011;415(1): S957–S964. https://doi.org/10.1016/j.jnucmat.2011.01.114

4. Zucchetti M., Di Pace L., El-Guebali L., Kolbasov B.N., Massaut V., Pampin R., Wilson P.H. The back end of the fusion materials cycle. *Fusion Science and Technology*. 2009:109–139. https://doi.org/10.13182/FST09-12
5. Gervash A., Mazul I., Yablokov N. Alternative SS/CuCrZr joining methods for ITER. In: *ICFRM-10*. Baden-Baden, 2001. P. 129–134.
6. Tavassoli A.A. Assessment of austenitic stainless steel. *Fusion Engineering and Design*. 1995;29:371–390. https://doi.org/10.1016/0920-3796(95)80044-X
7. Asano K., Katsura R., Kawano S., Koshiishi M. Thick plate welding of irradiated stainless steel. Effect of irradiation on materials: In: *19th International Symposium. ASTM STP12443S*. 2000. P. 944–958. https://www.doi.org/10.1520/STP12443S
8. Korostelev A., Abramov V., Bashnin A. Assessment of metallurgical quality and mechanical properties of the 316LN-IG steel produced by different technologies. *Abstracts 8 International Conference on Fusion Reactor Materials*, October 26–31, 1997, Sendai, Japan. P. 207.
9. Ivanov A.D., Nikolaev A.K., Kalinin G.M, Rodin M.E. Effect of heat treatment on the properties of CuCrZr alloys. *Journal Nuclear Material*. 2002;307-311(1):673–676. https://doi.org/10.1016/S0022-3115(02)01110-8
10. Gervash A., Mazul I., Yablokov N., Ganenko A. Comparative strength analysis and therma fatigue testing of Be/CuCrZr and Be/GlidCop joints produced by fast brazing. *Fusion Technology*. 2000;38(3):278–282.
11. Kolbasov B.N., Khripunov V.I., Biryukov A.Yu. Some thoughts about beryllium resources, impurities in it and necessity of its detritiation after irradiation. *Voprosy atomnoi nauki i tekhniki. Seriya: Termoyadernyi sintez*. 2013;36(4):3–12. (In Russ.).

    Колбасов Б.Н., Хрипунов В.И., Бирюков А.Ю. Применение бериллия в термоядерных реакторах: ресурсы, примеси, детритизация после облучения. *Вопросы атомной науки и техники. Серия: Термоядерный синтез*. 2013;36(4):3–12.
12. Barabash V., Eaton R., Hirai T., Kupriyanov I., Nikolaev G., Zhanhong Wang, Xiang Liu, Roedig M., Linke J. Beryllium qualification activity for ITER first wall applications. In: *13th International Workshop on Plasma-Facing Materials and Components for Fusion Applications / 1st International Conference on Fusion Energy Material Science* (Rosenheim, Germany, 09–13 May, 2011). P. 3–12.
13. Kupriyanov I.B., Khomutov A.M., Nikolaev G.N., Gorlevsky V.V., Markushkin Yu.E., Chakin V.P., Gervash A.A., Kalashnikov A.N., Kolbasov B.N. Status of beryllium R&D activities in Russian Federation. In: *Proceedings 7th IEA International Workshop on Beryllium Technology* (Santa Barbara, California, USA, 29 November – 2 December 2005). P. 8–16.
14. Frants Ye., Kolmakov M., Zorin B., Kylyshkanov M., Podoinikov M., Udartsev S., Vechkutov A., Vladimirov P., Chakin V., Gaisin R. Beryllides – experience of UMP JSC in development and testing. In: *Proceedings of the 15th International Workshop on Beryllium Technology (BeWS-15)* (Karlsruhe, Germany, 14–15 September, 2022). P. 52–61. http://dx.doi.org/10.5445/KSP/1000156312
15. Zmitko M., Vladimirov P., Chakin V., Spagnuolo A.G. The HCPB test blanket module: current status in development and qualification of beryllium materials and an overview of open issues. In: *Proceedings of the 15th International Workshop on Beryllium Technology (BeWS-15)* (Karlsruhe, Germany, 14–15 September, 2022). P. 6–19. http://dx.doi.org/10.5445/KSP/1000156312
16. Smith K., Frehn A. Overview of the United States beryllium industry – 2022 Update. In: *Proceedings of the 15th International Workshop on Beryllium Technology (BeWS-15)* (Karlsruhe, Germany, 14–15 September, 2022). P. 36–51. http://dx.doi.org/10.5445/KSP/1000156312
17. Belyakov V., Mazul I., Strebkov Yu. Manufacturing and testing of large-scale mock-ups of ITER plasma facing components in Russia. *Fusion Engineering and Design*. 2002;61–62:129–134. https://doi.org/10.1016/S0920-3796(02)00225-9
18. Gervash A., Giniyatulin R., Mazul I., Watson R. Beryllium armoured mock-ups for fusion high heat flux application. In: *Proceedings of the 20th SOFT*. Marseille, France, 1998. P. 47–50.
19. Gervash A., Giniyatulin R., Komarov V., Mazul I. Comparative thermal cyclic testing and strength investigation of different Be/Cu joints. *Fusion Engineering and Design*. 1998;(39–40):543–549.
20. Gervash A., Mazul I., Belyakov V., Yablokov N. Manufacturing and testing of Be first wall mock-up for ITER. In: *5 IEA Workshop on Beryllium technologies for fusion. Perspektivnye materiali. Special issue*. Moscow; Interkontakt Nauka, 2002.

    Gervash A., Mazul I., Belyakov V., Yablokov N. Manufacturing and testing of Be first wall mock-up for ITER. В сб.: *Труды V рабочей группы Международного энергетического агенства по бериллию. Перспективные Материалы. Спец. выпуск.* М.: Интерконтакт Наука, 2002. С. 20–23.
21. Lyshinsky A.V. Diffusion welding of dissimilar materials. Moscow: Izdatelskii Tsentr «Academiya», 2006. 208 p. (In Russ.).

    Люшинский А.В. Диффузионная сварка разнородных материалов. М.: Изд. центр «Академия», 2006. 208 с.
22. Trykov Yu.P., Gurevich L.M., Arisova V.N. Diffusion in layered composites. Volgograd: RPK «Polytechnik», 2006. 402 p.

    Трыков Ю.П., Гуревич Л.М., Арисова В.Н. Диффузия в слоистых композитах. Волгоград: РПК «Политехник», 2006. 402 с.
23. Barwinok V.A., Bordakov P.A., Mordasov V.I., Usoltsev A.L., Oleksiyko S.M. Increasing the strength of joints made of dissimilar materials during diffusion welding and soldering. *Problemy mashinostroenija i avtomatizatsii*. 1999;3:79–83. (In Russ.).

    Барвинок В.А., Бордаков П.А., Мордасов В.И., Усольцев А.Л., Олексийко С.М. Повышение прочности соединений из разнородных материалов при диффузионной сварке и пайке. *Проблемы машиностроения и автоматизации*. 1999;3:79–83.

24. Gervash A., Mazul I., Litunovsky N., Pokrovsky A. Thermal fatigue properties and results of in-pile integrated test of Be/CuCrZr and Be/GlidCop joints produced by fast brazing. In: *Sb. tr. V rabochei gruppy Mezhdunarodnogo Energeticheskogo Agenstva po berilliyu. Perspektivnie Materialy. Special issue*. Moscow: Interkontakt Nauka, 2002. P. 44–47.

Gervash A., Mazul I., Litunovsky N., Pokrovsky A. Thermal fatigue properties and results of in-pile integrated test of Be/CuCrZr and Be/GlidCop joints produced by fast brazing. В сб.: *Труды V рабочей группы Международного энергетического агенства по бериллию. Перспективные Материалы. Спец. выпуск.* М.: Интерконтакт Наука, 2002. С. 44–47.

25. Ananyin V.M., Gladkov V.P., Zotov V.S., Skorov D.M. Diffusion processes in beryllium. Moscow: Energoatomizdat, 1981. 75 p. (In Russ.).

Ананьин В.М., Гладков В.П., Зотов В.С., Скоров Д.М. Диффузионные процессы в бериллии. М.: Энергоатомиздат, 1981. 75 с.

26. Powder metallurgy. Sintered and composite materials (Ed. V. Shatt). Moscow: Metallurgiya, 1983. 520 p. (In Russ.).

Порошковая металлургия. Спеченные и композиционные материалы. Под ред. В. Шатта. М.: Металлургия, 1983. 520 с.

27. Diffusion welding of materials. Directory (Ed. Kazakov N.F.). Moscow: Mashinostroenie, 1981. 271 p. (In Russ.).

Диффузионная сварка материалов: Справочник. Под ред. Казакова Н.Ф. М.: Машиностроение, 1981. 271 с.

28. Papirov I.I. Structure and properties of beryllium alloys: Directory. Moscow: Energoizdat, 1981. 367 p. (In Russ.).

Папиров И.И. Структура и свойства сплавов бериллия: Справочник. М.: Энергоиздат, 1981. 367 с.

Information about the Authors

Boris V. Syrnev – Dr. Sci. (Eng.), Leading Researcher at Research Center "Veritas", East Kazakhstan Technical University (EKTU)
ORCID: 0000-0002-3085-3341
E-mail: izusan@mail.ru

Oleg I. Maslennikov – Leading Process Engineer at Research Center "Veritas", EKTU
ORCID: 0000-0003-4375-5959
E-mail: a.mpk@mail.ru

Oksana V. Semilutskaya – Senior Lecturer at the School of Metallurgy and Mineral Processing, EKTU
ORCID: 0000-0001-9494-9572
E-mail: 2009genius@mail.ru

Сведения об авторах

Борис Владимирович Сырнев – д.т.н., вед. науч. сотрудник научного центра «Веритас» Восточно-Казахстанского технического университета (ВКТУ)
ORCID: 0000-0002-3085-3341
E-mail: izusan@mail.ru

Олег Иванович Масленников – вед. инженер-технолог научного центра «Веритас», ВКТУ
ORCID: 0000-0003-4375-5959
E-mail: a.mpk@mail.ru

Оксана Валерьевна Семилуцкая – ст. преподаватель школы «Металлургия и обогащение полезных ископаемых», ВКТУ
ORCID: 0000-0001-9494-9572
E-mail: 2009genius@mail.ru

Contribution of the Authors

B. V. Syrnev – provided scientific supervision, set research objectives, participated in experiments, processed research results, wrote the article.
O. I. Maslennikov – organized and conducted the experiments, discussed the results.
O. V. Semilutskaya – performed calculations, processed and discussed the results, wrote a specific section of the article.

Вклад авторов

Б. В. Сырнев – научное руководство, постановка задач, участие в экспериментах, обработка результатов, оформление и написание текста статьи.
О. И. Масленников – организация и проведение экспериментальных работ, обсуждение результатов.
О. В. Семилуцкая – проведение расчетов, обработка и обсуждение результатов, написание раздела статьи.

Received 01.12.2022
Revised 11.05.2023
Accepted 22.07.2023

Статья поступила 01.12.2022 г.
Доработана 11.05.2023 г.
Принята к публикации 22.07.2023 г.

Refractory, Ceramic, and Composite Materials
Тугоплавкие, керамические и композиционные материалы

UDC 621.762
https://doi.org/10.17073/1997-308X-2024-2-23-34

Research article
Научная статья

Phase composition, structure and properties of B_4C–TiB_2 ceramics produced by hot pressing

R. R. Khabirov[1], N. Yu. Cherkasova[1], T. S. Gudyma[1], Yu. L. Krutskii[1], A. V. Mass[1], T. S. Ogneva[1], R. I. Kuzmin[1], A. G. Anisimov[2]

[1] **Novosibirsk State Technical University**
20 Karl Marx Prosp., Novosibirsk 630073, Russia
[2] **Lavrentyev Institute of Hydrodynamics of Siberian Branch of Russian Academy of Sciences**
15 Academician Lavrentiev Prosp., Novosibirsk 630090, Russia

xabirov.2016@stud.nstu.ru

Abstract. Composite ceramic materials based on B_4C with the addition of TiB_2 in amounts of 0, 10, 20, 25 and 30 mol. % have been studied. Titanium diboride was synthesized from TiO_2 powder and nanofibrous carbon using the boron carbide method in an induction furnace at 1650 °C in an argon atmosphere. The samples were produced by hot pressing at 2100 °C and 25 MPa in an argon environment. The phase composition was determined, and the apparent density and open porosity of the experimental materials were measured. The microstructure was assessed using optical and scanning electron microscopy. The investigations revealed that an increase in the TiB_2 content reduces the open porosity while concurrently enhancing the relative density of the boron carbide ceramics. For a sample containing 30 mol. % TiB_2, the open porosity and relative theoretical density were 1.6 and 99 %, respectively. Using XRD and XRS analyses established that the synthesized materials are comprised of two phases: B_4C and TiB_2. The average grain size of TiB_2 was 0.85 ± 0.02 μm for the sample with 10 mol. % TiB_2 and 8.90 ± 0.25 μm for the material with 30 mol. % TiB_2. It was found that at higher TiB_2 concentrations, large clusters of grains are formed. The destruction pattern of B_4C grains is intragranular, while TiB_2 grains are characterized by intergranular destruction. For a sample containing 30 mol. % TiB_2, the fracture toughness was 4.97 ± 0.23 MPa·$m^{0.5}$, and the hardness was 3320 ± 120 $HV_{0.5}$. Therefore, the addition of TiB_2 at these specified concentrations facilitated a 30 % enhancement in fracture toughness relative to single-phase B_4C while preserving a high level of hardness.

Keywords: composite ceramics, B_4C, TiB_2, fracture toughness, crack deflection

Acknowledgements: The research was conducted at the core facility "Structure, mechanical and physical properties of materials", NSTU (No. 13. TsKP.21.0034, 075-15-2021-698).

For citation: Khabirov R.R., Cherkasova N.Yu., Gudyma T.S., Krutskii Yu.L., Mass A.V., Ogneva T.S., Kuzmin R.I., Anisimov A.G. Phase composition, structure and properties of B_4C–TiB_2 ceramics produced by hot pressing. *Powder Metallurgy and Functional Coatings*. 2024;18(2):23–34. https://doi.org/10.17073/1997-308X-2024-2-23-34

Фазовый состав, структура и свойства B_4C–TiB_2-керамики, полученной горячим прессованием

Р. Р. Хабиров[1], Н. Ю. Черкасова[1], Т. С. Гудыма[1], Ю. Л. Крутский[1], А. В. Масс[1], Т. С. Огнева[1], Р. И. Кузьмин[1], А. Г. Анисимов[2]

[1] Новосибирский государственный технический университет
Россия, 630073, г. Новосибирск, пр-т Карла Маркса, 20
[2] Институт гидродинамики им. М.А. Лаврентьева СО РАН
Россия, 630090, г. Новосибирск, пр-т Академика Лаврентьева, 15

xabirov.2016@stud.nstu.ru

Аннотация. Исследованы композиционные керамические материалы на основе B_4C с добавлением TiB_2 в количестве 0, 10, 20, 25, 30 мол. %. Диборид титана был синтезирован из порошка TiO_2 и нановолокнистого углерода карбидоборным методом в индукционной печи при температуре 1650 °C в потоке аргона. Образцы получены методом горячего прессования при температуре 2100 °C и давлении 25 МПа в атмосфере аргона. Определен фазовый состав и измерены кажущаяся плотность и открытая пористость экспериментальных материалов. Микроструктуру оценивали методами оптической и растровой электронной микроскопии. Выявлено, что увеличение содержания TiB_2 снижает открытую пористость и увеличивает относительную плотность керамики на основе карбида бора. Для образца, содержащего 30 мол. % TiB_2, открытая пористость и относительная от теоретической плотность составили 1,6 % и 99 % соответственно. Методами рентгенофазового и микрорентгеноспектрального анализов установлено, что полученные материалы состоят из двух фаз – B_4C и TiB_2. Средний размер зерен TiB_2 составил 0,85 ± 0,02 мкм для образца с 10 мол. % TiB_2 и 8,90 ± 0,25 мкм для материала с 30 мол. % TiB_2. Установлено, что при более высокой концентрации TiB_2 образуются крупные скопления зерен. Характер разрушения B_4C-зерен – внутризеренный, а для TiB_2-зерен характерно межзеренное разрушение. Для образца, содержащего 30 мол. % TiB_2, трещиностойкость составила 4,97 ± 0,23 МПа·м^{0,5}, твердость – 3320 ± 120 $HV_{0,5}$. Таким образом, добавка TiB_2 в таком количестве позволила увеличить трещиностойкость на 30 % по сравнению с однофазным B_4C и сохранить высокий уровень твердости.

Ключевые слова: композиционная керамика, B_4C, TiB_2, трещиностойкость, отклонение трещины

Благодарности: Исследования проведены на оборудовании ЦКП «Структура, механические и физические свойства материалов» НГТУ. (№ 13.ЦКП.21.0034, 075-15-2021-698).

Для цитирования: Хабиров Р.Р., Черкасова Н.Ю., Гудыма Т.С., Крутский Ю.Л., Масс А.В., Огнева Т.С., Кузьмин Р.И., Анисимов А.Г. Фазовый состав, структура и свойства B_4C–TiB_2-керамики, полученной горячим прессованием. *Известия вузов. Порошковая металлургия и функциональные покрытия*. 2024;18(2):23–34. https://doi.org/10.17073/1997-308X-2024-2-23-34

Introduction

Ceramics based on B_4C are garnering significant interest from the research community due to their distinct combination of properties, including a high level of hardness (50 GPa) and low density (2.52 g/cm^3), positioning them as a promising candidate for the fabrication of sandblasting nozzles [1–3].

Achieving a density in B_4C ceramics that approximates the theoretical maximum is challenging due to the presence of strong covalent B–C bonds, a low self-diffusion coefficient, and substantial resistance to grain boundary slippage. B_4C also presents limitations in terms of its relatively modest fracture toughness (3.1–3.2 MPa·m$^{0.5}$) [4] and bending strength (475–579 MPa) [5].

Suppressing the growth of B_4C grains through the establishment of a two-phase structure has been shown to enhance sintering conditions, thereby facilitating the production of ceramics with a relative density nearing the theoretical ideal [6; 7]. Furthermore, the development of composite materials derived from boron carbide impacts the pattern of destruction. Introducing dispersed particles that exhibit greater plasticity into the B_4C matrix promotes the dissipation of crack energy within the ceramics [8], culminating in an increase in material fracture toughness [9].

Titanium diboride is frequently utilized as an additive that favorably influences the characteristics of B_4C ceramics. The B_4C–TiB_2 system is characterized by an absence of significant mutual solubility, with TiB_2 establishing a mechanical mixture alongside B_4C. A composition comprising 75–78 mol. % B_4C and 22–25 mol. % TiB_2 aligns with a eutectic point that has a melting temperature of 2200 °C [10; 11]. Consequently, the sintering process for the B_4C–TiB_2 composite material is executed at a reduced temperature, resulting in a structure that features isolated TiB_2 grains dispersed throughout a polycrystalline B_4C matrix [12]. The coefficients of linear thermal expansion for titanium boride

and boron carbide are markedly different ($5.5 \cdot 10^{-6}$ °C^{-1} for B_4C, $7.8 \cdot 10^{-6}$ °C^{-1} for TiB_2) [13]. In this regard, in such materials, upon cooling after sintering, residual stresses arise, which, according to the authors of [14], reach 1 GPa. Therefore, upon cooling after sintering, residual stresses emerge within the material, which, as suggested by [14], can reach up to 1 GPa. Here, not only the magnitude but also the distribution of these stresses is of critical importance. Tensile stresses and microcracks tend to form along the grain boundaries, whereas the compressive stresses within B_4C crystallites act to inhibit their growth and the subsequent development of macrocracks [15]. This stress distribution significantly contributes to the elevated fracture toughness observed in these ceramics [16; 17].

B_4C–TiB_2 composites produced via hot pressing (HP) attain a relative density of 99.8 % and a fracture toughness of 9.4 MPa·m$^{0.5}$, albeit with a slight reduction in hardness (26 GPa) when contrasted with additive-free B_4C [5; 14; 18–21]. It has been observed that the *in-situ* formation of titanium diboride within the material – arising from the synthesis of B_4C, TiB_2, and carbon during ceramic sintering – contributes to enhanced mechanical properties of the sintered composite relative to composites incorporating directly added TiB_2 powders [5; 14; 22]. Nevertheless, the mechanisms governing the evolution of the microstructure of B_4C ceramics with varying concentrations of TiB_2 additive, as well as its impact on the properties of the composites, remain insufficiently elucidated in the literature.

In the studies reported in [6], the properties and microstructure of B_4C ceramics were analyzed in correlation with the concentration of the TiB_2 additive. An increase in fracture toughness was observed with an increase in TiB_2 content beyond 10 %; however, the incorporation of more than 30 mol. % TiB_2 resulted in diminished hardness and bending strength, attributable to the intrinsically lower strength attributes of TiB_2. Additionally, an elevated TiB_2 content exceeding 30 mol. % was correlated with a decrease in the composite's relative density [12; 23], potentially due to TiB_2 limited sinterability [6].

In the current research, TiB_2 was synthesized through the boron carbide method using B_4C, TiO_2, and a carbonaceous agent. Typically, acetylene black with a specific surface area (S_{sp}) of approximately 50 m^2/g is utilized as a carbon source in the synthesis of refractory oxygen-free compounds. In this instance, nanofibrous carbon, also with an S_{sp} of around 50 m^2/g, was employed. The use of carbon materials with an expansive specific surface area is known to expedite solid-phase reactions, hence their application represents a promising avenue in the exploration of methodologies for synthesizing composite ceramics [24].

The objective of this study is to delineate the patterns in the formation of phase composition, microstructure, and properties of B_4C composite ceramics that incorporate TiB_2 synthesized with the aid of nanofibrous carbon.

Materials and methods

Highly dispersed B_4C powders (98.5 % purity, 2.1 μm particle size), synthesized according to the method given in [25], TiO_2 (99 %, purity, 1 μm particle size) and nanofibrous carbon (99 % purity) were utilized as the initial components. The latter consisted of granules 0.4–8.0 mm in size, which were composed of intertwined fibers with an average diameter of 73 nm, and was produced by the catalytic decomposition of natural and hydrocarbon gases [26]. To enhance reactivity, the nanofibrous carbon granules were pre-milled in an AGO-2S planetary mill for 5 min at an acceleration of 15*g* and a ball-to-material weight ratio of 15:1. The drums and milling media were made of ZrO_2. The average particle size of the nanofibrous carbon granules post-milling was 3.9 μm. The proportions of the initial powders in the mixture were calculated to facilitate the formation of 10, 20, 25 and 30 mol. % TiB_2 in the sintered ceramics. Samples of B_4C without additives were also prepared.

The composition of the powder mixtures was determined based on an analysis published data. Titanium diboride was synthesized in a solid phase reaction using the boron carbide method [27], according to the following reaction [22]

$$(1 - 0.5x)B_4C + xTiO_2 + 1.5xC =$$
$$= (1 - x)B_4C + xTiB_2 + 2xCO,$$

where x is the mole fraction of TiB_2 in the mixture.

The mixing of boron carbide, titanium oxide, and nanofibrous carbon powders occurred in an AGO-2S planetary mill for 5 min at an acceleration of 20*g*, using a ball-to-material weight ratio of 30:1. Only powders that had been sieved through a 100 μm mesh were used. The synthesis of TiB_2 was performed in an indirect heating induction furnace under an argon atmosphere at 1650 °C, with a dwell time of 20 min. The median particle sizes (d_{50}) for the synthesized powders containing 10, 20, 25 and 30 mol. % TiB_2 were 7.4, 8.3, 8.4 and 13.4 μm, respectively.

The synthesized powders were employed to fabricate samples by hot pressing (HP) at 2100 °C under a pressure of 25 MPa in an argon atmosphere. The HP process lasted for 70 min, with a dwell time at the maximum temperature of 25 min. The dimensions of the sintered samples were 20 mm in diameter and 4 mm in height. The HP parameters were chosen with consideration

of published findings. For instance, research detailed in [28] indicates that a HP temperature of 2100 °C yields the highest relative density in ceramics. Other studies [29; 30] have also conducted hot pressing of B_4C ceramics at this temperature.

Diffraction patterns were captured using an ARL X'TRA diffractometer (Thermo Scientific, Switzerland) equipped with a θ–θ goniometer. The end surfaces of the samples which had been cleared of any residues from the graphite paper used as a separator during the hot pressing process, were photographed after a meticulous grinding process.

The phase composition was determined utilizing the corundum number method. A profile analysis of the diffraction pattern was carried out in the Fityk software package (Poland) to assess the integral intensity of the largest phase peaks. The weight fraction of the phases was calculated according to the formula

$$w_k = \frac{\frac{I_k^{\max}}{RIR_k}}{\sum \frac{I_i^{\max}}{RIR_k}},$$

where $I_k^{\max}$ is the integral intensity of the largest peak of the given phase, RIR_k is the corundum number of that phase.

The apparent density and open porosity of the ceramics were measured by hydrostatic weighing. The relative density was determined as the ratio of the apparent density to the theoretical value:

$$\rho_{\text{rel}} = \frac{\rho_{\text{app}}}{\rho_{\text{theor}}} \cdot 100\ \%.$$

The theoretical density for each composite was calculated using the rule of mixtures, referencing the *X*-ray density values of the components found in the literature B_4C (2.5 g/cm^3) and TiB_2 (4.5 g/cm^3) [31–33].

The average particle size of the powder was determined using a MicroSizer 201 VA Instrument laser particle size analyzer (VA Instalt, Russia). Microstructural examination was performed on polished sections and fracture surfaces employing EVO 50 optical and scanning electron microscopes (Carl Zeiss, Germany). To enhance the electrical conductivity of the samples under investigation, a copper layer approximately 20 nm in thickness was sputtered onto the polished surfaces. The chemical composition of the samples was analyzed through energy dispersive *X*-ray spectroscopy (EDX) using the INCA X-ACT system, and maps depicting the distribution of chemical elements were generated.

Hardness and fracture resistance measurements were conducted utilizing a 402MVD hardness tester (Wolpert Group, Germany) equipped with a diamond tetrahedral Vickers pyramidal indenter. Hardness was measured by the Vickers method under an indenter load of 500 g, while fracture toughness tests were administered with a load of 5 kg. The values of this index were initially computed using various methods, inclusive of equations from [34; 35]. The utilization of equations that consider Young's modulus (E) yields more accurate values of the critical stress intensity factor (K_{Ic}), especially when investigating composite materials with significant discrepancies in E values. Employing simplified equations often results in overestimations that deviate substantially from actual values [36]. Consequently, most literature concentrating on the evaluation techniques for calculating the critical stress intensity factor use equations that include Young's modulus [34; 35]:

$$K_{Ic} = 0.048\left(\frac{l}{a}\right)^{-0,5}\left(\frac{H_v}{E\varphi}\right)^{-0,4}\frac{H_v a^{0,5}}{\varphi},$$

where H_v is the hardness, GPa; l is the crack length, μm; a is the indentation half diagonal, μm; φ = 3 is the constant.

The Young's modulus of the experimental materials was determined using the rule of mixtures:

$$E = \frac{100}{\frac{m_i}{E_i} + \frac{m_j}{E_j}},$$

where E_i and E_j are the Young's modulus values of B_4C and TiB_2, respectively, GPa; m_i and m_j are their weight fractions, %.

For these calculations, the values of Young's modulus for hot-pressed B_4C (450 GPa) and TiB_2 (530 GPa) were taken from [31–33].

Results and discussion

Open porosity and density of composite ceramic materials

The study evaluated the impact of varying titanium diboride concentrations on the alteration of (ρ_{rel}) and open porosity (P). The findings are illustrated in Fig. 1. In the B_4C ceramics devoid of additives, a high ρ_{rel} was observed at 97.66 ± 0.49 %, with P = 0.07 ± 0.02 %. These figures confirm the appropriateness of the selected hot pressing parameters, which facilitated the production of low-porosity ceramics.

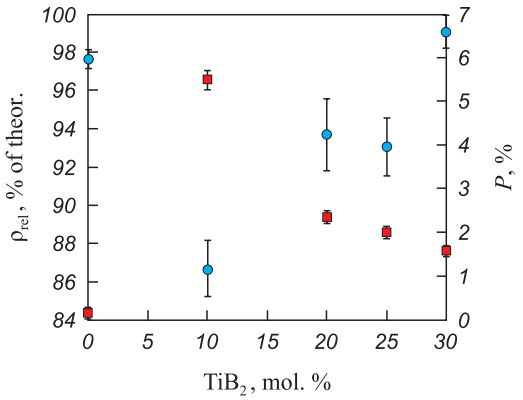

Fig. 1. Relative density (●) and open porosity (■) of experimental materials as a function of the amount of TiB_2 additive

Рис. 1. Относительная от теоретической плотность (●) и открытая пористость (■) экспериментальных материалов в зависимости от количества добавки TiB_2

Nevertheless, the sample containing 10 mol. % TiB_2 exhibited a lower ρrel and increased *P*.

With the escalation of TiB_2 content to 30 mol. %, there was a 15 % increase in relative density and a 42 % reduction in open porosity in comparison to the specimen with 10 mol. % TiB_2. The resulting material's relative density is on par with that of composite B_4C ceramics reported in other studies [6; 7; 37].

Phase analysis

Fig. 2 presents the *X*-ray diffraction pattern of a composite material consisting of boron carbide and 30 mol. % titanium diboride, which is characterized by the highest relative density. The sample's composition by weight percentage is: $65B_4C$, $31TiB_2$ and 4C.

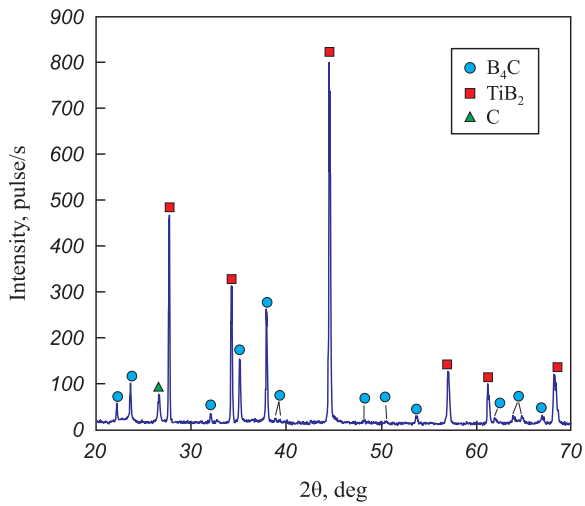

Fig. 2. XRD pattern of B_4C ceramic sample with 30 mol. % TiB_2

Рис. 2. Рентгеновская дифракционная картина образца керамики B_4C с 30 мол. % TiB_2

Graphite paper served as a barrier between the punch and the powder during hot pressing. It is possible that particles of the graphite penetrated into the more profound pores evident on the sample's surface. This could account for the carbon reflection observed in the diffraction pattern.

The lack of TiO_2 reflections in Fig. 2 suggests the complete reaction of the starting powder materials. Furthermore, the absence of ZrO_2 reflections implies that there was no significant attrition of the milling media during the milling process.

Microsrtructural study

The microstructure of composite ceramics with a 30 mol. % addition of TiB_2 comprises a matrix (appearing gray in images) interspersed with light-colored clusters of varying sizes (Fig. 3, *a*). To elucidate the consti-

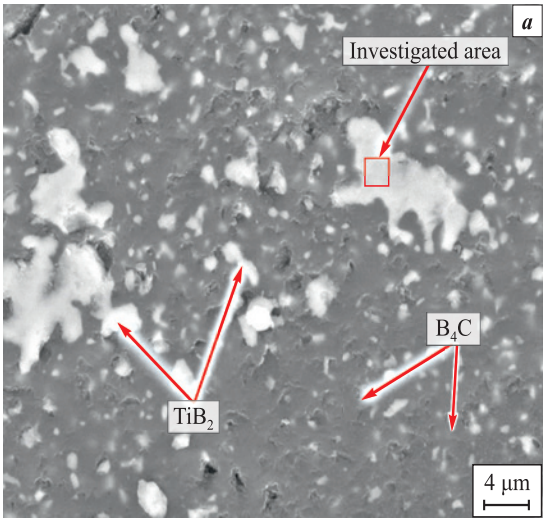

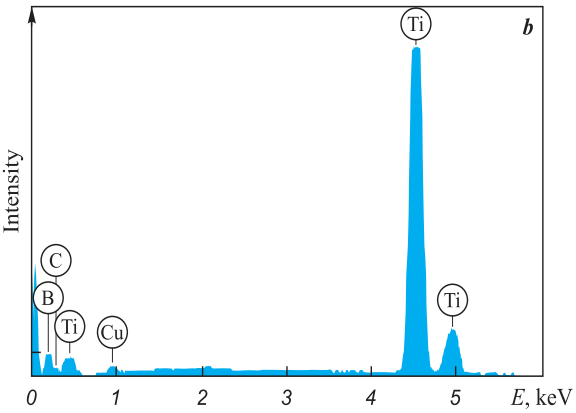

Fig. 3. Results of EDX analysis of ceramics containing 30 mol. % TiB_2

a – general view of the investigated area, ***b*** – EDX spectrum

Рис. 3. Результаты EDX-анализа керамики, содержащей 30 мол. % TiB_2

a – общий вид исследуемой области, ***b*** – характеристический рентгеновский спектр

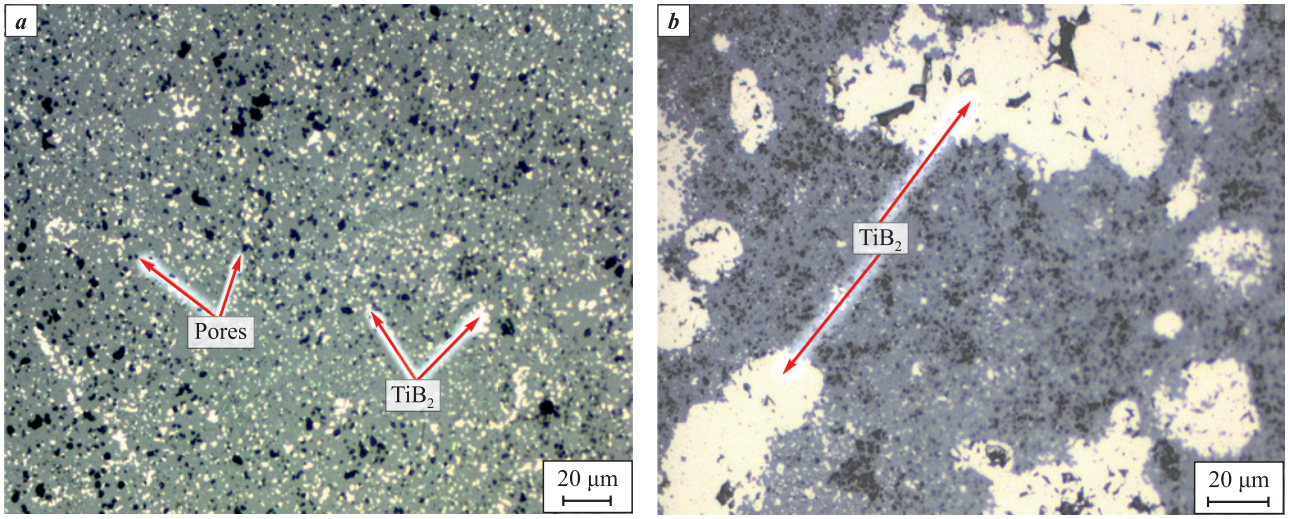

Fig. 4. Microstructure of B_4C samples with 10 mol. % (***a***) and 20 mol. % (***b***) TiB_2 additions

Рис. 4. Микроструктура образцов B_4C с добавкой TiB_2 в количестве 10 мол. % (***a***) и 20 мол. % (***b***)

tuents of the structure, maps detailing the distribution of chemical elements were generated, and reflections indicative of boron and titanium were observed within these light clusters (Fig. 3, *b*). Consequently, these clusters have been identified as the TiB_2 phase. The absence of zirconium in the spectral analysis further corroborates the lack of significant wear on the grinding media during processing.

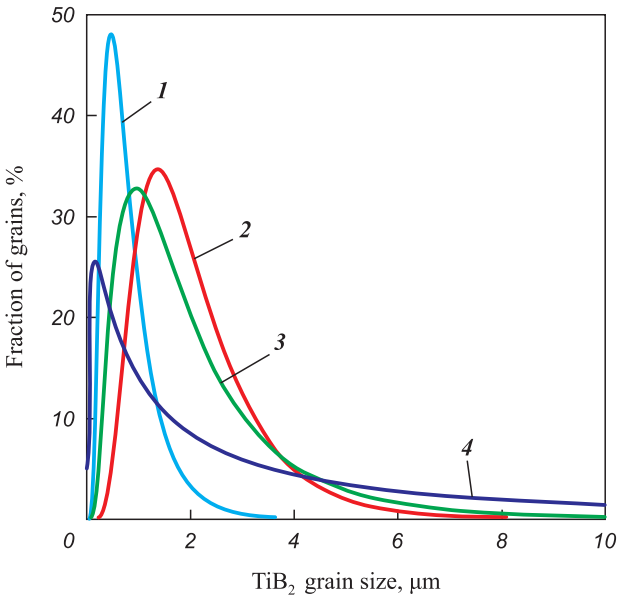

Fig. 5. Histogram plot of TiB_2 grain size distribution in sintered ceramics:
1 – 10 mol. % TiB_2; ***2*** – 20 mol. % TiB_2;
3 – 25 mol. % TiB_2; ***4*** – 30 mol. % TiB_2

Рис. 5. Участок гистограммы распределения размера зерен TiB_2 в спеченной керамике:
1 – 10 мол. % TiB_2; ***2*** – 20 мол. % TiB_2;
3 – 25 мол. % TiB_2; ***4*** – 30 мол. % TiB_2

The material with 10 mol. % TiB_2 exhibits a low relative density and elevated open porosity, which is attributed to the large number of pores (Fig. 4, *a*). TiB_2 grains are evenly dispersed throughout the B_4C matrix. However, an increase in TiB_2 content is associated with the emergence of larger aggregates of this phase (Fig. 4, *b*).

Fig. 5 provides histograms that portray the distribution of TiB_2 grain size across composites of varying compositions, while an accompanying table lists their mean size (d_{avg}) along with the d_{50} and d_{90} statistics. The grain size distribution curves for the composite ceramics exhibit a unimodal configuration with a single pronounced peak. A lognormal function was employed to model the distribution curve of TiB_2 grain sizes in the fabricated materials.

With an increment in TiB_2 content within the material's composition, there is a corresponding increase in the average size of the diboride grains, as well as the formation of large clusters. In the specimen containing 10 mol. % TiB_2, the largest grain clusters do not exceed 4.5 μm. The restricted range of size distribution in this

Average size and parameters d_{50}, d_{90} of TiB_2 grains in B_4C + TiB_2 ceramic samples

Средний размер и параметры d_{50}, d_{90} зерен TiB_2 в образцах композиционной керамики B_4C + TiB_2

TiB_2, mol. %	d_{avg}, μm	d_{50}, μm	d_{90}, μm
10	0.85 ± 0.02	0.72	1.37
20	2.05 ± 0.04	1.62	3.47
25	2.40 ± 0.09	1.40	5.26
30	8.90 ± 0.25	1.82	35.89

ceramic suggests a uniform growth of the second phase inclusions. Conversely, clusters measuring up to 320 μm were identified in the sample with 30 mol. % TiB_2. The distribution function graph for the TiB_2 grain sizes in this sample demonstrates an asymmetrical profile, with a considerable presence of coarse grains, as indicated by the elevated d_{90} values. Meanwhile, the d_{50} parameter shows only a minor increase with the rise in TiB_2 concentration. Therefore, the microstructure of the ceramics is characterized by a combination of uniformly distributed fine TiB_2 grains and larger grains and clusters. This phenomenon is likely due to the high degree of agglomeration present in the initial powder mixtures and the subsequent growth of these agglomerates during the TiB_2 synthesis process.

Microstructural images from studies [18; 23] also affirm that the size of grain clusters for this phase expands as the TiB_2 concentration increases. Findings by researchers in [38] demonstrate that employing finer B_4C powder aids in creating fine-grained B_4C–TiB_2 ceramics with a more homogeneously distributed TiB_2 phase.

To mitigate the inhomogeneity of the grain structure, it is advisable to extend the milling duration of the powder mixtures prior to the synthesis of TiB_2 powder, and also to perform additional milling of the synthesized powder mixture.

Mechanical properties

The incorporation of TiB_2, which possesses a lower hardness than B_4C, results in a decrease in the hardness of the B_4C–TiB_2 composite as depicted in Fig. 6 and corroborated by numerous studies [7; 15]. The diminished fracture toughness observed in samples containing 10, 20, and 25 mol. % TiB_2 additives is attributed to their high open porosity and low relative density. The presence of large pores within the ceramic matrix adversely affects its resistance to crack propagation [39]. Nevertheless, enhancing the TiB_2 content to 30 mol. % yielded improvements in both hardness and fracture toughness over materials with lesser additive amounts and the pure B_4C sample.

Research in [6] reported the fabrication of ceramics with 30 mol. % TiB_2 from commercial B_4C and TiB_2 powders through spark plasma sintering (P = 50 MPa, t = 2000 °C). The resultant material's relative density was 97.91 % of theoretical, with a hardness of 28.86 ± 0.29 GPa and fracture resistance of 4.36 ± 0.1 MPa·m$^{0.5}$, figures that are inferior to those achieved in the current study. The authors of [6] suggest that the decreased performance metrics with TiB_2 contents exceeding 5 mol. % are due to TiB_2's limited sinterability. In contrast, our study demonstrates an increase in the relative density of ceramics with rising TiB_2 concentrations, underscoring the enhanced sinterability of titanium diboride synthesized via the boron carbide method compared to that of commercial powders.

The research presented in [38] involved synthesizing ceramics using commercial powders of B_4C and 30 vol. % (37.5 mol. %) TiB_2 by hot pressing at 2000 °C and 35 MPa. This process produced a material with a uniform distribution of TiB_2 grains, a theoretical relative density of 100 %, and mechanical properties (H_v = 30.42 ± 0.79 GPa, K_{Ic} = 5.16 ± 0.19 MPa·m$^{0.5}$) comparable to those observed in the present study, likely facilitated by intensive milling for 12 h.

Similarly, [12] describes ceramics with 30 vol. % (37.5 mol. %) TiB_2 and 100 % relative density, prepared from commercial B_4C and TiB_2 powders subjected to 24 h of grinding and subsequently sintered by spark plasma sintering at 2000 °C and 60 MPa. This material exhibited a hardness of 31 ± 0.5 GPa and a fracture toughness of 3.75 ± 0.25 MPa·m$^{0.5}$.

These comparative analyses indicate that the mechanical properties of the experimental material developed in this work are competitive with those of ceramics fabricated from commercial TiB_2 powders. Hence, synthesizing TiB_2 from relatively inexpensive starting materials such as TiO_2, carbon, and B_4C emerges as a viable strategy to enhance the properties of B_4C ceramics.

On the fracture surfaces of the initial B_4C sintered sample (Fig. 7) and the sample containing 10 mol. % TiB_2 (Fig. 8, *a*), transgranular fracture of B_4C was

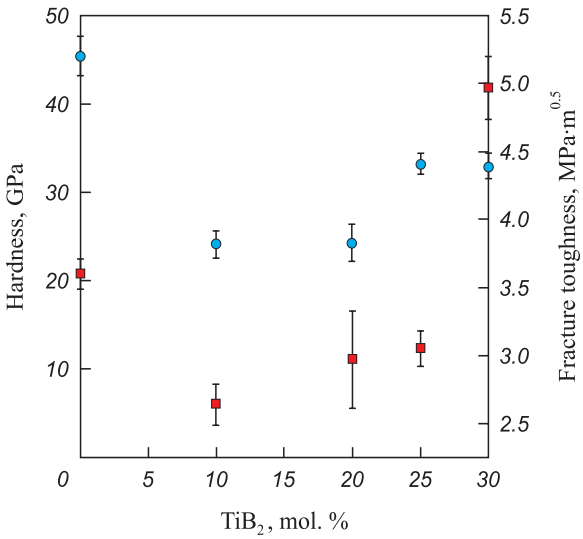

Fig. 6. Hardness (●) and fracture toughness (■) of composite ceramics as a function of amount of TiB_2 additive

Рис. 6. Твердость (●) и трещиностойкость (■) композиционной керамики в зависимости от количества добавки TiB_2

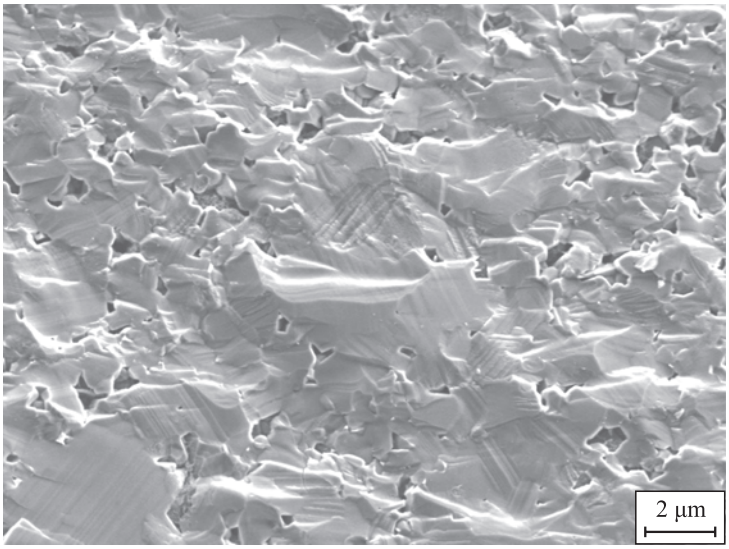

Fig. 7. Fracture surface of sintered B_4C without additives

Рис. 7. Поверхность разрушения спеченного B_4C без добавок

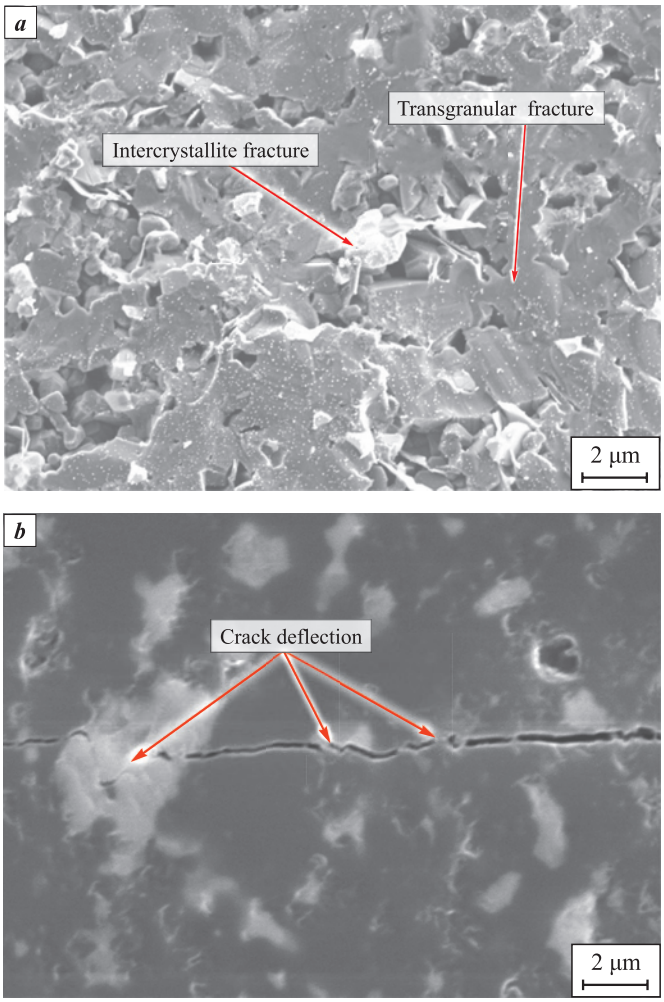

Fig. 8. Microstructure of ceramics with addition of 10 mol. % TiB_2

a – fracture surface, ***b*** – crack deflection on TiB_2 grains and agglomerates

Рис. 8. Микроструктура керамики с добавкой 10 мол. % TiB_2

a – поверхность разрушения, ***b*** – отклонение трещины на зернах и агломератах TiB_2

observed. This indicates a significantly strong cohesive strength among the intergranular bonds. According to ceramic materials fracture theory, the dominance of a transgranular fracture mechanism positively influences fracture toughness.

In certain TiB_2 grains, a variation in the fracture pattern within the intergranular regions is noted (Fig. 8, *b*). Similar observations were made in previous studies [15; 22], especially when a crack transitions from B_4C to TiB_2. Such variations could stem from alterations in the crack's path as it approaches grains possessing a fracture toughness superior to that of the B_4C matrix. This crack deflection process is likely to facilitate the dissipation of energy, thereby enhancing the mechanical properties of the composite ceramics [6]. In the examined material, such crack deflection was distinctly visible upon interaction with TiB_2 grains (refer to Fig. 8, *b*), accounting for the observed increase in fracture toughness in the composite with 30 mol. % TiB_2 in comparison to the additive-free B_4C.

Conclusions

The investigation has established clear trends in the alterations to the microstructure and properties of B_4C-based composite ceramics as a function of their composition.

1. *X*-ray phase analysis has verified that the sintered composite materials are composed of boron carbide and titanium diboride. The absence of TiO_2 reflections in the *X*-ray diffraction patterns substantiates the complete synthesis of TiB_2.

2. An increment in the TiB_2 content results in an enlarged average grain size of the diboride, with the formation of substantial clusters ranging between 100–320 μm. This phenomenon may contribute to increased anisotropy in the properties of the ceramics.

3. The prevalent fracture mechanism in B_4C is observed to be transgranular, while TiB_2 exhibits intergranular failure. This distinction underscores a modulation in the trajectory of cracks when encountering TiB_2 particles, where crack deviation is associated with the dissipation of energy, thereby enhancing the composite's fracture toughness.

4. The material incorporating 30 mol. % TiB_2 exhibits a synergy of high fracture toughness and hardness. This composition is distinguished by its elevated relative density, diminished open porosity, and a robust cohesive strength among grains.

References / Список литературы

1. Jianxin D. Erosion wear of boron carbide ceramic nozzles by abrasive air-jets. *Materials Science and Engineering A*. 2005;408(1-2):227–233. https://doi.org/10.1016/j.msea.2005.07.029

2. Wang C., Lu Z., Zhang K. Microstructure, mechanical properties and sintering model of B_4C nozzle with microholes by powder injection molding. *Powder Technology*. 2012;228:334–338. https://doi.org/10.1016/j.powtec.2012.05.049

3. Junlong S., Changxia L., Jin T., Baofu F. Erosion behavior of B_4C based ceramic nozzles by abrasive air-jet. *Ceramics International*. 2012;38(8):6599–6605. https://doi.org/10.1016/j.ceramint.2012.05.045

4. Lee H., Speyer R. F. Hardness and Fracture Toughness of Pressureless-Sintered Boron Carbide (B_4C). *Journal of the American Ceramic Society*. 2002;85(5):1291–1293. https://doi.org/10.1111/j.1151-2916.2002.tb00260.x

5. Yamada S., Hirao K., Yamauchi Y., Kanzaki S. High strength B_4C–TiB_2 composites fabricated by reaction hot-pressing. *Journal of the European Ceramic Society*. 2003;23(7):1123–1130. https://doi.org/10.1016/S0955-2219(02)00274-1

6. Liu Y., Li Z., Peng Y., Huang Y., Huang Z., Zhan D. Effect of sintering temperature and TiB_2 content on the grain size of B_4C–TiB_2 composites. *Materials Today Communications*. 2020;23:100875. https://doi.org/10.1016/j.mtcomm.2019.100875

7. Guo W., Wang A., He Q., Tian T., Liu C., Hu L., Shi Y., Liu L., Wang W., Fu Z. Microstructure and mechanical properties of B_4C–TiB_2 ceramic composites prepared via a two-step method. *Journal of the European Ceramic Society*. 2021;41(14):6952–6961. https://doi.org/10.1016/j.jeurceramsoc.2021.07.013

8. Zhao S.M, Zhao L.R. Mechanical properties of hot-pressed B_4C–TiB_2 composites synthesized from B_4C–TiO_2 and B_4C–TiC. *Key Engineering Materials*. 2021;902:81–86. https://doi.org/10.4028/www.scientific.net/KEM.902.81

9. Yuan Y., Ye T., Wu Y., Xu Y. Mechanical and ballistic properties of graphene platelets reinforced B_4C ceramics: Effect of TiB_2 addition. *Materials Science and Engineering: A*. 2021;817:141294. https://doi.org/10.1016/j.msea.2021.141294

10. Ordan'yan S.S., Nesmelov D.D., Danilovich D.P., Udalov Yu.P. SiC–B_4C–Me^dB_2 systems and the prospects for creating composite ceramic materials based on them. *Powder Metallurgy and Functional Coatings*. 2016;(4):41–50. (In Russ.). https://doi.org/10.17073/1997-308X-2016-4-41-50

Орданьян С.С., Несмелов Д.Д., Данилович Д.П., Удалов Ю.П. О строении систем SiC–B_4C–Me^dB_2 и перспективах создания композиционных керамических материалов на их основе. *Известия вузов. Порошковая металлургия и функциональные покрытия*. 2016;(4):41–50. https://doi.org/10.17073/1997-308X-2016-4-41-50

11. Gunjishima I., Akashi T., Goto T. Characterization of directionally solidified B_4C–TiB_2 composites prepared by a floating zone method. *Materials Transactions*. 2002; 43(4):712–720. https://doi.org/10.2320/matertrans.43.712

12. Huang S.G., Vanmeensel K., Malek O.J.A., Van der Biest O., Vleugels J. Microstructure and mechanical properties of pulsed electric current sintered B_4C–TiB_2

composites. *Materials Science and Engineering: A*. 2011;528(3): 1302–1309. https://doi.org/10.1016/J.MSEA.2010.10.022

13. Carter C.B., Norton M.G. Ceramic materials. New York: Springer, 2013. 766 p.
14. Skorokhod V.V., Krstic V.D. Processing, microstructure, and mechanical properties of B_4C–TiB_2 particulate sintered composites. II. Fracture and mechanical properties. *Powder Metallurgy and Metal Ceramics*. 2000;39(9):504–513. https://doi.org/10.1023/A:1011378825628
15. Dai J., Pineda E.J., Bednarcyk B.A., Singh J., Yamamoto N. Macro-scale testing and micromechanics modeling of fracture behaviors for boron carbide composites with hierarchical microstructures. In: *AIAA Scitech 2021 Forum* (11–15 and 19–21 January 2021). USA, American Institute of Aeronautics and Astronautics, 2021. P. 14. https://doi.org/10.2514/6.2021-0405
16. Skorokhod V., Krstic V.D. High strength-high toughness B_4C–TiB_2 composites. *Journal of Materials Science Letters*. 2000;19(3):237–239. https://doi.org/10.1023/A:1006766910536
17. Ivanov Y.F., Khasanov O.L., Polisadova V.V., Petyukevich M.S., Milovanova T.V., Teresov A.D., Bikbaeva Z.G., Kalashnikov M.P., Bratukhina A.S. The analysis of the mechanisms for plasticization of boron carbide ceramics irradiated by an intense electron beam. *Key Engineering Materials*. 2016;685:700–704. https://doi.org/10.4028/www.scientific.net/KEM.685.700
18. Yue X.Y., Zhao S.M., Yu L., Ru H.Q. Microstructures and mechanical properties of B_4C–TiB_2 composite prepared by hot pressure sintering. *Key Engineering Materials*. 2010;34:50–53. https://doi.org/10.4028/www.scientific.net/KEM.434-435.50
19. Yue X.Y., Zhao S.M., Lü P., Chang Q., Ru H.Q. Synthesis and properties of hot pressed B_4C–TiB_2 ceramic composite. *Materials Science and Engineering: A*. 2010;527(27-28):7215–7219. https://doi.org/10.1016/J.MSEA.2010.07.101
20. Liu A.D., Qiao Y.J., Liu Y.Y. Pressureless sintering and properties of boron carbide-titanium diboride composites by *in situ* reaction. *Key Engineering Materials*. 2012;525:321–324. https://doi.org/10.4028/www.scientific.net/KEM.525-526.321
21. Li A., Zhen Y., Yin Q., Ma L., Yin Y. Microstructure and properties of (SiC, TiB_2)/B_4C composites by reaction hot pressing. *Ceramics International*. 2006;32(8):849–856. https://doi.org/10.1016/j.ceramint.2005.05.022
22. Skorokhod V.V., Krstic V.D. Processing, microstructure, and mechanical properties of B_4C–TiB_2 particulate sintered composites. Part I. Pressureless sintering and microstructure evolution. *Powder Metallurgy and Metal Ceramics*. 2000;39(7):414–423. https://doi.org/10.1023/A:1026625909365
23. Wang Y., Peng H., Ye F., Zhou Y. Effect of TiB_2 content on microstructure and mechanical properties of in-situ fabricated TiB_2/B_4C composites. *Transactions of Nonferrous Metals Society of China*. 2011;21:369–373. https://doi.org/10.1016/S1003-6326(11)61608-7
24. Gudyma T.S., Krutskii Y.L., Maskimovskii E.A., Ukhina A.V., Aparnev A.I., Smirnov A.I., Uvarov N.F. Synthesis of B_4C/ZrB_2 composite powders via boron carbide reduction for ceramic fabrication. *Inorganic Materials*. 2022;58(9):912–921. https://doi.org/10.1134/S0020168522090059
25. Krutskii Y.L., Bannov A. G., Sokolov V.V., Dyukova K.D., Shinkarev V.V., Ukhina A.V., Maksimovskii E.A., Pichugin A.Yu., Solov'ev E.A., Krutskaya T.M., Kuvshinov G.G. Synthesis of highly dispersed boron carbide from nanofibrous carbon. *Nanotechnologies in Russia*. 2013;8(3): 191–198. https://doi.org/10.1134/S1995078013020109

    Крутский Ю.Л., Баннов А.Г., Соколов В.В., Дюкова К.Д., Шинкарев В.В., Ухина А.В., Максимовский Е.А., Пичугин А.Ю., Соловьев Е.А., Крутская Т.М., Кувшинов Г.Г. Синтез высокодисперсного карбида бора из нановолокнистого углерода. *Российские нанотехнологии*. 2013;8(3-4):43–48
26. Kurmashov P.B., Maksimenko V.V., Bannov A.G., Kuvshinov G.G. Horizontal vibrofluidized bed pilot reactor for nanofibrous carbon synthesis process. *Khimicheskaya tehnologiya*. 2013;14(10):635–640. (In Russ.).

    Курмашов П.Б., Максименко В.В., Баннов А.Г., Кувшинов Г.Г. Горизонтальный пилотный реактор с виброожиженным слоем для процесса синтеза нановолокнистого углерода. *Химическая технология*. 2013;14(10):635–640.
27. Krutskii Y.L., Krutskaya T.M., Gudyma T.S., Gerasimov K.B., Khabirov R.R., Mass A.V. Carbothermal and boron carbide reduction of oxides of some transition metals. In: *Proceedings of VII International Russian–Kazakhstan Conference «Chemical Technologies of Functional Materials»* (Novosibirsk, Russia, 28–30 April 2021). MATEC Web of Conferences, 2021. P. 01040. https://doi.org/10.1051/matecconf/202134001040
28. Angers R., Beauvy M. Hot-pressing of boron carbide. *Ceramics International*. 1984;10(2):49–55. https://doi.org/10.1016/0272-8842(84)90025-7
29. Hwang C., DiPietro S., Xie K.Y., Yang Q., Celik A.M., Khan A.U., Domnich V., Walck S., Hemker K.J., Haber R.A. Small amount TiB_2 addition into B_4C through sputter deposition and hot pressing. *Jouranl of the American Ceramic Society*. 2019;102(8):4421–4426. https://doi.org/10.1111/jace.16457
30. He P., Dong S., Kan Y., Zhang X., Ding Y. Microstructure and mechanical properties of B_4C–TiB_2 composites prepared by reaction hot pressing using Ti_3SiC_2 as additive. *Ceramics International*. 2016;42(1A):650–656. https://doi.org/10.1016/j.ceramint.2015.08.160
31. Thevenot F. Boron carbide – A comprehensive review. *Journal of the European Ceramic Society*. 1990;6(4): 205–225. https://doi.org/10.1016/0955-2219(90)90048-K
32. Tee K.L., Lu L., Lai M.O. In situ processing of Al–TiB_2 composite by the stir-casting technique. *Journal of Materials Processing Technology*. 1999;89-90:513–519. https://doi.org/10.1016/S0924-0136(99)00038-2
33. Yi H., Ma N., Zhang Y., Li X., Wang H. Effective elastic moduli of Al–Si composites reinforced in situ with TiB_2 particles. *Scripta Materialia*. 2006;54(6):1093–1097. https://doi.org/10.1016/j.scriptamat.2005.11.070
34. Khasanov A.O. Development of compositions and technology of spark-plasma sintering of ceramic materials, composites based on micro- and nanopowders B_4C: Diss. Cand Sci. (Eng.). Tomsk: TPU, 2015. (In Russ.).

Хасанов А.О. Разработка составов и технологии спарк-плазменного спекания керамических материалов, композитов на основе микро- и нанопорошков B_4C: Дис. … канд. техн. наук. Томск: ТПУ, 2015.

35. Niihara K., Morena R., Hasselman D.P.H. Evaluation of K_{Ic} of brittle solids by the indentation method with low crack-to-indent ratios. *Journal of Materials Science Letters*. 1982;1(1):13–16. https://doi.org/10.1007/BF00724706

36. Khasanov O.L., Struts V.K., Sokolov V.M., Polisadova V.V., Dvilis E.S., Bikbaeva Z.G. Methods for measuring microhardness and crack resistance of nanostructured ceramics. Tomsk: Publishing House of Tomsk Polytechnic University, 2011. 101 p. (In Russ.).

Хасанов О.Л., Струц В.К., Соколов В.М., Полисадова В.В., Двилис Э.С., Бикбаева З.Г. Методы измерения микротвердости и трещиностойкости наноструктурных керамик. Томск: Изд-во Томского политехнического университета, 2011. 101 с.

37. Chen D., Zhang K., Zeng J., Guo H., Li B. High-strength TiB_2–B_4C composite ceramics sintered by spark plasma sintering. *International Journal of Applied Ceramic Technology*. 2022;19(4):1949–1955. https://doi.org/10.1111/ijac.14051

38. Liu Z., Deng X., Li J., Sun Y., Ran S. Effects of B_4C particle size on the microstructures and mechanical properties of hot-pressed B_4C–TiB_2 composites. *Ceramics International*. 2018;44(17):21415–21420. https://doi.org/10.1016/j.ceramint.2018.08.200

39. Yaşar Z. A., Celik A.M., Haber R.A. Improving fracture toughness of B_4C–SiC composites by TiB_2 addition. *International Journal of Refractory Metals and Hard Materials*. 2022;108:105930. https://doi.org/10.1016/j.ijrmhm.2022.105930

Information about the Authors

Roman R. Khabirov – Postgraduate Student at the Department "Materials Science in Mechanical Engineering", Novosibirsk State Technical University (NSTU)
ORCID: 0000-0003-4720-2876
E-mail: xabirov.2016@stud.nstu.ru

Nina Yu. Cherkasova – Cand. Sci. (Eng.), Junior Researcher of the Research Laboratory of Physical and Chemical Technologies and Functional Materials, NSTU
ORCID: 0000-0002-5603-7852
E-mail: cherkasova.2013@corp.nstu.ru

Tatiana S. Gudyma – Junior Researcher of the Laboratory of Chemical Technology of Functional Materials, NSTU
ORCID: 0000-0002-4724-3371
E-mail: gudymatan@mail.ru

Yurii L. Krutskii – Dr. Sci. (Eng.), Associate Professor at the Department of Chemistry and Chemical Technology, NSTU
ORCID: 0000-0003-2524-4143
E-mail: krutskij@corp.nstu.ru

Anna V. Mass – Postgraduate Student at the Department "Materials Science in Mechanical Engineering", NSTU
ORCID: 0000-0003-2053-7422
E-mail: a.mass@corp.nstu.ru

Tatiana S. Ogneva – Cand. Sci. (Eng.), Senior Researcher of the Research Laboratory of Physical and Chemical Technologies and Functional Materials, NSTU
ORCID: 0000-0002-0081-283X
E-mail: ogneva@corp.nstu.ru

Ruslan I. Kuzmin – Cand. Sci. (Eng.), Junior Researcher at the Center for Technological Excellence, NSTU
ORCID: 0000-0001-7712-4296
E-mail: kuzmin.2010@corp.nstu.ru

Alexander G. Anisimov – Cand. Sci. (Phys.-Math.), Senior Researcher of the Laboratory "Synthesis of Composite Materials", Lavrentyev Institute of Hydrodynamics of the Siberian Branch of the Russian Academy of Sciences
ORCID: 0000-0002-0244-2246
E-mail: anis@hydro.nsc.ru

Сведения об авторах

Роман Рафаэлович Хабиров – аспирант кафедры материаловедения в машиностроении, Новосибирский государственный технический университет (НГТУ)
ORCID: 0000-0003-4720-2876
E-mail: xabirov.2016@stud.nstu.ru

Нина Юрьевна Черкасова – к.т.н., мл. науч. сотрудник научно-исследовательской лаборатории физико-химических технологий и функциональных материалов, НГТУ
ORCID: 0000-0002-5603-7852
E-mail: cherkasova.2013@corp.nstu.ru

Татьяна Сергеевна Гудыма – мл. науч. сотрудник лаборатории химической технологии функциональных материалов, НГТУ
ORCID: 0000-0002-4724-3371
E-mail: gudymatan@mail.ru

Юрий Леонидович Крутский – д.т.н., доцент кафедры химии и химической технологии, НГТУ
ORCID: 0000-0003-2524-4143
E-mail: krutskij@corp.nstu.ru

Анна Владимировна Масс – аспирант кафедры материаловедения в машиностроении, НГТУ
ORCID: 0000-0003-2053-7422
E-mail: a.mass@corp.nstu.ru

Татьяна Сергеевна Огнева – к.т.н., ст. науч. сотрудник научно-исследовательской лаборатории физико-химических технологий и функциональных материалов, НГТУ
ORCID: 0000-0002-0081-283X
E-mail: ogneva@corp.nstu.ru

Руслан Изатович Кузьмин – к.т.н., мл. науч. сотрудник Центра технологического превосходства, НГТУ
ORCID: 0000-0001-7712-4296
E-mail: kuzmin.2010@corp.nstu.ru

Александр Георгиевич Анисимов – к.ф.-м.н., ст. науч. сотрудник лаборатории синтеза композиционных материалов, Институт гидродинамики им. М.А. Лаврентьева СО РАН
ORCID: 0000-0002-0244-2246
E-mail: anis@hydro.nsc.ru

Contribution of the Authors

R. R. Khabirov – formulated the main concept, defined the goal and objectives of the work, conducted experiments, processed and analyzed the study results, and wrote the manuscript
N. Yu. Cherkasova – formulated the main concept, defined the goal and objectives of the work, conducted structural studies, and wrote the manuscript.
T. S. Gudyma – formulated the main concept, defined the goal and objectives of the work, synthesized powder mixtures, and wrote the manuscript.
Yu. L. Krutskii – provided scientific management and conducted experiments.
A. V. Mass – conducted structural studies and participated in the discussion of the results.
T. S. Ogneva – carried out *X*-ray phase analysis and participated in the discussion of the results.
R. I. Kuzmin – conducted experiments and participated in the discussion of the results.
A. G. Anisimov – conducted experiments and participated in the discussion of the results.

Вклад авторов

Р. Р. Хабиров – формирование основной концепции, постановка цели и задач работы, проведение экспериментов, обработка и анализ результатов исследования, составление текста статьи.
Н. Ю. Черкасова – формирование основной концепции, постановка цели и задач работы, проведение структурных исследований, написание текста статьи.
Т. С. Гудыма – формирование основной концепции, постановка цели и задач работы, синтез порошковых смесей, написание текста статьи.
Ю. Л. Крутский – научное руководство, проведение экспериментов.
А. В. Масс – проведение структурных исследований, участие в обсуждении результатов.
Т. С. Огнева – проведение рентгенофазового анализа, участие в обсуждении результатов.
Р. И. Кузьмин – проведение экспериментов, участие в обсуждении результатов.
А. Г. Анисимов – проведение экспериментов, участие в обсуждении результатов.

Received 08.12.2022
Revised 19.07.2023
Accepted 22.07.2023

Статья поступила 08.12.2022 г.
Доработана 19.07.2023 г.
Принята к публикации 22.07.2023 г.

Porous Materials and Biomaterials
Пористые материалы и биоматериалы

UDC 504.06, 622.7, 628.31
https://doi.org/10.17073/1997-308X-2024-2-35-44

Research article
Научная статья

Removal of heavy metal ions from industrial (mining) wastewater using electromagnetically activated carbonaceous sorbent

A. S. Smolyanichenko ✉, E. V. Yakovleva

Don State Technical University
1 Gagarin Sqr., Rostov Region, Rostov-on-Don 344003, Russia

arpis-2006@mail.ru

Abstract. Mining wastewater, characterized by elevated salt levels, necessitates effective treatment to prevent contamination of underground and surface water. Traditional methods for treating large volumes of mining wastewater with high total dissolved solids are expensive, and cost-effective alternatives are limited. In this study, we propose a solution to this challenge: the sorption of dissolved substances using a carbonaceous sorbent derived from waste, specifically rice husk biochar. To enhance the sorbent's efficiency, we subjected it to electromagnetic activation, resulting in increased carbon content (from 43.3 to 78.5 % compared to the initial biochar), reduced impurities, and particle size reduction to the nanoscale (1–50 nm) with the formation of mesopores (mean diameter from the adsorption isotherm is 167 Å) and micropores (4.92 Å). This process contributes to improved compositional homogeneity. The effectiveness of the proposed sorbent was validated through the treatment of wastewater from Kirov Mine (Novoshakhtinsk, Rostov Region) under laboratory conditions. The removal rates for dissolved heavy metal ions (iron, zinc, manganese) were found to be 89, 84 and 26 %, respectively. A recommended two-stage sorption treatment involves: (1) static sorption using electromagnetically treated rice husk biochar at a concentration of 0.5 g/dm^3; (2) subsequent reagent treatment of the suspension (SKiF-180 reagent, 1.0 mg/dm^3), addition of potassium permanganate for manganese removal, settling for 30 min, and non-pressure filtration with a rice husk biochar filter.

Keywords: mining wastewater, water pollution, static sorption, dynamic sorption, industrial waste, rice husk, electromagnetic treatment, activator

Acknowledgements: This study was supported by the Innovation Promotion Fund (Russia). We express our gratitude to the Fund management for their financial support of the research and publication endeavors.

For citation: Smolyanichenko A.S., Yakovleva E.V. Removal of heavy metal ions from industrial (mining) wastewater using electromagnetically activated carbonaceous sorbent. *Powder Metallurgy and Functional Coatings*. 2024;18(2):35–44. https://doi.org/10.17073/1997-308X-2024-2-35-44

Очистка производственных сточных вод от ионов тяжелых металлов углеродным сорбентом с электромагнитной обработкой (на примере шахтных вод)

А. С. Смоляниченко, Е. В. Яковлева

Донской государственный технический университет
Россия, 344003, Ростовская обл., г. Ростов-на-Дону, пл. Гагарина, 1

arpis-2006@mail.ru

Аннотация. Загрязненная шахтная вода с большим количеством солей делает непригодными для хозяйственно-питьевых нужд подземные и поверхностные источники воды. В связи с необходимостью огромных затрат на очистку высокоминерализованных вод и недостаточной разработанностью дешевых технологий обезвреживания крупных объемов попытки очистить сбрасываемые или стекающие шахтные воды до безопасного уровня оказываются практически безрезультатными. В данной работе предложено одно из решений этой проблемы – сорбция растворенных в воде веществ на углеродсодержащем сорбенте, полученном из отходов производств. В качестве сорбционного углеродного материала применен биоуголь из плодовых оболочек зерен риса (рисовой соломы). Для наиболее эффективного действия сорбента выбран способ его подготовки электромагнитным методом в установке активации процессов, что позволило повысить содержание углерода в сорбенте с 43,3 до 78,5 % по сравнению с исходным биоуглем, снизить концентрации в нем примесей, а также измельчить его до 1–50 нм с образованием мезопор (средний диаметр по десорбции – 167 Å) и микропор (4,92 Å), тем самым улучшив однородность состава. Подтверждена эффективность полученного сорбента при обработке им сточных вод шахты им. Кирова (г. Новошахтинск, Ростовская обл.) в лабораторных условиях, в частности достигнуто снижение количества растворенных ионов тяжелых металлов – железа, цинка, марганца, на 89, 84 и 26 % соответственно. Рекомендована двухступенчатая сорбционная обработка шахтной воды: (1) сорбция в статических условиях с применением биоугля из плодовых оболочек зерен риса с электромагнитной обработкой дозой 0,5 г/дм^3; (2) последующая реагентная обработка полученной суспензии СКиФ-180 дозой 1,0 мг/дм^3, ввод перманганата калия с целью удаления содержащегося марганца, затем отстаивание в течение 30 мин в отстойных сооружениях и доочистка фильтрованием через безнапорный фильтр, загруженный биоуглем из рисовой соломы.

Ключевые слова: шахтные сточные воды, загрязнение водоемов, сорбция в статических условиях, сорбция в динамических условиях, отходы производств, плодовые оболочки зерен риса (рисовая солома), электромагнитная обработка, установка активации процессов

Благодарности: Исследования проведены за счет средств Фонда содействия инновациям (РФ). Выражаем благодарность руководству Фонда за финансовую поддержку научных изысканий и возможность публикации полученных результатов.

Для цитирования: Смоляниченко А.С., Яковлева Е.В. Очистка производственных сточных вод от ионов тяжелых металлов углеродным сорбентом с электромагнитной обработкой (на примере шахтных вод). *Известия вузов. Порошковая металлургия и функциональные покрытия*. 2024;18(2):35–44. https://doi.org/10.17073/1997-308X-2024-2-35-44

Introduction

Discharge of highly concentrated mining wastewater into the environment poses a significant hazard due its elevated levels of heavy metal ions, including iron, manganese, zinc, nickel and others, as well as high total dissolved solids (5.0–15.0 g/dm^3) [1; 2].

Groundwater contamination by heavy metal ions, such as soluble Fe^{2+} and Mn(II) compounds, further exacerbates the environmental impact. Russian environmental standards specify maximum allowable concentrations (MAC) for iron (0.3 mg/dm^3) and manganese (0.1 mg/dm^3) in drinking water [3; 4].

It is essential to recognize that the treatment of mine wastewater is a multifaceted process. The initial stage involves mechanical treatment, including clarification, filtration, and the separation of solid particles through centrifugal forces. Subsequent stages encompass chemical processes (coagulation, flocculation, sorption, neutralization, decontamination), physical treatments (ultrasonic, UV, magnetic exposure), and biological treatments [5; 6]. A mandatory step in the treatment of mine and quarry wastewater involves decontamination through chemical methods (ozonation) and physical methods (UV) before discharge into the environment [7–9].

This study proposes a sorption process for removing heavy metal ions dissolved in wastewater. The process utilizes a carbonaceous sorbent derived from agro-industrial waste and subjected to electromagnetic treatment. The suggested solution can be applied in mining wastewater treatment plants.

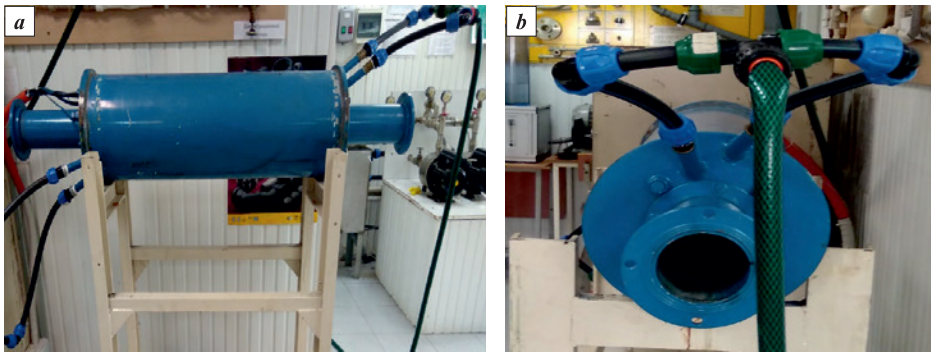

Fig. 1. The activator
a – general view, ***b*** – body

Рис. 1. Установка активации процессов
a – общий вид, ***b*** – рабочий корпус

Materials and methods

We utilized biochar derived from rice husks (rice straw) as the carbonaceous sorbent. This biochar was produced by carbonizing pre-washed rice husks in a muffle furnace at 600 °C for 30 min, followed by treatment in an activator (Fig. 1). A portion of the biochar was then mixed in distilled water, transferred to a non-magnetic cylinder containing ferromagnetic particles with a weight of m = 200 g, and subjected to a rotating electromagnetic field for 30 s within the activator. Subsequently, it was dried in a desiccator for 4 h at t = 105 °C (Fig. 2).

The rotation of ferromagnetic particles in the electromagnetic field induces a magnetostrictive effect, leading to the reduction of oxides on the particle surface. This process results in an increase in the carbon content of the sorbent from 43.3 to 78.5 %, as compared to the initial biochar, and a reduction in impurities, including silicon, from 8.2 to 2.1 % (refer to Table 1).

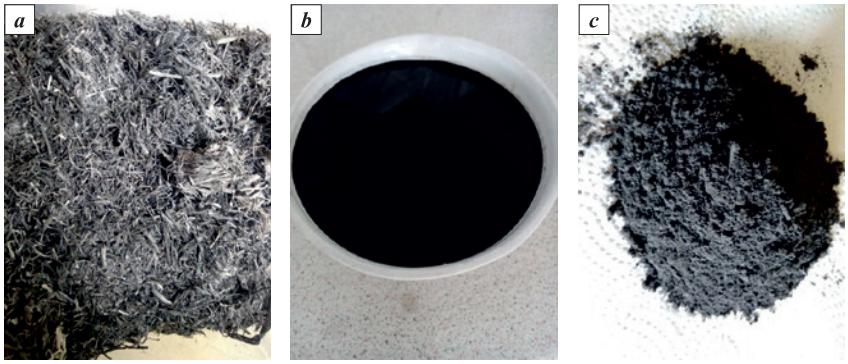

Fig. 2. The sorbent at each stage of preparation
a – after carbonization of the initial fruit shells of rice grains in a muffle furnace at t = 600 °C;
b – after processing in the PAU; ***c*** – after drying in an oven at t = 105 °C

Рис. 2. Внешний вид сорбента на разных стадиях подготовки
a – после карбонизации исходных плодовых оболочек зерен риса в муфельной печи при t = 600 °C;
b – после обработки в УАП; ***c*** – после просушивания в сушильном шкафу при t = 105 °C

Table 1. **Chemical composition of rice husk biochar samples with and without electromagnetic activation**

Таблица 1. **Химический состав полученных образцов биоугля из плодовых оболочек зерен риса с электромагнитной обработкой и без нее**

Sorbent sample	Content, wt. %									
	C	O	Si	K	Ca	Mg	Na	Cl	Fe	Al
Original biochar	43.3	42.5	8.2	1.0	1.1	0.9	0.4	0.1	–	2.7
After electromagnetic activation	78.5	18.5	2.1	0.5	0.1	0.1	0.1	–	0.1	–

The alterations in the chemical composition of biochar stem from various processes occurring within the activator. The increase in carbon content can be attributed to the disruption of intermolecular bonds [10]. Additionally, the interaction of SiO_2 with ferromagnetic particles leads to the formation of chemical compounds on their surface layer, resulting in a reduction in silicon content [11]. The activation process not only pulverizes the sorbent into the nanoscale range (1–50 nm) but also generates mesopores (with a mean diameter of 167 Å) and micropores (4.92 Å) while enhancing the homogeneity of the composition. Following the preparation of the carbonaceous sorbent as described above, we assessed its effectiveness for mining wastewater treatment under laboratory conditions.

Table 1 presents the properties of the initial biochar derived from rice husks and the biochar following electromagnetic activation *1*.

We conducted thermogravimetric analysis (TGA) of the sorbent, and the summarized results are provided below:

Ash content, %	35.8
Moisture content, %	Not found
Specific surface area, m^2/g	7.45
The relative volume of pores up to 900 Å in dia., cm^3/g	0.034
Average mesopore diameter from the adsorption isotherm, Å	196
Micropore volume, cm^3/g	0.0026
Average micropore diameter, Å	4.08
Iodine adsorption, %	24
Methylene blue adsorption, %	None

The sorbent sample, post-activation, underwent calcination at $t = 450$ °C for 3 h. During this process, its color transitioned from black to brown, and there was a slight reduction in volume. The observed 0.7 % loss upon heating to 450 °C suggests the potential presence of a minimal amount of moisture absorbed during sample preparation. Given the requirement for a very small sample size (less than 20 mg) in thermal analysis, even a minor influence from ambient air moisture during sample preparation could impact the results. Upon heating to 500 °C, the calcined sample experienced almost negligible weight loss. In the temperature range of 500 to 688 °C, a weight loss of approximately 3.3 % occurred, as indicated by the endothermic effect in the DSC curve (Fig. 3).

The observed process is likely analogous to transformations occurring at $t = 620 \div 685$ °C, involving the release of chemically bound moisture and some

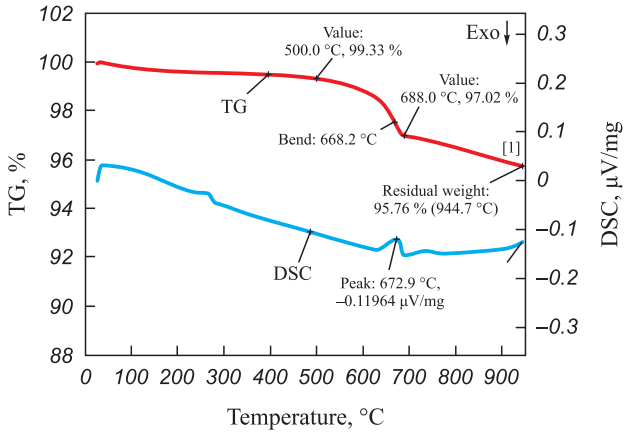

Fig. 3. TGA derivatogram of the sorbent sample *1*

Рис. 3. Дериватограмма термогравиметрического анализа образца *1* приготовленного сорбента

organic volatiles. Continued heating to 950 °C led to a gradual decline in the rate of weight loss. The residual weight at 950 °C was determined to be 95.76 %. Notably, the TGA curve does not reach a plateau, indicating ongoing decomposition of the sample.

In this study, the wastewater sourced from the Kirov mine (Novoshakhtinsk, Rostov Region) was employed. The mine generates an estimated daily volume of approximately 40,000 m^3 of wastewater, which is pumped from the mine and directed to the primary settling basin for the removal of suspended solids. Despite undergoing clarification, the treated wastewater remains unsuitable for discharge into the environment, leading to the imposition of environmental pollution penalties.

An illustration of the mine wastewater composition post-treatment at the existing treatment plant is provided in Table 2. Notably, this composition does not adhere to the stipulated environmental requirements [12; 13].

Our investigation encompassed both the steady-state and dynamic reduction of dissolved heavy metal ion concentrations, specifically iron, manganese, copper, and zinc, under laboratory conditions. In static conditions, a fluid element remains stationary relative to the sorbent particle, indicating that they move together. Conversely, in dynamic conditions, the fluid element moves relative to the sorbent particle, with the absorbed substance present in a mobile liquid phase that is filtered through the sorbent layer.

Condition 1. Static sorption conditions:

– introduction of rice husk biochar, subjected to electromagnetic treatment, into the original mine wastewater at various amounts (0.1; 0.3; 0.5; 0.7 and 1.0 g/dm^3), followed by mixing in a flocculator at 45 rpm for 30 min;

Table 2. **Composition of mine wastewater before and after treatment at the existing water treatment plant**

Таблица 2. **Состав шахтных вод до и после существующей водоочистки**

Mine wastewater	Concentration of contaminants, mg/dm^3									pH	Total hardness, mg eq/L
	Suspended solids	Dissolved oxygen	Chloride ions	Sulfate ions	Total iron	Ca^{2+} ions	Mg(II) ions	BOD_5	Petroleum products		
Original	52	11.58	443	2805	3.5	386	320	17.5	0.06	7.7	40.1
After treatment	28	10.63	252	2641	0.95	362	309	2.5	0.04	7.9	40.1
Environmental requirements*	0.75	4.0	350	500	0.3	3.5	20	20	0.3	6.5–8.5	–

* Standard values for recreational water and water bodies in populated areas [12; 13].

– treatment of the resulting suspension with the SKiF-180 reagent, consisting of aluminum polyoxychloride as the coagulant and polydiallyldimethylammonium chloride (PolyDADMAC) as the cationic flocculant, at a dosage of 1.0 mg/dm^3. This treatment involves stirring for 2 min at 200 rpm and an additional 10 min at 45 rpm;

– allowing the wastewater to settle for 30 min to facilitate coagulation;

– filtration through a quartzite pressure filter.

Condition 2. Dynamic sorption conditions (filtration):

– treatment of the initial wastewater with the SKiF-180 reagent (1.0 mg/dm^3) through stirring for 2 min at 200 rpm and an additional 10 min at 45 rpm;

– settling the wastewater for 30 min to induce coagulation;

– filtration through a non-pressure filter containing rice husk biochar particles sized 1–3 mm.

Results and discussion

All mine drainage samples collected during testing were analyzed by a certified laboratory, following standard test procedures for total iron (PND F 14.1:2:4.50-96), manganese (PND F 14.1:2:61-96), copper (PND F 14.1:2:4.48-96), and zinc (PND F 14.1:2:4.60-96). The laboratory employed a UNICO 1201 spectrophotometer (UNITED PRODUCTS & INSTRUMENTS, USA).

Table 3 presents the concentrations of the mentioned chemical elements in mining wastewater after static sorption using rice husk biochar (condition *1*). A notable reduction in iron ion concentration, ranging from 44 to 89 % compared to the initial concentration, was observed. The optimal treatment efficiency was achieved at a sorbent concentration of 0.5 g/dm^3. The largest decrease in zinc ion content, by 84 %, resulted in a concentration of 0.059 mg/dm^3. A marginal drop (4–26 %) in manganese ion concentration occurred when 0.3, 0.7 and 1.0 g/dm^3 of the sorbent were added, while in other cases, the concentration increased. Therefore, it is recommended to oxidize manganese using potassium permanganate. To remove 1.0 mg of Mn(II), 1.88 mg of $KMnO_4$ is required. As the initial copper ion concentration in the wastewater is below the rated threshold, evaluating copper removal efficiency is not feasible.

Fig. 4 depicts concentration curves illustrating the variation of controlled chemical elements (iron, manganese, zinc, and copper) in relation to the amount of sorbent (rice husk biochar after electromagnetic treatment).

Throughout the tests, we monitored the following parameters:

– redox potential, serving as an indicator of the substance's ability to accept or donate electrons (oxidation-reduction capability);

– total dissolved solids, quantifying the amount of salts dissolved in water, measured using a TDS-3 meter, and pH levels.

The summarized results of these measurements are presented in Table 4 and visually represented in Fig. 5.

It is established that when a certain critical threshold of the hydrogen ion concentration (pH) is reached, doubly and triply charged simple and hydrolyzed cations react to form practically or poorly soluble metal hydroxides [14]. However, the measured pH values fall within the range of 6.15 to 6.39, indicating a neutral environment. The total dissolved solids (TDS) range from 258 to 271 mg/dm^3, which falls within the category

Table 3. **Results of mining wastewater treatment under Condition *1***

Таблица 3. **Результаты испытаний обработки шахтных сточных вод в режиме *1***

Property	Initial mining wastewater	Wastewater after sorbent treatment, g/dm³ (Removal efficiency, %)					
		0	0.1	0.3	0.5	0.7	1.0
Total iron, mg/dm³	36.47 ± 3.65	22.82 ± 2.28 (37 %)	20.34 ± 2.03 (44 %)	18.88 ± 1.89 (48 %)	**3.99 ± 0.60 (98 %)**	17.92 ± 1.79 (51 %)	11.46 ± 1.715 (69 %)
Manganese, mg/dm³	5.619 ± 1.124	5.288 ± 1.058 (6 %)	7.356 ± 1.471 (–)	4.150 ± 0.83 (26 %)	6.047 ± 1.209 (–)	4.321 ± 0.864 (23 %)	5.386 ± 1.077 (4 %)
Copper, mg/dm³	0.012 ± 0.002	0.007 ± 0.002 (42 %)	0.008 ± 0.002 (33 %)	0.023 ± 0.005 (–)	0.016 ± 0.003 (–)	0.011 ± 0.002 (8 %)	0.012 ± 0.002 (–)
Zinc, mg/dm³	0.376 ± 0.128	0.177 ± 0.060 (53 %)	0.064 ± 0.022 (83 %)	0.185 ± 0.063 (51 %)	**0.059 ± 0.02 (84 %)**	0.147 ± 0.05 (61 %)	0.153 ± 0.052 (59 %)

of low TDS, resembling potable water conditions [15]. Notably, these TDS values exhibit independence from the amount of sorbent used. Given these findings, it can be inferred that a broader range of values for pH and TDS may be necessary to establish a relationship with the amount of sorbent.

Upon introducing the coagulant (SKiF-180 reagent with pH = 0.5÷3.0), the redox potential shifts from negative to positive, signifying a transition from reducing to oxidizing water properties. With an increase in sorbent quantity, the water's oxidizing properties intensify. However, at a biochar dose of 0.5 mg/dm³, the redox potential decreases from +108 to +50 mV. This reduction is attributed to the decline in iron concentration at this specific sorbent quantity (Fig. 5).

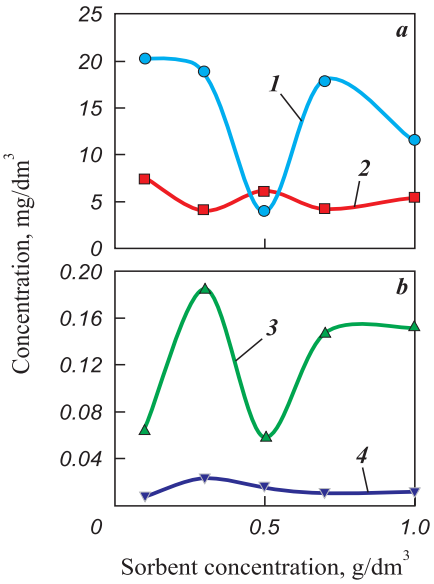

Fig. 4. Concentrations of iron and manganese (***a***), zinc and copper (***b***) ions vs. sorbent amount

1 – Fe, ***2*** – Mn, ***3*** – Cu, ***4*** – Zn

Рис. 4. Зависимости концентрации ионов железа и марганца (***a***), цинка и меди (***b***) от количества введенного сорбента

1 – Fe, ***2*** – Mn, ***3*** – Cu, ***4*** – Zn

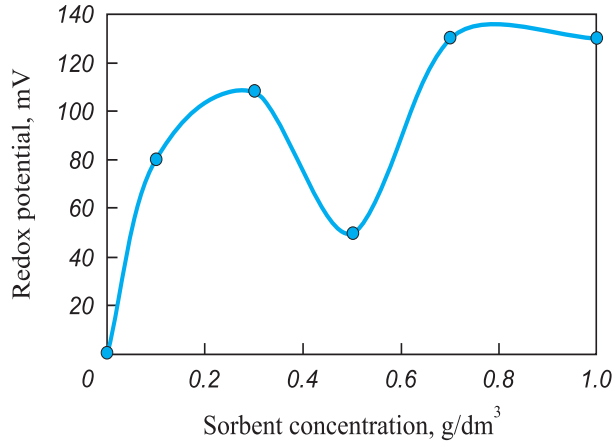

Fig. 5. Redox potential of water vs. sorbent amount

Рис. 5. Зависимость ОВП обрабатываемой воды от количества введенного сорбента

Table 4. **Results of mining wastewater treatment under Condition *1***

Таблица 4. **Результаты контроля параметров среды после обработки в режиме *1***

Property	Initial mining wastewater	Wastewater after sorbent treatment, g/dm³					
		0	0.1	0.3	0.5	0.7	1.0
pH	6.76	6.35	6.39	6.30	6.35	6.15	6.20
TDS, mg/dm³	267	278	258	262	271	266	262

Using iron as an example, we calculated its removal efficiency (E, %) and the sorption capacity of the sorbent (A, mg/g) using the following formulas:

$$A = \frac{(C_0 - C)V}{m}, \quad (1)$$

where C_0 and C are the initial and equivalent concentrations of iron, mg/dm^3; V is the volume of the adsorbate volume, dm^3; m is the weight of the sorbent, g;

$$E = \frac{C_0 - C}{C_0} \cdot 100\ \%, \quad (2)$$

where C_0 and C are the iron concentrations in the initial and treated wastewater, mg/dm^3.

The results of these calculations are presented in Table 5.

Based on these computations, we generated curves illustrating the sorption capacity and iron removal efficiency as functions of the amount of sorbent (Fig. 6).

The results from tests conducted under Condition *2* are presented in Table 6. The most effective removal was observed for divalent iron, with an efficiency of 98 %, leading to a residual concentration of 0.6 mg/dm^3. While this slightly exceeds the maximum allowable concentration, it suggests that a two-stage sorption process may be advisable. Manganese removal efficiency from the initial mining wastewater reached 52.07 %, meeting the maximum allowable concentration of 5.619 mg/dm^3 (actual concentration: 2.693 mg/dm^3). As the copper concentration in the initial wastewater is below the threshold, evaluating copper removal efficiency is not feasible.

Analyzing the obtained data, the following observations can be made. After coagulating the initial wastewater with the acidic SKiF-180 reagent (pH = 0.5÷3.0), the redox potential of the solution changes its sign from "–" to "+", indicating oxidizing properties. The pH value of the water experiences a slight change from 6.76 to 6.35, remaining within the rated range. Following filtration, the redox potential further increases from +73 to +215, along with a rise in the pH value (8.47), corresponding to a slightly alkaline environment.

As previously mentioned, the optimal sorbent amount for iron and zinc removal is 0.5 mg/dm^3.

***Table 5.* Sorption capacity and iron removal efficiency vs. sorbent amount**

***Таблица 5.* Определение сорбционной емкости и эффективности удаления железа в зависимости от количества введенного сорбента**

Property	Sorbent concentration, g/dm^3				
	0.1	0.3	0.5	0.7	1.0
Sorption capacity, mg/g	161.3	58.63	64.96	17.92	11.46
Removal efficiency, %	44.23	48.23	89.06	50.87	68.58

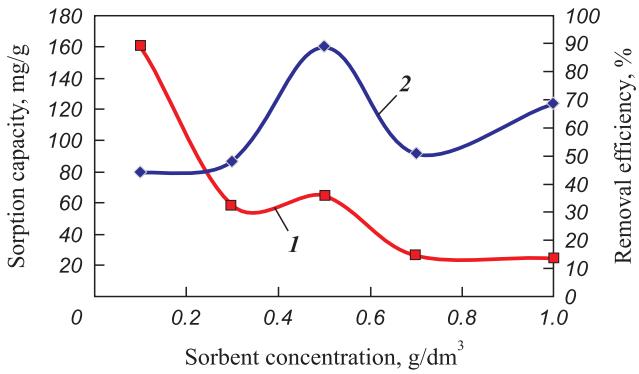

Fig. 6. Sorption capacity (***1***) and iron removal efficiency (***2***) vs. sorbent amount

Рис. 6. Зависимости сорбционной емкости (***1***) и эффективности удаления (***2***) железа от количества введенного сорбента

Table 6.* Results of mining wastewater treatment under Condition *2

Таблица 6.* Результаты испытаний обработки шахтных сточных вод в режиме *2

Property	Initial mining wastewater	Rated concentrations, mg/dm^3	Coagulation (SKiF-180 reagent) D = 1.0 mg/dm^3	Filtration through the sorbent	Removal efficiency, %
Total iron, mg/dm^3	36.47 ± 3.65	0.3	22.82 ± 2.28	0.60 ± 0.09	98.35
Manganese, mg/dm^3	5.619 ± 1.124	0.1	5.288 ± 1.058	2.693 ± 0.539	52.07
Copper, mg/dm^3	0.012 ± 0.002	1.0	0.007 ± 0.002	0.020 ± 0.004	–
Zinc, mg/dm^3	0.376 ± 0.128	5.0	0.177 ± 0.060	0.181 ± 0.062	50.68
Redox potential	–0.07	–	+073	+215	–
pH	6.76	–	6.35	8.47	–
TDS, mg/dm^3	267	–	278	262	–

However, when increased to 0.7 mg/dm^3, the efficiency of biochar sharply decreases. Iron removal efficiency drops from 89.06 to 50.86 % (Fig. 4, *a* and Fig. 6), and zinc removal efficiency drops from 84.31 to 60.9 % (Fig. 4, *b*). A similar drop in zinc removal efficiency is observed with increasing sorbent dose in the 0.1 to 0.3 mg/dm^3 range. This phenomenon might be attributed to a reduction in the effective specific surface area accessible to metal ions due to overlapping or aggregation of adsorption centers, thereby increasing the diffusion path length for these ions [16]. This aggregation tends to increase with the weight of the sorbent. Another plausible explanation is that a higher quantity of sorbent provides more active adsorption centers, causing them to remain unsaturated after adsorption [17–19].

Using equation (2), we estimated the removal efficiency for iron, manganese, copper, and zinc under static conditions using rice husk biochar as the sorbent in a range of concentrations, followed by electromagnetic treatment in condition *1* and filtration in condition *2* (Fig. 7).

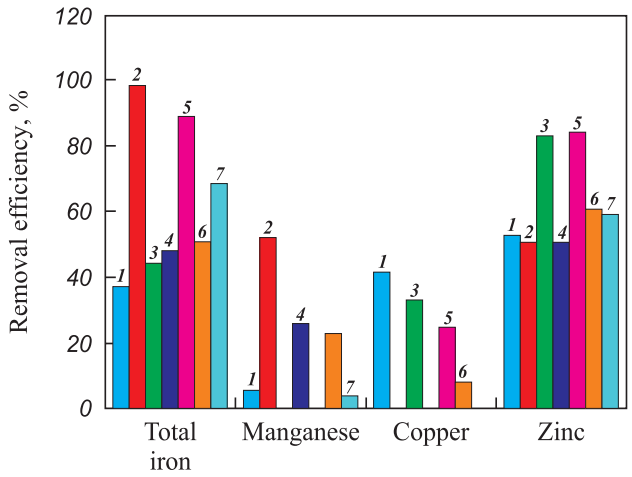

Fig. 7. Removal efficiency at different stages of mining wastewater treatment in two treatment conditions

1 – coagulation of SKiF 1.0 mg/dm^3 (condition *2*);
2 – dynamic sorption (condition *2*);
3 – static sorption, *D* = 0.1 mg/dm^3 (condition *1*);
4 – static sorption, *D* = 0.3 mg/dm^3 (condition *1*);
5 – static sorption, *D* = 0.5 mg/dm^3 (condition *1*);
6 – static sorption, *D* = 0.7 mg/dm^3 (condition *1*);
7 – static sorption, *D* = 1.0 mg/dm^3 (condition *1*)

Рис. 7. Эффективность удаления химических элементов на разных этапах обработки шахтных вод в 2 режимах очистки

1 – коагуляция СКиФ 1,0 мг/дм^3 (режим *2*);
2 – динамическая сорбция (режим *2*);
3 – статическая сорбция, Д = 0,1 мг/дм^3 (режим *1*);
4 – статическая сорбция, Д = 0,3 мг/дм^3 (режим *1*);
5 – статическая сорбция, Д = 0,5 мг/дм^3 (режим *1*);
6 – статическая сорбция, Д = 0,7 мг/дм^3 (режим *1*);
7 – статическая сорбция, Д = 1,0 мг/дм^3 (режим *1*)

Conclusions

In summary, the following conclusions can be drawn.

1. The proposed electromagnetic activation of rice husk biochar [20] demonstrates efficiency in treating mining wastewater under laboratory conditions.

2. The sorbent exhibits a chemical composition that is comparable to activated carbon, widely utilized in water treatment, affirming the applicability of the sorbent in water treatment plants.

3. To optimize the efficiency of mining wastewater treatment, we recommend a two-stage sorption process: static sorption utilizing electromagnetically treated rice husk biochar at a concentration of 0.5 g/dm^3 (Table 3) (Stage 1), followed by reagent treatment of the suspension (SCiF-180 reagent, 1.0 mg/dm3), addition of potassium permanganate for manganese removal, settling for 30 min, and non-pressure filtration with a rice husk biochar filter (dynamic sorption, Stage 2).

4. Implementation of this process in mining wastewater treatment facilities is anticipated to reduce the concentrations of dissolved heavy metal ions, particularly iron, zinc, and manganese, below the maximum allowable concentrations, enabling the discharge of treated water into the environment.

References / Список литературы

1. Wright I.A., Paciuszkiewicz K., Belmer N. Increased water pollution after closure of Australia's longest operating underground coal mine: a 13-month study of mine drainage. *Water Chemistry and River Ecology Water. Air Soil Pollut*. 2018;229(55):1–20. https:/doi.org/10.1007/s11270-018-3718-0
2. Phuong T.D., Vu C.D. Mine water treatment in Hongai coal mines. *E3S Web of Conf.* 2018;35(01007):1–5. https://doi.org/10.1051/e3sconf/20183501007
3. Arefieva O.D., Shapkin N.P., Gruschakova N.V., Prokuda N.A. Mine water: Chemical composition and treatment. *Water Practice and Technology*. 2016;11(3):540–546. https:/doi.org/10.2166/wpt.2016.060
4. Kulikova A.A., Sergeeva Yu.A., Ovchinnikova T.I., Xabarova E.I. Formation of mine water composition and analysis of treatment methods. *MIAB. Mining informational and analytical bulletin*. 2020;7:135–145. (In Russ.). https:/doi.org/10.25018/0236-1493-2020-7-0-135-145

   Куликова А.А., Сергеева Ю.А., Овчинникова Т.И., Хабарова Е.И. Формирование шахтных вод и анализ способов их очистки MIAB. *Горный информационно-аналитический бюллетень*. 2020;(7):135–145. https:/doi.org/10.25018/0236-1493-2020-7-0-135-145
5. Maksimovich N.G., Pyankov S.V., Khayrulina E.A. Environmental assessment of closeded coal mine territory using G1S analysis. *Mine Water and Circular Economy Mine Water and Circular Economy*. 2017;212–217.
6. Tarasenko I.A., Zin`kov A.V. Assessment of the environmental safety of the underground water basin during

the closure of the mines of Primorsky Krai (on the example of the Lipovetskaya mine). *Mining informational and analytical bulletin*. 2013;2:362–373. (In Russ.).

Тарасенко И.А., Зиньков А.В. Оценка экологической безопасности подземного водного бассейна при закрытии шахт Приморского края (на примере шахты «Липовецкая»). *Горный информационно-аналитический бюллетень*. 2013;2:363–373.

7. Budykina T.A. Treatment of wastewater resulting from iron ore beneficiation. *Magazine of Civil Engineering*. 2018;6(82):163–169. (In Russ.). https:/doi.org/10.18720/MCE.82.15

   Будыкина Т.А. Очистка сточных вод обогащения железных руд. *Инженерно-строительный журнал*. 2018;6(82):163–169. https:/doi.org/10.18720/MCE.82.15
8. Gubina N.A., Ylesin M.A., Karmanovskaya N.V. Ways to increase the productivity and quality of mine water treatment. *Journal of Environmental Management and Tourism*. 2018;9(3):423–427. https://doi.org/10.14505//jemt.v9.3(27).03
9. Stavitskaya S.S., Goba V.E., Petrenko T.P., Kovtun M.F., Kartel' N.T. Industrial wastewater treatment using modified anthracite and other carbon sorbents. *Khimiya tverdogo topliva*. 2003;2:56–62. (In Russ.).

   Ставицкая С.С., Гоба В.Е., Петренко Т.П., Ковтун М.Ф., Картель Н.Т. Очистка производственных сточных вод с использованием модифицированных антрацитов и других углеродных сорбентов. *Химия твердого топлива*. 2003;2:56–62.
10. Rempel' A.A., Valeeva A.A. Materials and methods of nanotechnology. Yekaterinburg: UrFU, 2015. 136 p. (In Russ.).

    Рempель А.А., Валеева А.А. Материалы и методы нанотехнологий. Екатеринбург: Изд-во УрФУ, 2015. 136 с.
11. Serzhanov G.M., Shevko V.M., Lavrov B.A., Amanov D.D. Thermodynamic modeling of silicon reduction from aluminum oxide. *Mezhdunarodnyi zhurnal prikladnykh i fundamental'nykh issledovanii*. 2015;11(2): 161–166. (In Russ.). https://applied-research.ru/ru/article/view?id=7698 (accessed: 03.03.2024).

    Сержанов Г.М., Шевко В.М., Лавров Б.А., Аманов Д.Д. Термодинамическое моделирование восстановления кремния из оксида алюминием. *Международный журнал прикладных и фундаментальных исследований*. 2015;11(2):161–166. https://applied-research.ru/ru/article/view?id=7698 (дата обращения: 03.03.2024).
12. Sanitary norms and rules 2.1.3684-21 "Sanitary and epidemiological requirements for the maintenance of territories of urban and rural settlements, for water bodies, drinking water and drinking water supply, atmospheric air, soils, residential premises, operation of industrial, public premises, organization and conduct of sanitary and anti-epidemic (preventive) measures", 2021. (In Russ.). URL: https://www.rospotrebnadzor.ru/files/news/SP2.1.3684-21_territorii.pdf (accessed: 01.02.2023).

    СанПиН 2.1.3684-21 «Санитарно-эпидемиологические требования к содержанию территорий городских и сельских поселений, к водным объектам, питьевой воде и питьевому водоснабжению, атмосферному воздуху, почвам, жилым помещениям, эксплуатации производственных, общественных помещений, организации и проведению санитарно-противоэпидемических (профилактических) мероприятий», 2021. URL: https://www.rospotrebnadzor.ru/files/news/SP2.1.3684-21_territorii.pdf (дата обращения: 01.02.2023).
13. Hygienic standards 2.1.5.1315-03 Maximum permissible concentrations (MPC) of chemicals in the water of water bodies of economic and drinking and cultural and domestic water use. Moscow: Ministry of Health of Russia, 2003. (In Russ.). URL: https://files.stroyinf.ru/Data1/41/41363/index.htm (accessed: 01.02.2023).

    ГН 2.1.5.1315-03 Предельно допустимые концентрации (ПДК) химических веществ в воде водных объектов хозяйственно-питьевого и культурно-бытового водопользования. М.: Минздрав России, 2003. URL: https://files.stroyinf.ru/Data1/41/41363/index.htm (дата обращения: 01.02.2023).
14. Vigdorovich V.I., Tsygankova L.E., Protasov A.S. Features of sorption purification of aqueous solutions from heavy metal cations. Message 1. Media with non-hydrolyzable anion. *Vestnik TGU*. 2013;(1):401–404. (In Russ.).

    Вигдорович В.И., Цыганкова Л.Е., Протасов А.С. Особенности сорбционной очистки водных растворов от катионов тяжелых металлов. Сообщение 1. Среды с негидролизующимся анионом. *Вестник ТГУ*. 2013;18(1):401–404.
15. Sanitary norms and rules 2.1.4.1175-02 Hygienic requirements for the quality of non-centralized water supply. Sanitary protection of sources, 2003. (In Russ.). URL: https://files.stroyinf.ru/Data2/1/4294845/4294845751.pdf (accessed: 01.02.2023).

    СанПиН 2.1.4.1175-02 Гигиенические требования к качеству воды нецентрализованного водоснабжения. Санитарная охрана источников, 2003. URL: https://files.stroyinf.ru/Data2/1/4294845/4294845751.pdf (дата обращения: 01.02.2023).
16. Li Y., Xia B., Zhao Q., Liu F., Zhang P., Du Q., Wang D., Li D., Wang Z., Xia Y. Removal of copper ions from aqueous solution by calcium alginate immobilized kaolin. *Journal Environmental Science*. 2011;23(3):404–411. https://doi.org/10.1016/s1001-0742(10)60442-1
17. Raji C., Anirudhan T.S. Kinetics of Pb (II) adsorption by polyacrylamide grafted sawdust. *Indian Journal of Chemical Technology*. 1997;4:157–162.
18. Hayrapetyan S.S., Hayrapetyan M.S. A Method for evaluating the sorption capacity of the sorbents. *International Journal of modern engineering research (IJMER)*. 2017;7(6):48–55.
19. Naumenko K., Frolova N., Petrusha O., Chepel N. The method of determination of the sorption capacity of activated carbon by gas chromatography. *Eureka: Life Sciences*. 2017;(1):12–18. https://doi.org/10.21303/2504-5695.2017.00290
20. Smolyanichenko A.S. Physical and chemical properties of silver-containing nanosorbent obtained from rice straw biochar. *Agriculture*. 2023;13(7):1288. https://doi.org/10.3390/agriculture13071288

Information about the Authors

Alla S. Smolyanichenko – Cand. Sci. (Eng.), Associate Professor, Water Supply and Disposal Department, Don State Technical University
ORCID: 0000-0002-1664-2986
E-mail: arpis-2006@mail.ru

Elena V. Yakovleva – Postgraduate Student, Senior Lecturer, Water Supply and Disposal Department, Don State Technical University
ORCID: 0000-0002-5255-1598
E-mail: ananas199021@yandex.ru

Сведения об авторах

Алла Сергеевна Смоляниченко – к.т.н., доцент кафедры «Водоснабжение и водоотведение», Донской государственный технический университет
ORCID: 0000-0002-1664-2986
E-mail: arpis-2006@mail.ru

Елена Вячеславовна Яковлева – аспирант, ст. преподаватель кафедры «Водоснабжение и водоотведение», Донской государственный технический университет
ORCID: 0000-0002-5255-1598
E-mail: ananas199021@yandex.ru

Contribution of the Authors

A. S. Smolyanichenko – research guidance; main concept, goals, and objectives; conclusions.

E. V. Yakovleva – data acquisition, primary data analysis and processing.

Both authors contributed equally to the manuscript and are responsible for any plagiarism, self-plagiarism, or other unethical issues.

Вклад авторов

А. С. Смоляниченко – руководство исследованием, постановка основной концепции, целей и задач исследования, формулировка выводов.
Е. В. Яковлева – сбор данных для исследования, анализ полученных первичных данных, обработка результатов исследований.

Оба автора в равной степени участвовали в написании рукописи, и несут ответственность при обнаружении плагиата, самоплагиата или других неэтических проблем.

Received 23.03.2023
Revised 29.05.2023
Accepted 05.06.2023

Статья поступила 23.03.2023 г.
Доработана 29.05.2023 г.
Принята к публикации 05.06.2023 г.

Modification of Surface Including Charged Particle Beams and Photon and Plasma Fluxes
Модифицирование поверхности, в том числе пучками заряженных частиц, потоками фотонов и плазмы

UDC 621.793.184
https://doi.org/10.17073/1997-308X-2024-2-45-52

Research article
Научная статья

Effects of ion-plasma treatment temperature of the aluminium coating on the structure and phase composition of the VT6 titanium alloy

A. A. Nikolaev, A. Yu. Nazarov, E. L. Vardanyan, V. R. Mukhamadeev

Ufa University of Science and Technology
32 Zaki Validi Str., Ufa 450076, Russia

alex.nkv8@gmail.com

Abstract. In this study, we studied the effects of aluminum coating treatment temperature on the microstructure and phase composition when applied to a VT6 titanium alloy substrate within a low-pressure arc discharge plasma environment. The ion-plasma treatment was conducted at 450 and 500 °C, employing argon shielding, while the aluminum coating was deposited using the vacuum-arc process, resulting in a coating thickness of ~3 μm. Microstructural analysis was performed using a scanning electron microscope, and the structural and phase composition were examined using *X*-ray diffraction (XRD) imaging in symmetric imaging mode with CuK_α radiation. Our findings demonstrate that the application of the aluminum coating initiates the formation of a near-surface α-stabilized layer, extending up to 2.5 μm in thickness due to the heat generated during the ion cleaning process. Subsequent ion-plasma treatment further results in the development of a $TiAl_3$ intermetallide site, reaching thicknesses of up to 1.5 μm, while the α-stabilized region expands to 5.5 μm. Higher temperatures during the treatment process contribute to an increase in the thickness of these aforementioned layers and also lead to the emergence of an intermediate TiAl intermetallic layer.

Keywords: ion-plasma treatment, intermetallide coatings, gradient coatings, titanium alloys

Acknowledgements: This research received support from the Russian Science Foundation under Grant No. 22-29-01463, https://rscf.ru/project/22-29-01463/.

For citation: Nikolaev A.A., Nazarov A.Yu., Vardanyan E.L., Mukhamadeev V.R. Effects of ion-plasma treatment temperature of the aluminium coating on the structure and phase composition of the VT6 titanium alloy. *Powder Metallurgy and Functional Coatings*. 2024;18(2):45–52. https://doi.org/10.17073/1997-308X-2024-2-45-52

Влияние температуры ионно-плазменной обработки алюминиевого покрытия на микроструктуру и фазовый состав титанового сплава ВТ6

А. А. Николаев, А. Ю. Назаров, Э. Л. Варданян, В. Р. Мухамадеев

Уфимский университет науки и технологий
Россия, 450076, г. Уфа, ул. Заки Валиди, 32

alex.nkv8@gmail.com

Аннотация. Представлены результаты исследования влияния температуры обработки поверхности алюминиевого покрытия на титановом сплаве ВТ6 в плазме дугового разряда низкого давления на микроструктурные и фазовые изменения. Ионно-плазменную обработку проводили в плазме дугового разряда низкого давления при температурах 450 и 500 °С в среде аргона. Алюминий наносили вакуумно-дуговым методом, толщина покрытия составляла ~3 мкм. Микроструктурные изменения

исследовали с помощью растровой электронной микроскопии. Структурно-фазовый состав определяли по результатам расшифровки дифрактограмм, полученных при симметричной съемке в CuK_α-излучении. Показано, что после нанесения алюминиевого покрытия в результате нагрева при ионной очистке формируется приповерхностный α-стабилизированный слой толщиной до 2,5 мкм. Последующая ионно-плазменная обработка приводит к формированию интерметаллидной области $TiAl_3$ толщиной до 1,5 мкм, α-стабилизированная область увеличивается до 5,5 мкм. Выявлено, что повышение температуры обработки приводит как к увеличению толщины указанных выше областей, так и к появлению промежуточной интерметаллидной зоны TiAl.

Ключевые слова: ионно-плазменная обработка, интерметаллидные покрытия, градиентные покрытия, титановые сплавы

Благодарности: Работа выполнена при поддержке Российского научного фонда в рамках гранта № 22-29-01463, https://rscf.ru/project/22-29-01463/.

Для цитирования: Николаев А.А., Назаров А.Ю., Варданян Э.Л., Мухамадеев В.Р. Влияние температуры ионно-плазменной обработки алюминиевого покрытия на микроструктуру и фазовый состав титанового сплава ВТ6. *Известия вузов. Порошковая металлургия и функциональные покрытия*. 2024;18(2):45–52. https://doi.org/10.17073/1997-308X-2024-2-45-52

Introduction

Titanium and its alloys fnd extensive application in the aerospace industry and medicine [1–3]. However, their wear resistance is low, with most titanium friction parts being susceptible to diffusion interaction between the contact surfaces and subsequent wear [4; 5]. There is a demand to enhance the wear resistance of titanium alloys.

One efficient approach to achieve this enhancement is through ion nitriding [6–8] and alloying [9; 10] of the surface layer, as well as applying coatings [11–13]. In the case of titanium alloys, ion nitriding requires high temperatures and extended holding periods [14; 15], while the low-temperature process [16; 17] proves to be less efficient. The application of coatings enables to create super-hard films on surfaces based on nitrides, carbides, and oxides of transition metal [18–20]. However, these coatings may experience delamination when subjected to impacts [21; 22], inevitably leading to accelerated surface wear, intensified by detached coating particles.

Gradient coatings made from alloys with high impact resistance and resistance to aggressive media show better performance due to the absence of a distinct substrate-coating interface. In steel products, a combination of nitriding and coating (Duplex Treatment) is commonly employed [23; 24]. However, the application of duplex treatment to titanium alloys does not improve performance. In this scenario, the nitrided layer exhibits significantly lower hardness and depth compared to the same treatment time and temperature.

Titanium forms intermetallic compounds with various metals, and these compounds typically have enhanced physical and mechanical properties compared to pure titanium and its non-hardened alloys. Ti–Al intermetallides have a low specific gravity (3.3–4.2 g/cm^3) and show high hardness, heat resistance, oxidation resistance, and corrosion resistance. Some aerospace applications of this material have been reported by Lazurenko D. et al. [25]. Nevertheless, due to the high brittleness, particularly the $TiAl_3$ phase, intermetallides are unsuitable for manufacturing solid parts. Zhang Y. et al. [26], Liu Y. [27], and Parlikar C. [28] have investigated the application processes and resulting intermetallide coatings, reporting a significant increase in strength (up to 20 %) and wear resistance for coating thicknesses less than 16 μm.

Currently, primary Ti–Al intermetallic coating technologies include aluminizing [29], magnetron [30], and vacuum-arc [31] sputtering, as well as laser [32] and electron-beam [33] surfacing, ion implantation [34], often combined with subsequent heat treatment [35–37]. It is, however, challenging to control the phase composition of the resulting layers during coating deposition and ion implantation. When aluminum and/or Ti–Al coatings are deposited, followed by heat treatment at the aging temperature of the titanium alloy, the final coating consists only of the $TiAl_3$ phase. Subsequent ion-plasma treatment can intensify the formation of the TiAl and Ti_3Al intermetallides, which are more ductile compared to $TiAl_3$.

Our study focuses on a combination of vacuum-arc deposition used to create pure aluminum coatings, followed by plasma treatment with low-pressure non-self-powered arc discharges. The objective of this study is to analyze the effects of the ion-plasma treatment temperature on the aluminum coating on the structure and phase changes of the VT6 titanium alloy surface layers.

Materials and methods

We prepared samples in the form of 20 mm diameter disks, each measuring 4 mm in thickness, obtained from a titanium bar (VT6 alloy). The combined treatment involved two stages. In the initial stage, we deposited a pure aluminum layer, approximately 3 μm thick,

onto the surface of the titanium disk using vacuum arc deposition. The sample surface underwent an initial ion cleaning process in an Ar plasma (40 A discharge current, 800 V bias voltage) for 30 min, raising the surface temperature to 450 °C. Then it was exposed to Al plasma for 1 min, generated by a 60 A arc evaporator current. We monitored the surface temperature using a chromel-copel thermocouple and an AST250+ IR pyrometer (Accurate Sensors Technologies, India). In the second stage, the surface was treated in a PINK plasmatron with an incandescent cathode (ISE, Russia) [38] for 1 h under argon shielding. The bias voltage varied depending on the temperature, but the discharge current was always 50 A. We processed the samples at both 450 and 500 °C. Then the samples were vacuum-cooled in argon atmosphere at 1 Pa.

Following the treatment, we examined polished section structure of the samples using a Mira scanning electron microscope (Tescan, Czech Republic) operating in the secondary electron mode. For *X*-ray diffraction analysis (XRD), we used an Ultima IV diffractometer (Rigaku, Japan) with CuK_α-radiation in the symmetrical imaging mode.

Results and discussion

To investigate the interaction between the aluminum coating and the VT6 titanium substrate, we examined how the ion-plasma treatment temperature influenced changes in the structure and phase composition of the surface layers. Following the deposition of the aluminum coating onto the rough substrate surface (Fig. 1, *a*, *b*), an α-stabilized region I, approximately 2.5 ± 0.5 μm deep, is formed within the near-surface layer of the substrate. This formation results from the diffusion of the coating elements during the initial stage of deposition when the surface of the titanium alloy is still heated to 450–470 °C. The α-stabilized region can be distinguished from the substrate due to the dissolution of small recrystallized β-particles

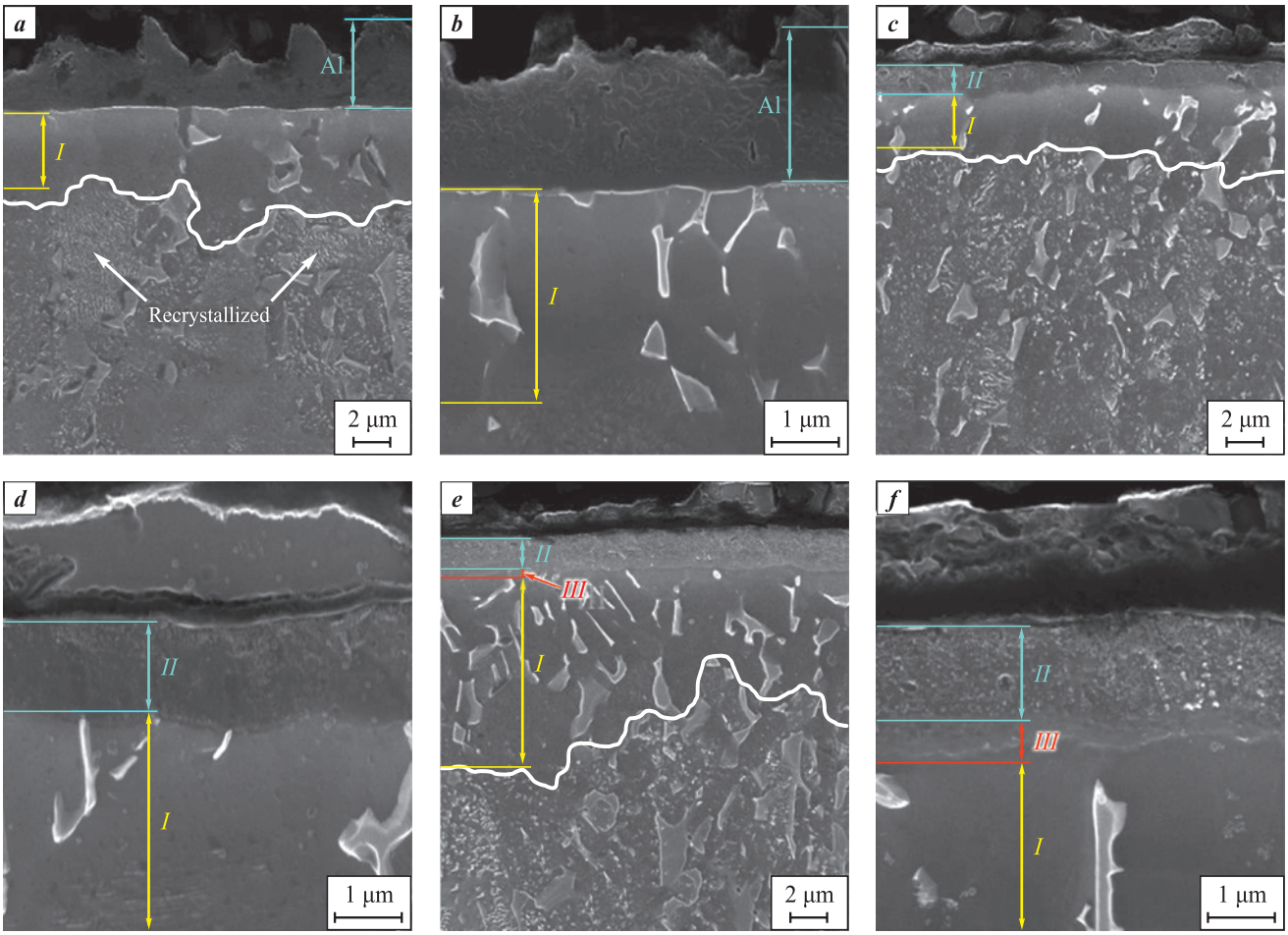

Fig. 1. Polished section structures of the aluminum-coated titanium samples
a, ***b*** – initial coating; ***c***–***f*** – after ion-plasma treatment at 450 (***c***, ***d***) and 500 °C (***e***, ***f***)

Рис. 1. Изображения структуры поперечного сечения образцов титана с покрытием из алюминия
a, ***b*** – исходное покрытие; ***c***–***f*** – после ионно-плазменной обработки при 450 (***c***, ***d***) и 500 °C (***e***, ***f***)

within the α-grains, a consequence of aluminum diffusion deep into the surface layer, and the α-phase stabilization facilitated by the presence of Al, which is known to be an α-stabilizing element.

The ion-plasma treatment conducted at 450 °C (Fig. 1, *c*, *d*) also led to the formation of an intermetallic site comprising the $TiAl_3$ phase with a high aluminum content. The total length of the modified site increased to 5 ± 0.5 μm. Plasma etching reduced the thickness of the aluminum coating to ~2 μm. The coating became brittle, as evidenced from its fracturing during our sample section polishing. This brittleness can be attributed to the presence of the brittle $TiAl_3$ intermetallic phase and its large volume concentration in the surface layers. Elevating the temperature to 500 °C resulted in the emergence of a transition layer between the substrate and layer *III* (Fig. 1, *e*, *f*). This transition layer, as reported by Ramos A. et al. [35] and Garbacz H. et al. [36], primarily consists of the TiAl intermetallide. As indicated by the gradient of aluminum concentration, the layer above it consists mainly of the $TiAl_3$ phase, while the layer below it comprises Ti_3Al.

This assumption finds confirmation in the XRD analysis, as depicted in Fig. 2. The surface layers following treatment at 450 °C mostly contain the $TiAl_3$ intermetallide. No aluminum peaks were detected, possibly due to the low Al concentration in the surface layer of the coating. Additionally, aside from the intermetallic phases, a solid solution forms as aluminum substitutes into the titanium lattice, evidenced by the shift of titanium peaks towards larger diffraction angles, signifing a decrease in the lattice period. As the treatment temperature increased to 500 °C, the TiAl intermetallide was found in the surface layers, while no Ti_3Al peaks were observed. The intensity and number of the $TiAl_3$ phase grew, which correlates with the observed microstructure changes.

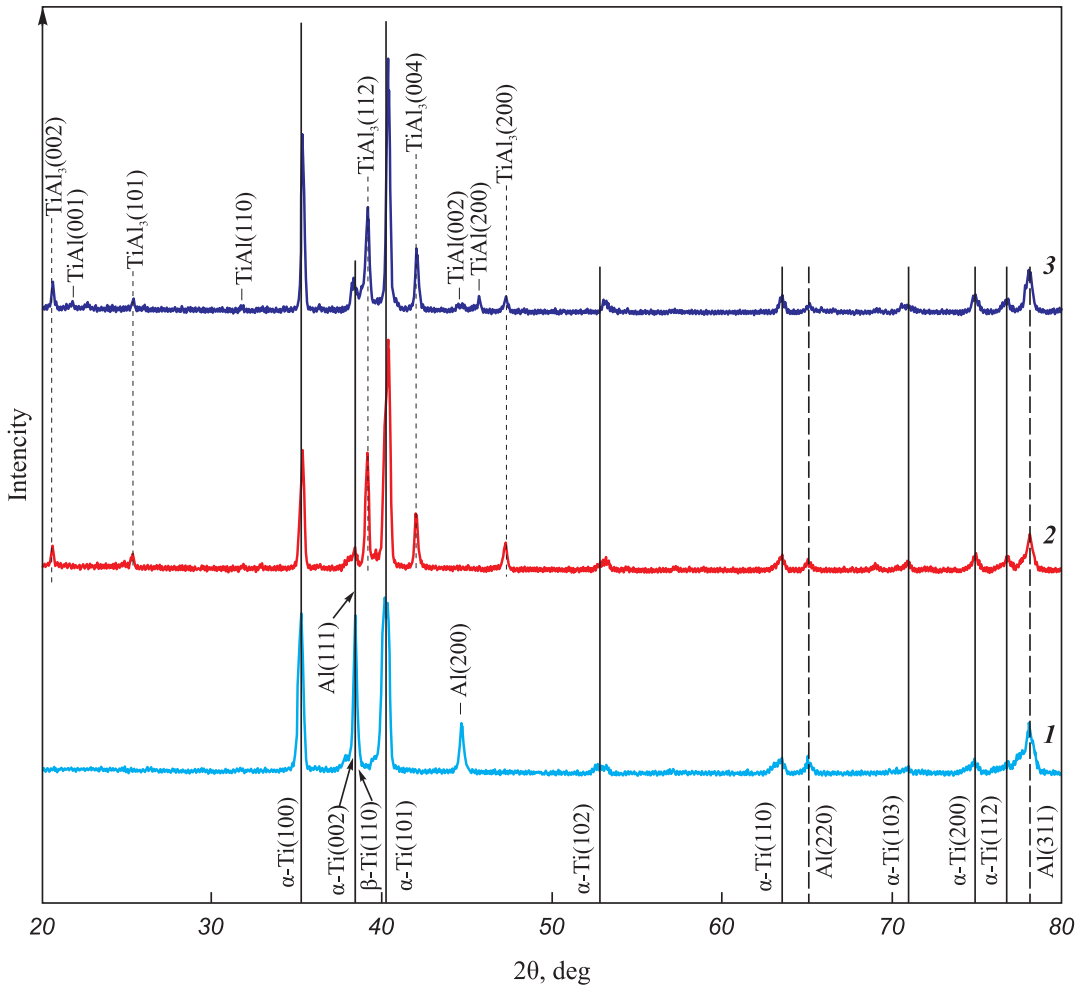

Fig. 2. XRD images of the samples

1 – initial coating; ***2*** and ***3*** – after ion-plasma treatment at 450 (***2***) and 500 °C (***3***)

Рис. 2. Дифрактограммы исследуемых образцов

1 – исходное покрытие; ***2*** и ***3*** – после ионно-плазменной обработки при 450 (***2***) и 500 °C (***3***)

Given the inherent brittleness of the coatings, we intend to explore the impact of ion-plasma treatment duration and the thickness of the initial aluminum coating on the elemental and phase compositions, as well as the wear resistance of these coating layers.

Conclusion

We conducted experimental investigations on intermetallic surface layers created through the deposition of an aluminum coating onto a titanium substrate, followed by low-pressure non-self-sustained gas plasma treatment.

Our findings reveal that such treatment results in the development of intermetallic and α-stabilized layers within the near-surface layer of the VT6 titanium alloy. Treatment at 450 °C yields an intermetallic layer, approximately 1.5 μm thick, composed only of the $TiAl_3$ phase. Raising the temperature to 500 °C leads to the formation of an additional TiAl intermetallide layer, measuring 300 nm in thickness, situated beneath the 1.8 μm thick $TiAl_3$ layer. Importantly, XRD analysis does not detect any Ti_3Al peaks.

The creation of the α-stabilized layer commences during the deposition of the aluminum coating itself. As the ion-plasma temperature increases, the layer's thickness increases as well, attributed to the accelerated diffusion rate of aluminum into the titanium substrate.

References / Список литературы

1. Pavlova T.V., Kashapov O.S., Nochovnaya N.A. Titanium alloys for gas turbine engines. *Vse materialy. Entsiklopedicheskiy spravochnik*. 2012;5:8–14. (In Russ.).

   Павлова Т.В., Кашапов О.С., Ночовная Н.А. Титановые сплавы для газотурбинных двигателей. *Все материалы. Энциклопедический справочник*. 2012;5:8–14.
2. Khorev A.I. Fundamental and applied work on structural titanium alloys and promising areas of their development. *Trudy VIAM*. 2013;2:4. (In Russ.).

   Хорев А.И. Фундаментальные и прикладные работы по конструкционным титановым сплавам и перспективные направления их развития. *Труды ВИАМ*. 2013;2:4.
3. Pawlak W., Kubiak K.J., Wendler B.G., Mathia T.G. Wear resistant multilayer nanocomposite WC_{1-x}/C coating on Ti–6Al–4V titanium alloy. *Tribology International*. 2015;82(B):400–406. https://doi.org/10.1016/j.triboint.2014.05.030
4. Bansal D.G., Eryilmaz O.L., Blau P.J. Surface engineering to improve the durability and lubricity of Ti–6Al–4V alloy. *Wear*. 2011;271(9-10):2006–2015. https://doi.org/10.1016/j.wear.2010.11.021
5. Xing Y.Z., Wang G., Zhang Y., Chen Y.N., Dargusch M. Development in plasma surface diffusion techniques of Ti–6Al–4V alloy: A review. *The International Journal of Advanced Manufacturing Technology*. 2017;92(5):1901–1912. https://doi.org/10.1007/s00170-017-0302-5
6. Ahmadeev Yu.Kh, Goncharenko I.M., Ivanov Yu.F., Koval' N.N., Shchanin P.M. Nitriding of commercially pure titanium in a glow discharge with a hollow cathode. *Pis'ma v zhurnal tekhnicheskoi fiziki*. 2005;31(13):24–30. (In Russ.).

   Ахмадеев Ю.Х., Гончаренко И.М., Иванов Ю.Ф., Коваль Н.Н., Щанин П.М. Азотирование технически чистого титана в тлеющем разряде с полым катодом. *Письма в журнал технической физики*. 2005;31(13):24–30.
7. Koval' N.N., Shchanin P.M., Akhmadeev Yu.Kh., Lopatin I.V., Kolobov Yu.R., Vershinin D.S., Smolyakova M.Yu. Influence of the composition of the plasma-forming gas on the nitriding process in a non-self-sustained glow discharge with a large hollow cathode. *Poverhnost'. Rentgenovskie, sinhrotronnye i nejtronnye issledovaniya*. 2012;(2):62–67. (In Russ.).

   Коваль Н.Н., Щанин П.М., Ахмадеев Ю.Х., Лопатин И.В., Колобов Ю.Р., Вершинин Д.С., Смолякова М.Ю. Влияние состава плазмообразующего газа на процесс азотирования в несамостоятельном тлеющем разряде с полым катодом большого размера. *Поверхность. Рентгеновские, синхротронные и нейтронные исследования*. 2012;(2):62–67.
8. Denisov V.V., Akhmadeev Yu.Kh., Denisova Yu.A., Ivanov Yu.F., Koval' N.N., Ostroverkhov E.V., Shchanin P.M. Nitriding of titanium VT1-0 in constant and pulsed modes of combustion of a non-self-sustained glow discharge with a titanium hollow cathode. *Izvestiya vysshikh uchebnykh zavedeniy. Fizika*. 2017; 60(10-2):44–48. (In Russ.).

   Денисов В.В., Ахмадеев Ю.Х., Денисова Ю.А., Иванов Ю.Ф., Коваль Н.Н., Островерхов Е.В., Щанин П.М. Азотирование титана ВТ1-0 в постоянном и импульсном режимах горения несамостоятельного тлеющего разряда с титановым полым катодом. *Известия высших учебных заведений. Физика*. 2017;60(10-2):44–48.
9. Ryabchikov A.I., Sivin D.O., Bozhko I.A., Stepanov I.B., Shevelev A.E. Microstructure of titanium alloy modified by high-intensity implantation of low-and high-energy aluminium ions. *Surface and Coatings Technology*. 2020; 391:125722. https://doi.org/10.1016/j.surfcoat.2020.125722
10. Mikhailov V.V., Gitlevich A.E., Verkhoturov A.D., Mikhailyuk A.I., Belyakov A.V., Konevtsov L.A. Electrospark alloying of titanium and its alloys: The physical, technological, and practical aspects. Part I. The peculiarities of the mass transfer and the structural and phase transformations in the surface layers and their wear and heat resistance. *Surface Engineering and Applied Electrochemistry*. 2013;49(5):373–395. https://doi.org/10.3103/S1068375513050074
11. Mamaeva A., Kenzhegulov A., Panichkin A., Alibekov Z., Wieleba W. Effect of magnetron sputtering deposition

conditions on the mechanical and tribological properties of wear-resistant titanium carbonitride coatings. *Coatings*. 2022;12(2):193. https://doi.org/10.3390/coatings12020193

12. Walczak M., Pasierbiewicz K., Szala M. Adhesion and mechanical properties of TiAlN and AlTiN magnetron sputtered coatings deposited on the DMSL titanium alloy substrate. *Acta Physica Polonica: A*. 2019;136(2):294–298. https://doi.org/10.12693/APhysPolA.136.294
13. Lenivceva O.G., Bataev I.A., Golkovskiy M.G., Samoylenko V.V., Dostavalov R.A. Obtaining wear-resistant coatings on titanium alloys by non-vacuum electron beam processing. *Obrabotka metallov: Tekhnologiya, oborudovanie, instrumenty*. 2013;3(60):103–109. (In Russ.).

Ленивцева О.Г., Батаев И.А., Голковский М.Г., Самойленко В.В., Доставалов Р.А. Получение износостойких покрытий на титановых сплавах методом вневакуумной электронно-лучевой обработки. *Обработка металлов: Технология, оборудование, инструменты*. 2013;3(60):103–109.
14. Ramazanov K.N., Khayrullina I.Z., Kovalevich A.A. Formation of protective and hardening coatings on the surface of titanium alloys by ion nitriding. *Vestnik SGTU*. 2011;2(1(53)):96–101. (In Russ.).

Рамазанов К.Н., Хайруллина И.З., Ковалевич А.А. Формирование защитно-упрочняющих покрытий на поверхности титановых сплавов методом ионного азотирования. *Вестник СГТУ*. 2011;2(1(53)):96–101.
15. Belous V.A., Nosov G.I., Klimenko I.O. Hardening of titanium alloys by ion-plasma nitriding. *Voprosy atomnoy nauki i tekhniki*. 2017;5(111):75–82. (In Russ.).

Белоус В.А., Носов Г.И., Клименко И.О. Упрочнение титановых сплавов ионно-плазменным азотированием. *Вопросы атомной науки и техники*. 2017;5(111):75–82.
16. Vershinin D.S., Smolyakova M.Yu. Low-temperature nitriding of titanium in the plasma of a low-pressure non-self-sustained arc discharge. *Fizika i khimiya obrabotki materialov*. 2011;(5):15–20. (In Russ.).

Вершинин Д.С., Смолякова М.Ю. Низкотемпературное азотирование титана в плазме несамостоятельного дугового разряда низкого давления. *Физика и химия обработки материалов*. 2011;(5):15–20.
17. Farokhzadeh K., Edrisy A., Pigott G., Lidster P. Scratch resistance analysis of plasma-nitrided Ti–6Al–4V alloy. *Wear*. 2013;302(1-2):845–853. https://doi.org/10.1016/j.wear.2013.01.070
18. Vardanyan E.L., Ramazanov K.N., Nagimov R.S., Nazarov A.Y. Properties of intermetallic TiAl based coatings deposited on ultrafine grained martensitic steel. *Surface and Coatings Technology*. 2020;389:125657. https://doi.org/10.1016/j.surfcoat.2020.125657
19. Vereschaka A., Tabakov V., Grigoriev S., Sitnikov N., Milovich F., Andreev N., Bublikov J. Investigation of wear mechanisms for the rake face of a cutting tool with a multilayer composite nanostructured Cr–CrN–(Ti, Cr, Al, Si) N coating in high-speed steel turning. *Wear*. 2019;438:203069. https://doi.org/10.1016/j.wear.2019.203069
20. Pogrebnyak A.D., Kravchenko Ya.O., Bondar O.V., ZHollybekov B., Kupchishin A.I. Structural features and tribological properties of multilayer coatings based on refractory metals. *Fizikokhimiya poverhnosti i zashchita materialov*. 2018;54(2):152–172. (In Russ.).

Погребняк А.Д., Кравченко Я.О., Бондар О.В., Жоллыбеков Б., Купчишин А.И. Структурные особенности и трибологические свойства многослойных покрытий на основе тугоплавких металлов. *Физикохимия поверхности и защита материалов*. 2018;54(2):152–172.
21. Zhang H., Li Z., He W., Ma C., Liao B., Li Y. Mechanical modification and damage mechanism evolution of TiN films subjected to cyclic nano-impact by adjusting N/Ti ratios. *Journal of Alloys and Compounds*. 2019;809:151816. https://doi.org/10.1016/j.jallcom.2019.151816
22. Krella A.K. Degradation of protective PVD coatings. In: *Handbook of materials failure analysis with case studies from the chemicals, concrete and power industries*. Butterworth-Heinemann, 2016. P. 411–440. https://doi.org/10.1016/B978-0-08-100116-5.00016-8
23. Gronostajski Z., Kaszuba M., Widomski P., Smolik J., Ziemba J., Hawryluk M. Analysis of wear mechanisms of hot forging tools protected with hybrid layers performed by nitriding and PVD coatings deposition. *Wear*. 2019;(420):269–280. https://doi.org/10.1016/j.wear.2019.01.003
24. Grenadyorov A.S., Solovyev A.A., Oskomov K.V. The effect of duplex processing on the mechanical properties of grade 316L stainless steel. *Technical Physics Letters*. 2020;46(11):1060–1063. https://doi.org/10.1134/S106378502011005X

Гренадёров А.С., Соловьев А.А., Оскомов К.В. Воздействие дуплексной обработки на механические свойства нержавеющей стали марки 316L. *Письма в Журнал технической физики*. 2020;46(21):14–17.
25. Lazurenko D.V., Bataev I.A., Laptev I.S., Ruktuev A.A., Maliutina I.N., Golkovsky M.G., Bataev A.A. Formation of Ti–Al intermetallics on a surface of titanium by non-vacuum electron beam treatment. *Materials Characterization*. 2017;134: 202–212. https://doi.org/10.1016/j.matchar.2017.10.024
26. Zhang Y.B., Li H.X., Zhang K. Investigation of the laser melting deposited TiAl intermetallic alloy on titanium alloy. *Advanced Materials Research*. 2011;146:1638–1641. https://doi.org/10.4028/www.scientific.net/AMR.146-147.1638
27. Liu Y., Wang D., Deng C., Huo L., Wang L., Fang R. Novel method to fabricate Ti–Al intermetallic compound coatings on Ti–6Al–4V alloy by combined ultrasonic impact treatment and electrospark deposition. *Journal of Alloys and Compounds*. 2015;628:208–212. https://doi.org/10.1016/j.jallcom.2014.12.144
28. Parlikar C., Alam M.Z., Das D.K. Effect of Al_3Ti diffusion aluminide coating on tensile properties of a near α-Ti alloy. *Materials Science and Engineering: A*. 2011;530: 565–573. https://doi.org/10.1016/j.msea.2011.10.021
29. Kovtunov A.I., Khohlov Yu.Yu. The structure of coatings in the liquid-phase aluminizing of titanium. *Tekhnologiya*

metallov. 2021;(9):22–26. (In Russ.).
https://doi.org/10.31044/1684-2499-2021-0-9-22-26

Ковтунов А.И., Хохлов Ю.Ю. Структура покрытий при жидкофазном алитировании титана. *Технология металлов*. 2021;(9):22–26.
https://doi.org/10.31044/1684-2499-2021-0-9-22-26

30. Bauer P.P., Laska N., Swadźba R. Increasing the oxidation resistance of γ-TiAl by applying a magnetron sputtered aluminum and silicon based coating. *Intermetallics*. 2021;133:107177.
https://doi.org/10.1016/j.intermet.2021.107177
31. Zhang M., Shen M., Xin L., Ding X., Zhu, S., Wang F. High vacuum arc ion plating TiAl coatings for protecting titanium alloy against oxidation at medium high temperatures. *Corrosion Science*. 2016;112:36–43.
https://doi.org/10.1016/j.corsci.2016.07.005
32. Malyutina Yu.N., Si-Mohand Kh. Improvement of tribotechnical characteristics of titanium by laser cladding of γ-TiAl powder. In: *Electrical Engineering. Energy. Mechanical engineering: Collection of Scientific Works of the I International Scientific Conference of Young Scientists* (Novosibirsk, 02–06 December, 2014). Novosibirsk: Novosibirsk State Technical University, 2014. Part 3. P. 227–230. (In Russ.).

Малютина Ю.Н., Си-Моханд Х. Улучшение триботехнических характеристик титана путем лазерной наплавки порошка γ-TiAl. В сб.: *Электротехника. Энергетика. Машиностроение: Сборник научых трудов I Международной научной конференции молодых ученых* (г. Новосибирск, 02–06 декабря 2014 г.). Новосибирск: Новосибирский государственный технический университет, 2014. Ч. 3. С. 227–230.
33. Bataev I.A., Lazurenko D.V., Golkovskiy M.G., Laptev I.S., Chakin I.K., Ivanchik I.S. Surface alloying of titanium with aluminum using the method of non-vacuum electron-beam surfacing of powder mixtures. *Obrabotka metallov: Tekhnologiya, oborudovanie, instrumenty*. 2017;(1(74)):51–60. (In Russ.).

Батаев И.А., Лазуренко Д.В., Голковский М.Г., Лаптев И.С., Чакин И.К., Иванчик И.С. Поверхностное легирование титана алюминием с использованием метода вневакуумной электронно-лучевой наплавки порошковых смесей. *Обработка металлов: Технология, оборудование, инструменты*. 2017;(1(74)):51–60.
34. Nikonenko A.V., Popova N.A., Nikonenko E.L., Kalashnikov M.P., Oks E.M., Kurzina I.A. Influence of the aluminum ion implantation dose on the phase composition of submicrocrystalline titanium. *Vacuum*. 2021;189:110230.
https://doi.org/10.1016/j.vacuum.2021.110230
35. Ramos A.S., Calinas R., Vieira M.T. The formation of γ-TiAl from Ti/Al multilayers with different periods. *Surface and Coatings Technology*. 2006;200(22-23):6196–6200.
https://doi.org/10.1016/j.surfcoat.2005.11.023
36. Garbacz H., Pouquet J.M., García-Lecina E., Díaz-Fuentes M., Wieciński P., Martin R.H., Wierzchoń T., Kurzydlowski K.J. Microstructure, fatigue and corrosion properties of the Ti–Al intermetallic layers. *Surface and Coatings Technology*. 2011;205(19):4433–4440.
https://doi.org/10.1016/j.surfcoat.2011.03.072
37. Romankov S.E., Mukashev B.N., Ermakov E.L., Muhamedshina D.N. Structural formation of aluminide phases on titanium substrate. *Surface and Coatings Technology*. 2004;180:280–285.
https://doi.org/10.1016/j.surfcoat.2003.10.070
38. Koval' N.N., Ivanov Yu.F., Lopatin I.V., Akhmadeev Yu.Kh., Shugurov V.V., Krysina O.V., Denisov V.V. Generation of low-temperature gas-discharge plasma in large vacuum volumes for plasma-chemical processes. *Rossijskiy khimicheskiy zhurnal*. 2013;57(3-4):121–133. (In Russ.).

Коваль Н.Н., Иванов Ю.Ф., Лопатин И.В., Ахмадеев Ю.Х., Шугуров В.В., Крысина О.В., Денисов В.В. Генерация низкотемпературной газоразрядной плазмы в больших вакуумных объемах для плазмохимических процессов. *Российский химический журнал*. 2013;57(3-4):121–133.

Information about the Authors

Alexey A. Nikolaev – Postgraduate Student, Department of Manufacturing Technology, Ufa University of Science and Technology
ORCID: 0000-0002-2584-4790
E-mail: alex.nkv8@gmail.com

Almaz Yu. Nazarov – Cand. Sci. (Eng.), Senior Lecturer, Department of Manufacturing Technology, Ufa University of Science and Technology
ORCID: 0000-0002-4711-4721
E-mail: nazarov_almaz15@mail.ru

Eduard L. Vardanyan – Dr. Sci. (Eng.)
ORCID: 0000-0001-7047-6459

Vener R. Mukhamadeev – Senior Lecturer, Department of Mechanical Engineering and CAD, Ufa University of Science and Technology
ORCID: 0000-0002-2018-4877
E-mail: vener_muhamadeev@mail.ru

Сведения об авторах

Алексей Александрович Николаев – аспирант кафедры технологии машиностроения, Уфимский университет науки и технологий (УУНиТ)
ORCID: 0000-0002-2584-4790
E-mail: alex.nkv8@gmail.com

Алмаз Юнирович Назаров– к.т.н., старший преподаватель кафедры технологии машиностроения, УУНиТ
ORCID: 0000-0002-4711-4721
E-mail: nazarov_almaz15@mail.ru

Эдуард Леонидович Варданян– д.т.н.
ORCID: 0000-0001-7047-6459

Венер Рифкатович Мухамадеев– старший преподаватель кафедры механики и цифрового проектирования, УУНиТ
ORCID: 0000-0002-2018-4877
E-mail: vener_muhamadeev@mail.ru

Contribution of the Authors

A. A. Nikolaev – conceptualization, paper authoring, conclusions.

A. Yu. Nazarov – testing, paper authoring, paper proofreading, conclusion review.
E. L. Vardanyan – problem formulation, overall supervision.

V. R. Mukhamadeev – test preparation, testing, provision of equipment.

Вклад авторов

А. А. Николаев – формирование основной концепции, подготовка текста, формулировка выводов.
А. Ю. Назаров – проведение испытаний образцов, подготовка текста статьи, корректировка текста, корректировка выводов.
Э. Л. Варданян – постановка цели и задачи исследования, научное руководство.
В. Р. Мухамадеев – подготовка эксперимента, руководство проведением эксперимента, обеспечение ресурсами.

Received 30.12.2022
Revised 29.05.2023
Accepted 31.05.2023

Статья поступила 30.12.2022 г.
Доработана 29.05.2023 г.
Принята к публикации 31.05.2023 г.

Modification of Surface Including Charged Particle Beams and Photon and Plasma Fluxes
Модифицирование поверхности, в том числе пучками заряженных частиц, потоками фотонов и плазмы

UDC 621.785.4
https://doi.org/10.17073/1997-308X-2024-2-53-60

Research article
Научная статья

Formation of ceramic coating on VAL10 aluminum alloy surface via laser modification in polysilicate solution

D. G. Kalyuzhnyi[1, 2], M. V. Palabugin[1], I. N. Burnyshev[2], V. F. Lys[2], V. I. Ladyanov[2]

[1] **Kalashnikov Izhevsk State Technical University**
7 Studencheskaya Str., Izhevsk 426069, Russia
[2] **Udmurt Federal Research Center, Ural Branch of Russian Academy of Sciences**
34 Tatyany Baramzinoi Str., Izhevsk 426067, Russia

dikdik@mail.ru

Abstract. This article presents the results of an experimental study on the physical and mechanical properties of the surface layer of the VAL10 aluminum alloy after pulsed laser treatment, conducted in a bath with an aqueous solution of polysilicates (PS) at various concentrations. Ceramic coatings were produced on specimens measuring 10×10×3 mm. The laser processing of aluminum alloy specimens was carried out using an Nd:YAG laser. The study demonstrates that the quality of the resulting surface and its properties can vary depending on the laser exposure parameters, the concentration of the polysilicate solution, and the overall processing technique. The scattering of radiation by the PS solution layer leads to a significant reduction in surface roughness. In specimens processed in ambient air, the crater sizes on the surface exceeded 400 μm, while for specimens processed in a PS solution, they did not exceed 100 μm. A comparative analysis of the impact of solution concentration on elemental composition was performed. The study also included an investigation of friction characteristics and the measurement of microhardness of the modified surface. The research revealed that surface hardening processes occur as a result of the treatment, associated with the filling of recesses with high-strength oxides. This enabled the creation of a mixture containing silicon carbide and aluminum oxide in the surface layer of the specimens. Furthermore, wear tests of the modified surface were conducted using a “ball–specimen” tribological coupling. Specimens subjected to laser irradiation in a PS solution demonstrated increased wear resistance (a 40 % reduction in wear) and a 30 % decrease in the friction coefficient. Additionally, an increase in microhardness was observed.

Keywords: aluminum alloy, laser modification, polysilicates (PS), ceramic coating, surface structure, microhardness

For citation: Kalyuzhnyi D.G., Palabugin M.V., Burnyshev I.N., Lys V.F., Ladyanov V.I. Formation of ceramic coating on VAL10 aluminum alloy surface via laser modification in polysilicate solution. *Powder Metallurgy and Functional Coatings*. 2024;18(2): 53–60. https://doi.org/10.17073/1997-308X-2024-2-53-60

Формирование керамического покрытия на поверхности алюминиевого сплава ВАЛ10 при лазерном модифицировании в растворе полисиликатов

Д. Г. Калюжный[1, 2], М. В. Палабугин[1], И. Н. Бурнышев[2], В. Ф. Лыс[2], В. И. Ладьянов[2]

[1] **Ижевский государственный технический университет им. М.Т. Калашникова**
Россия, 426069, г. Ижевск, ул. Студенческая, 7
[2] **Удмуртский федеральный исследовательский центр УрО РАН**
Россия, 426067, г. Ижевск, ул. Татьяны Барамзиной, 34

dikdik@mail.ru

Аннотация. Представлены результаты экспериментального исследования физико-механических свойств поверхностного слоя алюминиевого сплава ВАЛ10 после лазерного импульсного воздействия на структуру материала, проводимого в ванне с водным раствором полисиликатов (ПС) различной концентрации. Покрытия формировались на образцах размером 10×10×3 мм. Лазерная обработка образцов алюминиевого сплава была произведена с использованием Nd:YAG-лазера. Показано, что качество формируемой поверхности и ее свойства могут меняться в зависимости от параметров лазерного воздействия, а также концентрации раствора полисиликатов и технологии процесса обработки в целом. Рассеяние излучения слоем раствора ПС приводит к существенному снижению шероховатости поверхности. Для образцов, обработанных на воздухе, размеры кратеров на поверхности составили более 400 мкм, а для образцов, обработанных в растворе ПС, они не превышали 100 мкм. Проведен сравнительный анализ влияния концентрации раствора на элементный состав. Исследованы фрикционные характеристики и измерена микротвердость модифицированной поверхности. Установлено, что в результате обработки протекают процессы упрочнения поверхности, связанные с заполнением углублений высокопрочными оксидами. Это позволило получить в поверхностном слое образцов смесь, содержащую карбид кремния и оксид алюминия. Проведены исследования износа модифицированной поверхности в трибосопряжении «шарик – образец». Для образцов, подвергнутых лазерному воздействию в растворе ПС, характерны повышение износостойкости (величина износа уменьшилась на 40 %) и снижение коэффициента трения на 30 %, также установлено увеличение микротвердости.

Ключевые слова: алюминиевый сплав, лазерное модифицирование, полисиликаты (ПС), керамическое покрытие, структура поверхности, микротвердость

Для цитирования: Калюжный Д.Г., Палабугин М.В., Бурнышев И.Н., Лыс В.Ф., Ладьянов В.И. Формирование керамического покрытия на поверхности алюминиевого сплава ВАЛ10 при лазерном модифицировании в растворе полисиликатов. *Известия вузов. Порошковая металлургия и функциональные покрытия*. 2024;18(2):53–60.
https://doi.org/10.17073/1997-308X-2024-2-53-60

Introduction

In modern mechanical engineering, the pursuit of reducing the weight of final products while maintaining high performance properties, such as strength and wear resistance, and achieving a high degree of process automation, is of major importance [1–3]. In this context, the surface hardening of aluminum alloys, known for their low density and high specific strength, holds great promise [4–9]. Nevertheless, one significant drawback of these materials is their low hardness [10; 11]. Surface hardening allows for an increase in the overall wear resistance of the part.

Various methods are currently available for surface hardening of metals and alloys [12], including thermal and chemical processes, spraying, shot blasting, and laser-based techniques [13]. Modern laser systems offer advantages such as high processing speed, precision, and the ability to finely adjust energy parameters and exposure duration within the processing zone [14].

Laser modification technologies for aluminum alloy surfaces, particularly laser alloying, have made significant progress in enhancing the corrosion resistance, mechanical durability, and resistance to adhesive and abrasive wear of aluminum alloys [15]. Fusion of alloying powders with the substrate using laser radiation is a promising method for creating protective coatings on aluminum alloys [16]. This process may involve the incorporation of both metals (e.g., Ni, Cr) and non-metals (e.g., B, Si) as dopants, with a binding element being introduced into the powder composition [17]. The resulting mixture is uniformly applied

to the substrate, and the surface is subsequently treated with a laser [18; 19]. t's crucial to note that the choice of components suitable for inclusion in the aluminum alloy's surface composition is limited, as they must have a melting point comparable to that of aluminum to ensure high-quality coating [20]. The use of other components often leads to a significant decrease in coating quality [21]. An alternative approach involves the introduction of alloying elements from the liquid phase. In this method, the part is immersed in a technological solution, and laser radiation, forming a vapor gas channel in the liquid, is directed onto the part's surface.

Recently, metal-ceramic composite materials with an aluminum-based matrix reinforced with refractory ceramic particles of silicon carbide (SiC) have been used [22]. Composite materials with an aluminum matrix are characterized by high specific strength combined with low density. Doping with silicon carbide particles allows for the creation of a material with a low coefficient of friction and high wear resistance [23].

The objective of this study is to investigate specific changes in the mechanical properties of ceramic coatings on an VAL10 aluminum alloy, produced using laser radiation in an aqueous polysilicate (PS) solution bath. Furthermore, we aim to determine the processing parameters that can enhance the microhardness of the surface layer and its abrasion resistance.

Materials and methods. Results and discussion

The most commonly used non-metallic dopant for aluminum alloys is silicon. Doping with silicon allows for the creation of a hypereutectic structure on the surface of hypoeutectic alloys while simultaneously increasing surface hardness. In this study, coatings were applied to 10×10×3 mm specimens of the VAL10 aluminum alloy. Surface laser processing was performed using a solid-state Nd:YAG laser with a radiation wavelength of 1.06 μm, integrated into the LIS-25 laser welding system (EIKTL Lagen LLC, Russia). Each laser pulse had a maximum energy of 25 J, a pulse duration of 5 ms, and a repetition rate of 3 Hz. During the processing, the specimen was immersed in a bath containing an aqueous solution of $(Na_2O)_n \cdot (SiO_2)_m$ polysilicate. The concentration of the polysilicate solution was experimentally determined to be in the range of 10–15 %. A higher concentration of polysilicate led to the release of gas bubbles from the medium, which significantly reduced the efficiency of laser radiation delivery to the specimen's surface and caused pronounced splashing of the polysilicate solution. On the other hand, a lower concentration resulted in a noticeable decrease in the silicon content within the coating (Fig. 1).

The layer of the liquid medium above the processed specimen's surface was consistently maintained at a 1 mm thickness. Reference specimens were also prepared and treated in both air and distilled water. Due to the scattering of radiation by the layer of PS solution positioned above the specimen's surface, the surface irregularities were significantly reduced.

As a result, for specimens treated in ambient air, crater sizes on the surface exceeded 400 μm, whereas when a PS solution was used, the exposure marks did not exceed a 100 μm diameter (Fig. 2).

The layer created by laser processing on the metal surface enhances the part's durability and performance. Laser processing of the aluminum alloy results in the redistribution of chemical elements throughout the depth of the material. The craters formed on the surface become filled with silicon and aluminum compounds. The chemical composition of the specimens was analyzed using a JAMP-10 S Auger analyzer (JEOL, Japan). The shape of the Auger lines indicated that aluminum exists in an oxidized state, while carbon and silicon are in the carbide state (Fig. 3).

The size and relative positioning of the surface recesses are determined by the processing mode and the concentration of the PS solution. The absence of crater overlap prevents complete coverage of the surface, leading to discontinuities in the ceramic layer. In untreated areas, the base metal remains exposed, resulting in a heterogeneous ceramic coating layer.

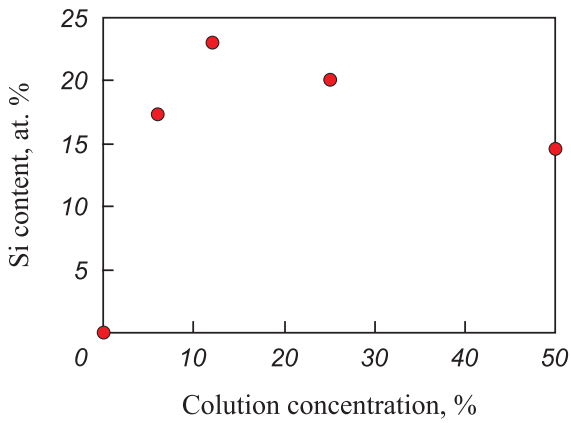

Fig. 1. Relationship between the silicon content in the coating at a depth of 3 nm and the concentration of the polysilicate solution

Рис. 1. Содержание кремния в покрытии на глубине 3 нм в зависимости от концентрации раствора полисиликата

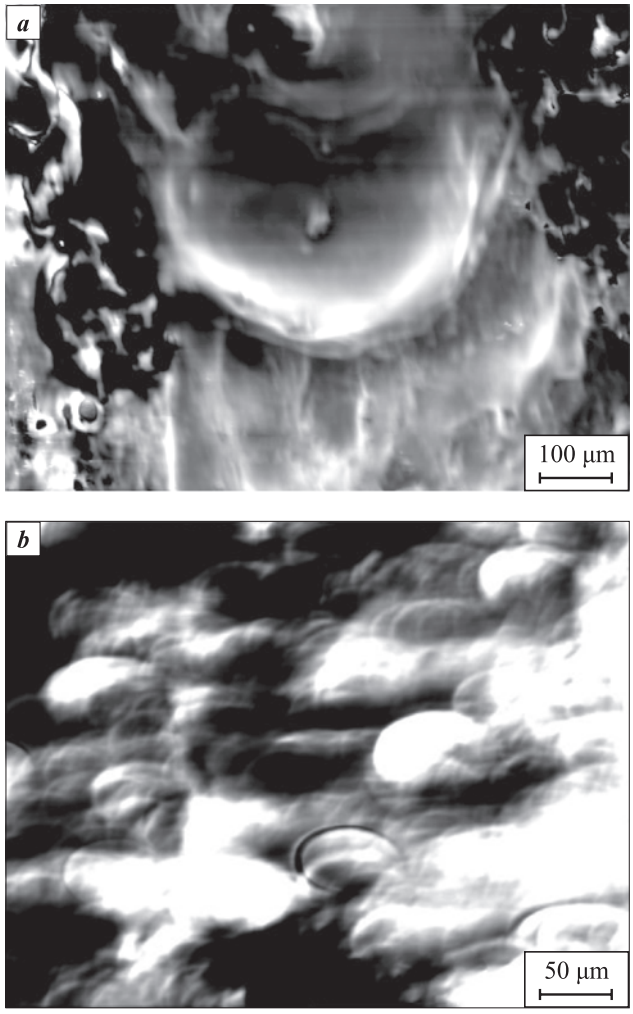

Fig. 2. Surface images of specimens treated in air (***a***) and in a polysilicate solution (***b***)

Рис. 2. Изображения поверхности образцов, обработанных на воздухе (***a***) и в растворе ПС (***b***)

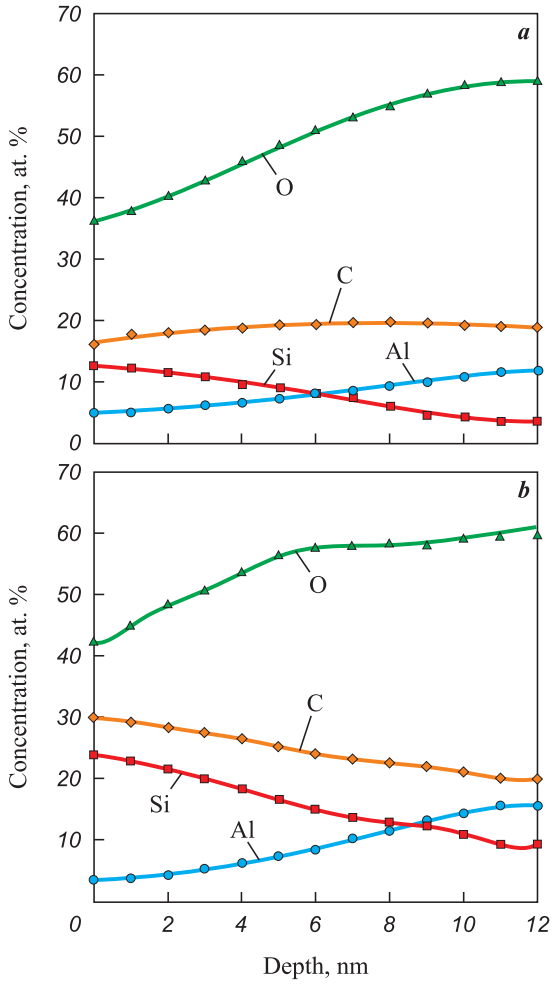

Fig. 3. Element distribution across the surface layer at polysilicate solution concentrations of 6 % (***a***) and 12 % (***b***)

Рис. 3. Распределение элементов по глубине поверхностного слоя при концентрациях раствора ПС 6 % (***a***) и 12 % (***b***)

One of the critical operational parameters influencing the quality of the surface-hardened layer is wear resistance. Fretting wear tests were conducted using an SRV Testsystem multifunctional testing device (Optimol Instruments, GmbH, Germany) at room temperature, following the disk-on-ball configuration without lubrication. The counterbody material was ShKh15 tool steel after hardening heat treatment. The tests were carried out with a vibration amplitude of 3 mm, a frequency of 2 Hz, a load of 10 N on the specimen, and a test duration of 10 min. Based on the results, it can be concluded that the amount of wear on the surface of the VAL10 alloy specimen after laser processing in a PS solution was less than 40 μm, while the untreated specimen exhibited 60 μm of wear. During testing, the friction coefficient for the treated specimen slightly exceeded 0.8, while the original specimen had a noticeably higher friction coefficient of over 1 (Fig. 4).

The presence of oxide and carbide components in the surface layer after laser processing is expected to influence microhardness. Microhardness of the surface of a VAL10 aluminum alloy specimen with an applied oxide coating was evaluated using a LOMO PMT-3M microhardness tester (LOMO, Russia). A 4-sided Vickers diamond pyramid served as the indenter. The results indicated that the average diagonal size of the indentation was 50 μm under a load of 0.196 N and a dwell time of 15 s, corresponding to a hardness of 14.8 kg/mm^2. In comparison, the microhardness of the original specimen was determined using the same method and measured 9.1 kg/mm^2, representing a 62.6 % decrease compared to the modified coated specimen. The formation of compounds with higher hardness on the surface of the aluminum alloy, in contrast to the base material, can also account for the reduction in the friction coefficient.

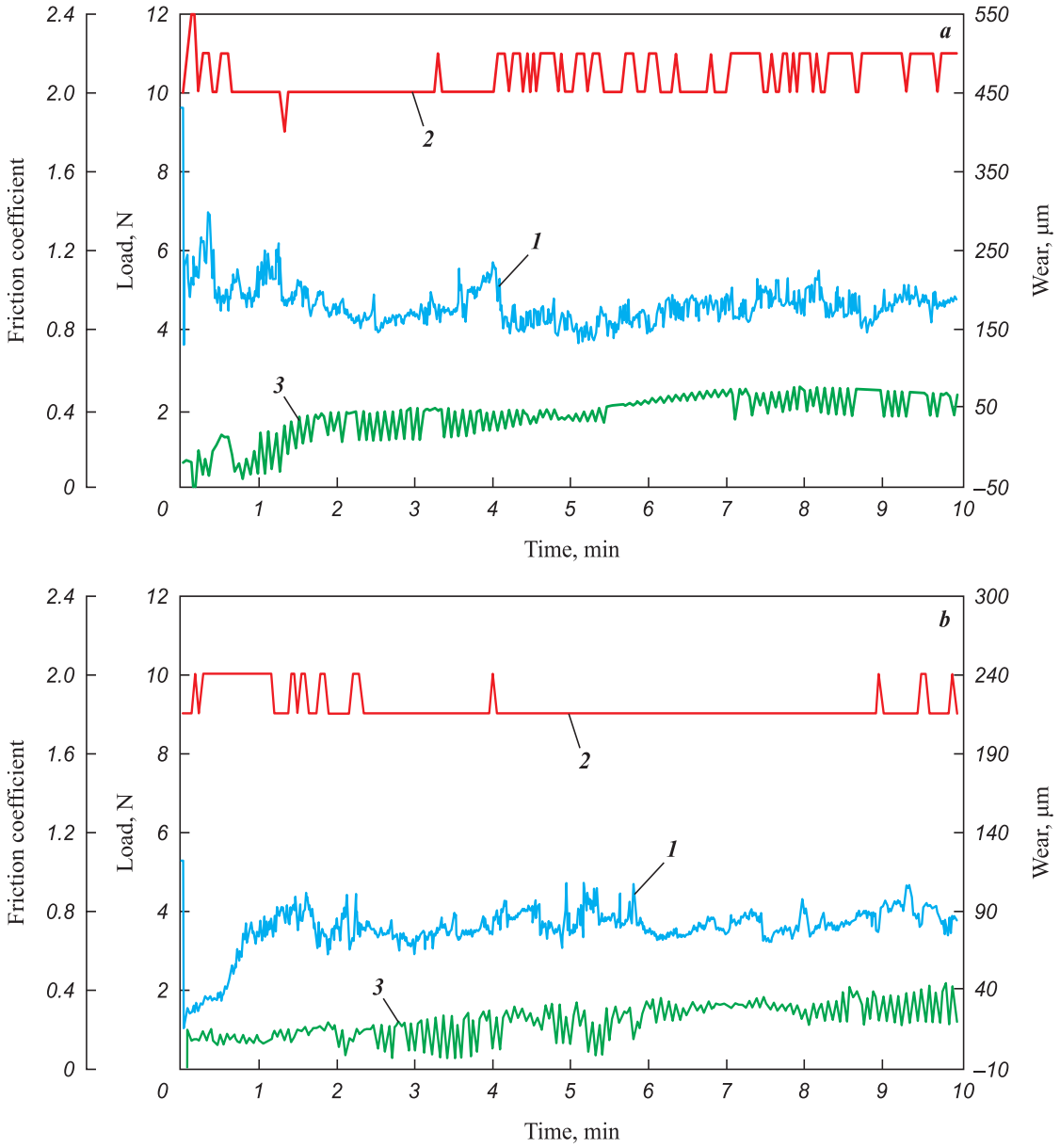

Fig. 4. Results of fretting wear tests of the original VAL10 alloy specimen (***a***) and specimen treated with laser radiation in a 12 % polysilicate solution (***b***):
1 – friction coefficient; ***2*** – load; ***3*** – wear

Рис. 4. Результаты испытаний на фреттинг-изнашивание исходного образца сплава ВАЛ10 (***a***) и обработанного лазерным излучением в растворе полисиликата концентрацией 12 % (***b***):
1 – коэффициент трения; ***2*** – нагрузка; ***3*** – износ

Conclusions

Analysis of the modified surface of VAL10 aluminum alloy specimens revealed the dependency of surface layer properties on the modification parameters. By adjusting laser processing parameters, such as pulse repetition rate, surface fill factor, concentration, and the thickness of the solution layer above the specimen's surface, it becomes possible to control the extent of the impact and, consequently, the chemical composition of the resulting coating.

The study conclusively demonstrated that laser processing of VAL10 alloy specimens in a polysilicate solution has a significant impact on their performance. In particular, it enhances surface abrasion resistance and promotes surface hardening.

References / Список литературы

1. Tarasova T.V., Gvozdeva G.O., Tikhonova E.P. Prospects for the use of laser radiation for surface treatment of non-ferrous alloys. *Vestnik of MGTU "Stankin"*.

2012;2(20):140–143. (In Russ.).
http://www.stankin-journal.ru/ru/articles/596

Тарасова Т.В., Гвоздева Г.О., Тихонова Е.П. Перспективы использования лазерного излучения для поверхностной обработки цветных сплавов. *Вестник МГТУ «Станкин»*. 2012;2(20):140–143.
http://www.stankin-journal.ru/ru/articles/596

2. Witkin D.B., Patel D.N., Helvajian H. Surface treatment of powder-bed fusion additive manufactured metals for improved fatigue life. *Journal of Materi Engineering and Perform*. 2019;28:681–692.
https://doi.org/10.1007/s11665-018-3732-9
3. Hatamleh M. I., Mahadevan J., Malik A. Prediction of residual stress random fields for selective laser melted A357 aluminum alloy subjected to laser shock peening. *Journal of Manufacturing Science & Engineering*. 2019; 141(10):101011. https://doi.org/10.1115/1.4044418
4. Smirnov S.V., Shandarov S.M., Karanskii V.V. Forced laser nanostructuring of the surface of alumina ceramics. *Uspekhi prikladnoi fiziki*. 2021;9(3):224–234. (In Russ.).
https://doi.org/10.51368/2307-4469-2021-9-3-224-234

Смирнов С.В., Шандаров С.М., Каранский В.В. Принудительное лазерное наноструктурирование поверхности алюмооксидной керамики. *Успехи прикладной физики*. 2021;9(3):224–234.
https://doi.org/10.51368/2307-4469-2021-9-3-224-234
5. Zhihao H., Wenjun W., Zelin M. Anti-icing ceramics surface induced by femtosecond laser. *Ceramics International*. 2022;48(7):10236–10243.
https://doi.org/10.1016/j.ceramint.2021.12.238
6. Sataeva N.E., Emel'yanenko K.A., Domantovskii A.G. Laser processing of aluminum alloys to create weather-resistant superhydrophobic coatings. *Rossiiskie nanotekhnologii*. 2020;15(2):158–163. (In Russ.).
https://doi.org/10.1134/S199272232002017X

Сатаева Н.Е., Емельяненко К.А., Домантовский А.Г. Лазерная обработка алюминиевых сплавов для создания атмосферостойких супергидрофобных покрытий. *Российские нанотехнологии*. 2020;15(2):158–163.
https://doi.org/10.1134/S199272232002017X
7. Jinliang Z.,Qingsong W., Dave B. A review of selective laser melting of aluminum alloys: Processing, microstructure, property and developing trends. *Journal of Materials Science & Technology*. 2019;35(2):270–284.
https://doi.org/10.1016/j.jmst.2018.09.004
8. Kisel' A.G., Belan D.Yu., Toder G.B. Investigation of the possibility of finishing laser processing of workpieces made of aluminum alloy D16. *Obrabotka metallov (tekhnologiya, oborudovanie, instrumenty)*. 2020;22(3):33–43. (In Russ.).
https://doi.org/10.17212/1994-6309-2020-22.3-33-43

Кисель А.Г., Белан Д.Ю., Тодер Г.Б. Исследование возможности чистовой лазерной обработки заготовок из алюминиевого сплава Д16. *Обработка металлов (технология, оборудование, инструменты)*. 2020;22(3):33–43.
https://doi.org/10.17212/1994-6309-2020-22.3-33-43
9. Riveiro A., Quintero F., Boutinguiza M. Laser cutting of aluminum alloy Al-2024-T3. *Procedia Manufacturing*. 2017;13:396–401.
https://doi.org/10.1016/j.promfg.2017.09.028
10. Kuis D.V., Volochko A.T., Shegidevich A.A., Svidunovich N.A., Omelyusik A.V., Lezhnev S.N., Mukhamedzyanova E.R., Kuznetsova O.N. Composite materials obtained by processing aluminum melt with ligatures containing carbon particles. *Vestnik Kazanskogo tekhnologicheskogo universiteta*. 2014;17(18):143–145. (In Russ.). https://www.elibrary.ru/item.asp?id=22480202

Куис Д.В., Волочко А.Т., Шегидевич А.А., Свидунович Н.А., Омелюсик А.В., Лежнев С.Н., Мухамедзянова Э.Р., Кузнецова О.Н. Композиционные материалы, полученные при обработке алюминиевого расплава лигатурами, содержащими углеродные частицы. *Вестник Казанского технологического университета*. 2014;17(18):143–145.
https://www.elibrary.ru/item.asp?id=22480202
11. Shinkaryov A.S., Ozherelkov D.Y., Pelevin I.A. Laser fusion of aluminum powder coated with diamond particles via selective laser melting: Powder preparation and synthesis description. *Coatings*. 2021;11(10):1219.
https://doi.org/10.3390/coatings11101219
12. Kozlova A.A., Kuznetsova V.A., Kozlov I.A. Influence of prolonged heating on the properties of protective coatings for aluminum alloy of the Al–Si–Mg system. *Aviatsionnye materialy i tekhnologii*. 2019;2(55):74–80. (In Russ.).
https://doi.org/10.18577/2071-9140-2019-0-2-74-80

Козлова А.А., Кузнецова В.А., Козлов И.А. Влияние длительных нагревов на свойства защитных покрытий для алюминиевого сплава системы Al–Si–Mg. *Авиационные материалы и технологии*. 2019;2(55):74–80.
https://doi.org/10.18577/2071-9140-2019-0-2-74-80
13. Mariappan T. Recent developments of intumescent fire protection coatings for structural steel: A review. *Journal of Fire Sciences*. 2016;34(2):120–163.
https://doi.org/10.1177/0734904115626720
14. Savrai R.A., Malygina I.Yu., Makarov A.V. Influence of laser alloying with Cu–Zn–Ti and Si–Cu powder mixtures on the structure and properties of cast aluminum alloy. *Obrabotka metallov (tekhnologiya, oborudovanie, instrumenty)*. 2019;21(4):70–84. (In Russ.).
https://doi.org/10.17212/1994-6309-2019-21.4-70-84

Саврай Р.А., Малыгина И.Ю., Макаров А.В. Влияние лазерного легирования порошковыми смесями Cu–Zn–Ti и Si–Cu на структуру и свойства литейного алюминиевого сплава. *Обработка металлов (технология, оборудование, инструменты)*. 2019; 21(4):70–84.
https://doi.org/10.17212/1994-6309-2019-21.4-70-84
15. Wang P., Deng L., Prashanth K.G. Microstructure and mechanical properties of Al–Cu alloys fabricated by selective laser melting of powder mixtures. *Journal of Alloys and Compounds*. 2018;735:2263–2266.
https://doi.org/10.1016/j.jallcom.2017.10.168
16. Tomida S., Nakata K. Fe–Al composite layers on aluminum alloy formed by laser surface alloying with

iron powder. *Surface and Coatings Technology*. 2003; 174-175:559–563. https://doi.org/10.1016/S0257-8972(03)00698-4

17. Aboulkhair N., Everitt N., Maskery I. Selective laser melting of aluminum alloys. *MRS Bulletin*. 2017;42(4): 311–319. https://doi.org/10.1557/mrs.2017.63
18. Aleksandrov V.D., Petrova L.G., Morshchilov M.V. Laser alloying of surface layers of aluminum alloys in order to increase their wear resistance. *Tekhnologiya metallov*. 2019;10:33–39. (In Russ.). https://doi.org/10.31044/1684-2499-2019-10-0-33-39

Александров В.Д., Петрова Л.Г., Морщилов М.В. Лазерное легирование поверхностных слоев алюминиевых сплавов с целью повышения их износостойкости. *Технология металлов*. 2019;10:33–39. https://doi.org/10.31044/1684-2499-2019-10-0-33-39

19. Yiming C., Guochao G., Huijun Y. Laser surface alloying on aluminum and its alloys: A review. *Optics and Lasers in Engineering*. 2018;100:23–37. https://doi.org/10.1016/j.optlaseng.2017.07.006
20. Olakanmi E.O., Cochrane R.F., Dalgarno K.W. A review on selective laser sintering/melting (SLS/SLM) of aluminium alloy powders: Processing, microstructure, and properties. *Progress in Materials Science*. 2015;74:401–477. https://doi.org/10.1016/j.pmatsci.2015.03.002
21. Quazi M.M., Fazal M.A., Farazila Y. Laser-based surface modifications of aluminum and its alloys. *Critical Reviews in Solid State and Materials Sciences*. 2016;41(2):106–131. https://doi.org/10.1080/10408436.2015.1076716
22. Shiganov I.N., Samarin P.E. Surface modification of aluminum alloys with silicon carbides by laser melting. *Vestnik MGTU im. N.E. Baumana. Seriya: Mashinostroenie*. 2012;5:62–68. (In Russ.). http://engjournal.ru/articles/226/html/files/assets/basic-html/page1.html

Шиганов И.Н., Самарин П.Е. Модифицирование поверхности алюминиевых сплавов карбидами кремния методом лазерного оплавления. *Вестник МГТУ им. Н.Э. Баумана. Серия: Машиностроение*. 2012;5:62–68. http://engjournal.ru/articles/226/html/files/assets/basic-html/page1.html

23. Pratik S., Subhasisa N., Guanjun W. Surface property modifications of silicon carbide ceramic following laser shock peening. *Journal of the European Ceramic Society*. 2017;37(9):3027–3038. https://doi.org/10.1016/j.jeurceramsoc.2017.03.005

Information about the Authors

Dmitriy G. Kalyuzhnyi – Cand. Sci. (Eng.), Assistant Professor of the Department "Physics and Optotechnics", Kalashnikov Izhevsk State Technical University; Senior Researcher of Scientific Center for Metallurgical Physics and Materials Science, Udmurt Federal Research Center of the Ural Branch of the Russian Academy of Sciences (UdmFRC UB RAS)
ORCID: 0000-0001-9704-3952
E-mail: dikdik@mail.ru

Mikhail V. Palabugin – Undergraduate of the Department "Instruments and Measurement, Control, Diagnostics", Kalashnikov Izhevsk State Technical University
ORCID: 0000-0002-8311-0779
E-mail: mr.kadochnikov777@mail.ru

Ivan N. Burnyshev – Cand. Sci. (Phys.-Math.), Leading Researcher Scientist of Scientific Center for Metallurgical Physics and Materials Science, UdmFRC UB RAS
ORCID: 0009-0001-8485-5123
E-mail: inburn@mail.ru

Vasiliy F. Lys – Leading Engineer of the Laboratory of Materials Science and Thermal Deformation Processes, UdmFRC UB RAS
ORCID: 0009-0005-0534-4608
E-mail: vflis@mail.ru

Vladimir I. Ladyanov – Dr. Sci. (Phys.-Math.), Chief Research Scientist of Scientific Center for Metallurgical Physics and Materials Science, UdmFRC UB RAS
ORCID: 0000-0002-7751-1007
E-mail: vilad@udman.ru

Сведения об авторах

Дмитрий Геннадьевич Калюжный – к.т.н., доцент кафедры «Физика и оптотехника», Ижевский государственный технический университет им. М.Т. Калашникова; ст. науч. сотрудник Научного центра металлургической физики и материаловедения, Удмуртский федеральный исследовательский центр УрО РАН
ORCID: 0000-0001-9704-3952
E-mail: dikdik@mail.ru

Михаил Вячеславович Палабугин – магистрант кафедры «Приборы и методы измерений, контроля, диагностики», Ижевский государственный технический университет им. М.Т. Калашникова
ORCID: 0000-0002-8311-0779
E-mail: mr.kadochnikov777@mail.ru

Иван Николаевич Бурнышев – к.ф.-м.н., вед. науч. сотрудник Научного центра металлургической физики и материаловедения, Удмуртский федеральный исследовательский центр УрО РАН
ORCID: 0009-0001-8485-5123
E-mail: inburn@mail.ru

Василий Федорович Лыс – вед. инженер лаборатории материаловедения и термодеформационных процессов, Удмуртский федеральный исследовательский центр УрО РАН
ORCID: 0009-0005-0534-4608
E-mail: vflis@mail.ru

Владимир Иванович Ладьянов – д.ф.-м.н., гл. научный сотрудник, Научного центра металлургической физики и материаловедения, Удмуртский федеральный исследовательский центр УрО РАН
ORCID: 0000-0002-7751-1007
E-mail: vilad@udman.ru

Contribution of the Authors

D. G Kalyuzhnyi – formulated the purpose of the work, research objectives, wrote the manuscript.
M. V. Palabugin – prepared initial specimens and coating mixtures, conducted experiments, participated in result discussions and manuscript writing.
I. N. Burnyshev – prepared initial specimens and coating mixtures, conducted experiments.
V. F. Lys – investigated fretting wear of the coatings, determined their microhardness.
V. I. Ladyanov – formulated the research objectives and methodology for its implementation.

Вклад авторов

Д. Г. Калюжный – определение цели работы, проведение экспериментов, написание текста статьи.
М. В. Палабугин – подготовка исходных образцов и смеси для нанесения покрытий, проведение экспериментов, участие в обсуждении результатов и написании статьи.
И. Н. Бурнышев – подготовка исходных образцов и смеси для нанесения покрытий, проведение экспериментов.
В. Ф. Лыс – исследование фреттинг-изнашивания полученных покрытий, определение микротвердости покрытий.
В. И. Ладьянов – определение цели исследования и методики его проведения.

Received 10.03.2023
Revised 02.06.2023
Accepted 05.06.2023

Статья поступила 10.03.2023 г.
Доработана 02.06.2023 г.
Принята к публикации 05.06.2023 г.

Materials and Coatings Fabricated Using the Additive Manufacturing Technologies
Материалы и покрытия, получаемые методами аддитивных технологий

UDC 62-405.8
https://doi.org/10.17073/1997-308X-2024-2-61-70

Research article
Научная статья

Transforming stereolithographic prototypes into metal or ceramic models by polymer substitution with titanium powder

M. A. Markov, S. A. Cherebylo, E. V. Ippolitov, S. V. Kamaev, M. M. Novikov, V. V. Vnuk

National Research Centre "Kurchatov Institute"
1 Kurchatov Sqr., Moscow 123182, Russia

Lc250@mail.ru

Abstract. The presented paper experimentally demonstrates the potential expansion of stereolithographic prototype utilization. Two methods for manufacturing plastic prototypes are proposed, enabling the subsequent substitution of the polymer material with either metal or ceramics. The first method involves additional actions by the prototype designer during the modeling stage. The second method necessitates alterations in the technological processes of model preparation and prototype manufacturing using a stereolithography apparatus. Material substitution occurs in two stages. Initially, cavities in the prototype are filled with powder material or a mixture of powder and water. Although titanium powder was chosen as the test material, the proposed technology permits the utilization of a broad spectrum of powder materials, encompassing both metallic and ceramic options. The subsequent stage involves heat treatment, where the polymer is eliminated, and the metal powder is sintered while retaining the original shape and dimensions of the prototype. Heat treatment of the acquired prototypes was conducted in both argon and atmospheric air environments. The utilization of different gas media might induce chemical transformations in the material filling the prototype. The experiments lead to the conclusion that the proposed approaches show promise and merit further development. Additionally, we contemplate amalgamating the two methods in the future to attain an optimized final outcome. The data we have gathered could significantly contribute to broadening the scope of stereolithography applications, given that this technology presently represents one of the most precise, widespread, and accessible additive manufacturing methods.

Keywords: additive technologies, titanium powder, 3D part, sintering

Acknowledgements: The study was conducted within the framework of the state assignment NRC "Kurchatov Institute".

For citation: Markov M.A., Cherebylo S.A., Ippolitov E.V., Kamaev S.V., Novikov M.M., Vnuk V.V. Transforming stereolithographic prototypes into metal or ceramic models by polymer substitution with titanium powder. *Powder Metallurgy and Functional Coatings*. 2024;18(2):61–70. https://doi.org/10.17073/1997-308X-2024-2-61-70

Преобразование стереолитографических прототипов в металлические или керамические модели замещением полимера порошковым титаном

М. А. Марков, С. А. Черебыло, Е. В. Ипполитов, С. В. Камаев, М. М. Новиков, В. В. Внук

Федеральное государственное бюджетное учреждение
«Национальный исследовательский центр «Курчатовский институт»
Россия, 123182, г. Москва, пл. Академика Курчатова, 1

Lc250@mail.ru

Аннотация. В работе экспериментально подтверждена возможность расширения области использования стереолитографических прототипов. Предложены два способа изготовления пластиковых прототипов, позволяющие впоследствии заместить полимерный материал моделей на металл или керамику. Первый из рассмотренных способов предполагает дополнительные действия конструктора, проектирующего прототип на стадии моделирования, второй – заключается во внесении изменений в технологические процессы подготовки модели и изготовления прототипа на стереолитографической установке. Замещение материала происходит в две стадии. Первая – это холодное заполнение полостей в прототипе порошковым материалом или его смесью с водой. В качестве тестового материала был выбран порошок титана, хотя предлагаемая технология подразумевает возможность использования широкого спектра порошковых материалов – как металлических, так и керамических. Вторая стадия – последующий отжиг. При этом происходят удаление полимера и спекание металлического порошка с сохранением исходной формы и размеров прототипа. Термическая обработка полученных прототипов проводилась как в атмосфере аргона, так и при свободном доступе атмосферного воздуха. Использование различных газовых сред может приводить к протеканию химических преобразований в составе материала, заполняющего прототип. Проведенные эксперименты позволяют сделать вывод о перспективности дальнейшего технологического развития представленных подходов. Также не исключается возможность соединения двух рассмотренных способов в один для достижения оптимального конечного результата. Полученные данные могут способствовать расширению области использования стереолитографических установок – наиболее точных, распространенных и доступных машин на данный момент из широкого типоряда аддитивных аналогов.

Ключевые слова: аддитивные технологии, титановый порошок, 3D-модель, спекание

Благодарности: Работа проведена в рамках выполнения государственного задания НИЦ «Курчатовский институт».

Для цитирования: Марков М.А., Черебыло С.А., Ипполитов Е.В., Камаев С.В., Новиков М.М., Внук В.В. Преобразование стереолитографических прототипов в металлические или керамические модели замещением полимера порошковым титаном. *Известия вузов. Порошковая металлургия и функциональные покрытия*. 2024;18(2):61–70.
https://doi.org/10.17073/1997-308X-2024-2-61-70

Introduction

Additive manufacturing using various materials finds widespread application across diverse fields. The list of such technologies and materials continually expands with the addition of new items [1–8]. Laser stereolithography, employed in photocurable polymers, stands out as one of the most extensively used additive technologies due to its diverse material options and a wide price range for equipment, ranging from costly industrial machines to affordable household devices. This equipment demonstrates the capability to produce highly accurate objects.

Converting polymer prototypes into metal or ceramic components requires specific equipment and skilled personnel, such as through methods like molding or cavityless casting.

In the realm of additive manufacturing for ceramic models, several noteworthy technological implementations exist. These include layer-by-layer sintering of powder ceramics, curing of photopolymerizing compositions with ceramic fillers, and local extrusion of ceramic-filled material [2–6]. Notably, these technologies involve high-temperature processing stages to eliminate the polymer binder, achieve surface gloss, conduct additional pore-filling impregnation, among other steps. Regarding additive manufacturing of metal models, methods encompass layer-by-layer sintering of metal powders, layer-by-layer model formation via polymerization of filled compositions, and local extrusion of filled material (followed by sintering) [4–12].

This paper explores the potential expansion of the application scope for stereolithography equipment that work with photopolymers. It specifically examines new possibilities for converting prototypes into ceramic or metal parts.

Experimental part

In our view, one solution to broaden the applicability of stereolithography involves producing polymer stereolithographic parts with available free volume. Such models could undergo subsequent cold filling with ceramic or metal powder, followed by heat treatment to eliminate the polymer component of the model (referred to as annealing) and the sintering of metal or ceramics (henceforth referred to as "sintering" without separately delineating the polymer burnout process).

During sintering, there is potential to synthesize a ceramic compound from the substance used to fill the model body [13; 14]. The sintering stage in this technology shares similarities with the method utilizing filled resins.

We have explored two straightforward methods to create models suitable for subsequent filling with alternate materials. These methods involve producing a thin-walled inverse fillable model, essentially a matrix, and a contourless model exhibiting significant free volume uniformly distributed throughout its body.

The process of obtaining the inverse model, or matrix, is depicted in Fig. 1. In this developed model, a matrix is created by indenting the working surface of the model by a specified thickness. The design incorporates a port for powder filling and includes a covering lid as integral parts.

This alternative approach shares some resemblance to sintering within a non-burnable mold [15]. However, in our scenario, the mold is combustible, and its intricacy is solely constrained by the designer's capabilities. In place of matrix models, we suggest employing original contourless prototypes. When creating a typical stereolithographic part, the process involves outlining both external and internal contours while filling the space between them. Additionally, denser outer hatching is necessary for horizontal outer surfaces.

To implement the contourless technology in stereolithography, several modifications to the conventional process are required, such as:

– eliminating contours;

– removing denser outer hatching;

– using only one coordinate (either X or Y) on each layer; the direction of hatching alternates through the layer;

– increasing the hatching step.

The sparse hatching serves as an internal frame structure that gets filled with the initial liquid resin during manufacturing. By the end of the process, the liquid resin naturally flows out from the model or is expelled by compressed air.

Fig. 2 illustrates both the conventional method and the validated contourless methods for creating a stereolithographic part of a cylinder.

The model produced using this technology adopts a cellular polymer structure, openly accessible on all sides, containing a uniformly distributed free volume internally. Experimental findings indicate that manipulating technological parameters, such as layer thickness (h) and hatching step (H_s), within the ranges

Fig. 1. Stages of part matrix construction for powder filling with sintered material
a – initial model, ***b*** – hollow matrix (sectional view), ***c*** – model displaying the matrix with a separated closing lid

Рис. 1. Построение матрицы модели для заполнения ее порошком спекаемого материала
a – исходная модель, ***b*** – пустотелая матрица (в разрезе), ***c*** – модель матрицы с отделенной крышкой

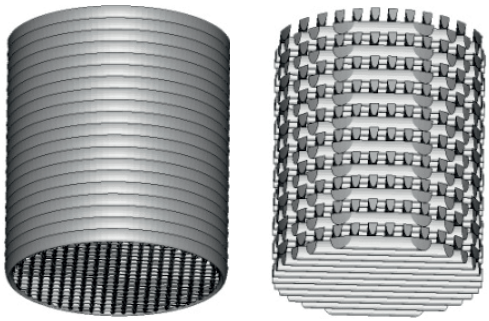

Fig. 2. The models fabricated via conventional (contour + X–Y hatching) (***a***) contourless (alternating X and Y hatching layer by layer) (***b***) stereolithography techniques

Рис. 2. Вид моделей, полученных по традиционной стереолитографической технологии (контуры + штриховка X–Y) (***a***) и бесконтурно, с чередующейся через слой штриховкой X и Y (***b***)

of h = 100 to 200 μm and H_s = 0.5 to 0.9 mm, results in varying proportions of free volume within the model, ranging from 30 to 80 %. A designer can replicate a similar internal hollow structure that fills the model. However, in such cases, the model's complexity significantly impacts the file size, potentially increasing it by several orders of magnitude. This could pose challenges for subsequent software processing to prepare the model for printing, potentially rendering it difficult or even impossible. In contrast, contourless models achieve the same effect by simply adjusting the model growing technology without burdening the file size with excessive complexity.

We opted for titanium powder with particle sizes ranging from 15 to 45 μm to explore the replacement of prototype material. Titanium is highly sought-after in engineering and medical applications. Additionally, both titanium and previously used silicon can serve as intermediate materials capable of forming ceramic compounds (such as nitride, oxide, and carbide) under suitable conditions, offering a wide array of structural properties [17–19].

The matrix models were dry-filled through the open facet, followed by sealing the closing lid with initial resin cured under a UV lamp.

For the filling of contourless models, a suspension of titanium powder and water was prepared. Filling the free volume in the models was conducted within an MK-mini vacuum chamber ("MK-Technology," Germany). Experimental findings revealed optimal results when the filler constituted approximately 50 ± 5 vol. % of the suspension.

Subsequently, all samples underwent heat treatment. Both matrix and contourless models were sintered under similar conditions using an SUOL-0.25.1/12-I1 furnace (manufactured in Russia). Sintering temperatures ranged from 900 to 1200 °C. The process was executed with gas purging (argon, nitrogen) and with exposure to atmospheric air. Sintering durations did not exceed 10 min.

Experimental results

Fig. 3 displays photographs of the test contourless models captured at various stages of the technological process.

The model obtained after sintering remarkably retained its original shape and dimensions, showcasing the initial color of the titanium powder and exhibiting adequate mechanical strength and electrical conductivity. The furnace utilized in our experimentation is well-suited for gas purging (specifically, Ar and N_2 in our case) and effectively prevents the temperature from exceeding 1200 °C. When using Ar purging, a minor quantity of weakly sintered metal powder (forming a loose layer up to 100 microns thick) was observed on the surface of the models. Sintering conducted at lower temperatures (1000 and 1100 °C) also yielded integral samples, albeit with inferior surface quality. Considering that the melting temperature of titanium is 1670 °C, it can be inferred that elevated temperatures might enhance the final model's quality.

As previously mentioned, the resulting samples exhibited the same colour as the original metal powder. Sintering the Ti-polymer model in an argon environment may instigate a reaction between titanium and the polymer of the initial prototype. Under such conditions, stoichiometric titanium carbide TiC, which conducts electrical current similar to Ti, can be formed, along with several non-stoichiometric carbides, such as Ti_xC_y [19; 20]. According to literature sources, titanium actively reacts with atmospheric gases like nitrogen and oxygen at high temperatures. This reaction results in the formation of titanium nitride and titanium oxide, respectively. It's essential to note that not only metallic titanium but also its compounds, such as carbides and nitrides, have the potential to interact with oxygen [18–22].

Fig. 3. Contourless samples

a – stereolithographic contourless model; ***b*** – the same model filled with titanium-water suspension; ***c*** – the model after a 10 min sintering at 1200 °C under argon purging

Рис. 3. Тестовые бесконтурные образцы

a – стереолитографическая бесконтурная модель; ***b*** – та же модель, заполненная титановодяной суспензией; ***c*** – модель после 10 мин спекания при t = 1200 °C с продувкой аргоном

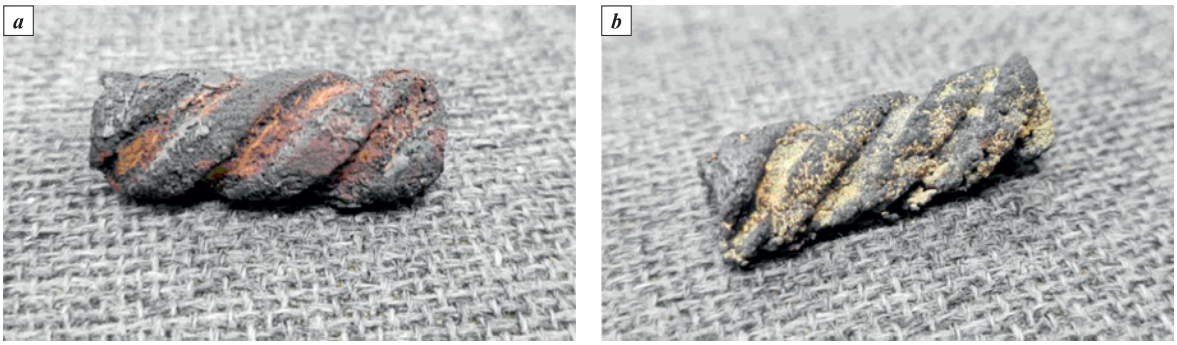

Fig. 4. Counterless samples following heat treatment at t =1100 °C under nitrogen purging (***a***) and in atmospheric air (***b***)

Рис. 4. Тестовые бесконтурные образцы после проведения спекания при t = 1100 °C с продувкой азотом (***a***) и в атмосферном воздухе (***b***)

Sintering the contourless models in a nitrogen environment resulted in samples that maintained the original shape and dimensions, akin to the experiments conducted in argon. These samples exhibited electrical conductivity, although at times, surface cleaning was necessary to verify this property. Both titanium nitride and titanium carbide act as metal-type conductors, particularly in the case of stoichiometric TiN or TiC compounds, while TiO_2 oxide functions as a dielectric material [23–25].

Sintering in a nitrogen environment imparted a reddish-brown color to the samples, characteristic of titanium nitride TiN (Fig. 4, *a*). However, upon discontinuing nitrogen purging and before the samples cooled completely, a layer of white or yellow color formed on their surfaces, typical of titanium oxide TiO_2. Fig. 4, *b* illustrates a sample obtained through heat treatment in atmospheric air. Both samples (Fig. 4, *a*, *b*) displayed a slightly molten surface, which is noticeable when compared with the sample in Fig. 3, *c*. According to reference data [26], the enthalpies of titanium dioxide and nitride formation are ΔH_f° = –944 ÷ –938 kJ/mol (for different modifications) and ΔH_f° = –323 kJ/mol, respectively. During sintering, after the removal of the polymer, the structure of the samples was notably porous, displaying a branched surface. Due to chemical reactions, the temperature on their surface increased, resulting in localized areas of melted material.

The matrix models underwent a sintering process akin to the previously described sintering of contourless prototypes. Fig. 5 illustrates the stages of sample preparation and the outcome of sintering with argon purging.

A layer of orange-colored substance developed on the surface of the sintered model, particularly noticeable on the protruding sections. A similar occurrence was observed on the contourless models with nitrogen purging, albeit in the recessed areas. The models generated in this manner, depicted in Fig. 5, *c*, more faithfully replicate the shape of the original model. Structurally, they also exhibit strength, and the orange layer can be removed from the surface using abrasive

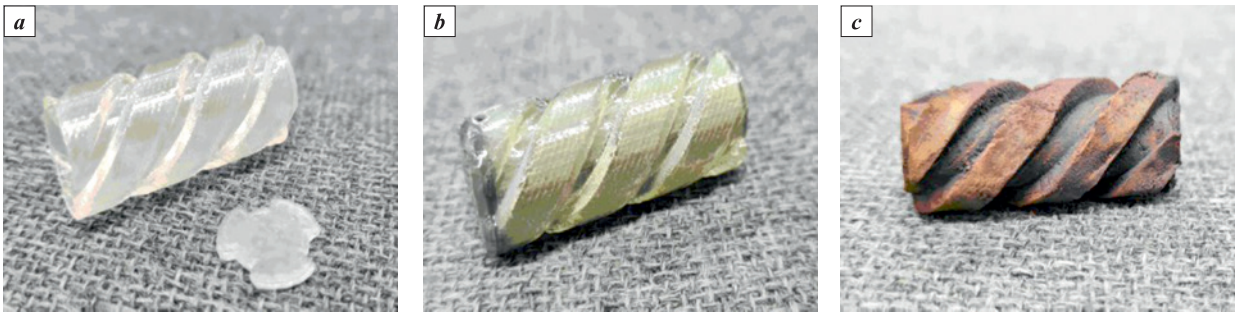

Fig. 5. Matrix samples

a – stereolithographic part depicting a component matrix with a lid; ***b*** – sealed matrix filled with titanium powder; ***c*** – the sample after a 10 min sintering at 1200 °C under argon purging

Рис. 5. Тестовые матричные объекты

a – стереолитографическая модель матрицы объекта с крышкой; ***b*** – заклеенная матрица, заполненная титановым порошком; ***c*** – образец после 10 мин спекания при t = 1200 °C с продувкой аргоном

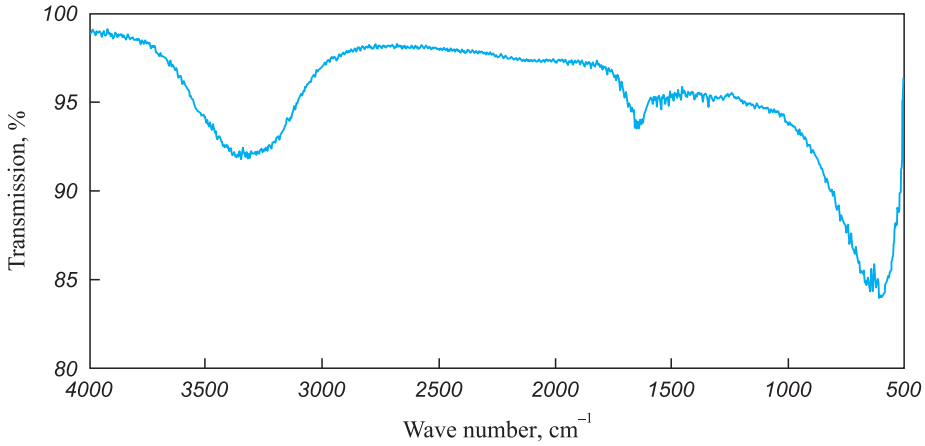

Fig. 6. FTIR spectrum analysis of substance from outer protruding parts of sintered matrix sample surface following 10 min sintering at 1200 °C under argon purging

Рис. 6. FTIR спектр вещества с внешних выступающих частей поверхности матричного образца после 10 мин спекания при t = 1200 °C с продувкой аргоном

materials or tools. Post-removal, the sample adopts a grey hue, akin to titanium powder.

Spectroscopy (FTIR) of the substance extracted from the surface of matrix models indicated (Fig. 6) the closest resemblance to the spectrum of non-stoichiometric Ti_3C_2 carbide. Notably, the spectrum obtained lacked characteristic lines indicative of Ti–N bonds [19; 27–34].

Figs. 7 and 8 depict matrix samples sintered under nitrogen purging and in an air environment, respectively. In the case of nitrogen purging, the samples sintered in this medium exhibited a more oxidized surface compared to those sintered in an air environment. The matrix samples prepared for sintering were densely packed with metal powder, as previously described. The metal was encapsulated from the surrounding medium by the matrix itself, formed by a layer of cured polymer. Heating initiated the thermal decomposition or combustion of the polymer, prompting the metal to react with the resulting decomposition products. Previous findings indicated that in an inert argon environment, this led to the formation of a layer composed of titanium-carbon compounds on the surface. As the polymer layer burned out, it gradually thinned and became permeable to atmospheric air or other gases, initiating competing processes between the formation of titanium carbide and titanium nitride [35; 36]. Titanium nitride reacted with heavier products of polymer thermal decomposition, containing a significant oxygen content, and transformed into oxide. It's noteworthy that oxidation of titanium nitride commences at lower temperatures compared to titanium carbide. The simultaneous occurrence of these exothermic reactions on the sample surface induced additional heating and surface melting, irrespective of the temperature used for heat treatment (refer to Fig. 7).

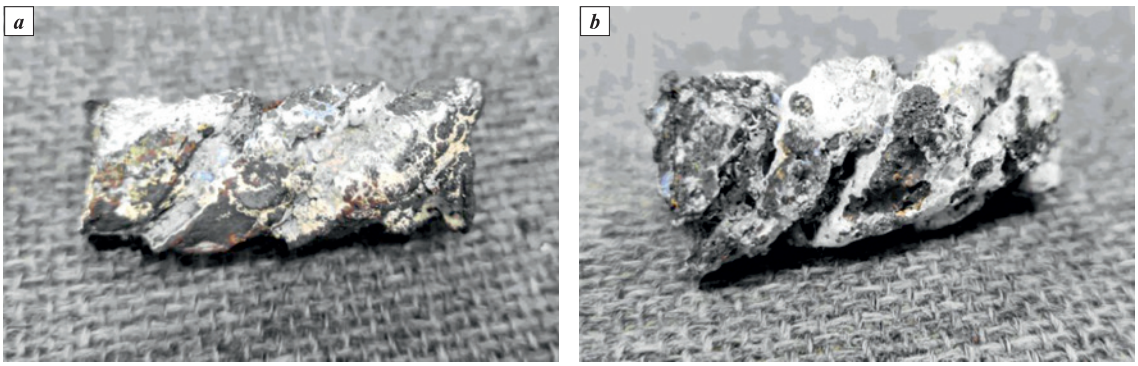

Fig. 7. Matrix samples following sintering under nitrogen purging at t = 1000 °C (***a***) and 1200 °C (***b***)

Рис. 7. Тестовые матричные образцы после спекания с продувкой азотом при t = 1000 °C (***a***) и 1200 °C (***b***)

Fig. 8. Matrix samples following sintering in air at t = 900 °C (***a***), 1000 °C (***b***) and 1100 °C (***c***)

Рис. 8. Тестовые матричные образцы после спекания на воздухе при t = 900 °C (***a***), 1000 °C (***b***) и 1100 °C (***c***)

Samples sintered in atmospheric air (Fig. 8) exhibited distinct differences from those treated with nitrogen purge. One notable characteristic was their sensitivity to the sintering temperature: lower temperatures (within specific limits) resulted in better retention of the sample's shape and a cleaner surface. Moreover, these samples, despite exposure to atmospheric oxygen, showed minimal amounts of generated titanium oxide, observed only at temperatures surpassing 1100 °C.

We hypothesize that such sintering behavior can be elucidated by the fact that in the presence of atmospheric oxygen, the polymer matrix underwent combustion rather than decomposition. The primary combustion products (H_2O and CO_2) were not retained on the surface of the sintered sample. Additionally, the outflow of hot gaseous combustion products from the reaction area hindered the entry of nitrogen and oxygen. Combustion of the polymer also resulted in a decreased presence of carbide on the titanium surface. Notably, at a sintering temperature of 900 °C, the samples with the cleanest surfaces, in comparison to others, were produced.

Results and discussion

Fig. 9 presents cross-sectional photos of the sintered samples purged with argon. The contourless sample retained a mesh structure at the edges, inverse to that of the original prototype. In the center, there's an area of sintered powder characterized by discontinuous pinpoint metallic luster. The matrix sample exhibited a darker outer layer, while the rest of the sample displayed a shiny metal appearance.

These investigations validate the feasibility of producing 3D metal models using a stereolithography apparatus, without necessitating foundry technologies. Each of the alternative technologies presented here holds distinct characteristics to be considered during the development of a final technological solution. Selecting a viable solution should follow a phase of experiments and tests evaluating the strength of the model.

All models created using the described methods required post-processing to eliminate the outer layer of the material. This post-processing step should be factored in during the computer modeling phase.

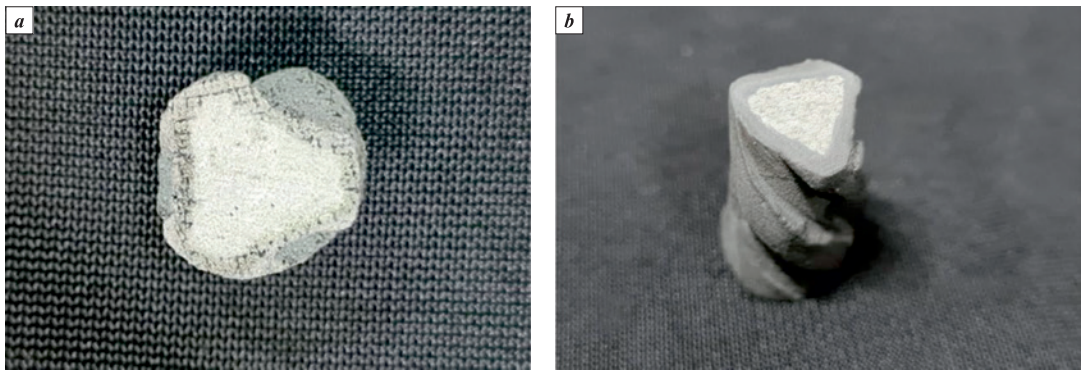

Fig. 9. Cross-sections of a sample sintered at t = 1000 °C
a – counterless sample; ***b*** – matrix sample

Рис. 9. Срезы образцов, спеченных при t = 1000 °C
a – бесконтурный образец; ***b*** – матричный образец

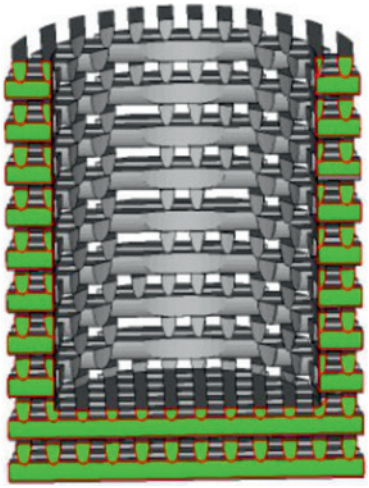

Fig. 10. Cross-section of a cylindrical sample model with contourless shell and internal cavity for metal powder or suspension filling

Рис. 10. Модель цилиндрической детали в разрезе, имеющая бесконтурную оболочку и внутреннюю полость для последующего заполнения металлическим порошком или суспензией

We are intrigued by the prospect of merging contourless and matrix technologies into one by creating a contourless matrix (as shown in Fig. 10). The wall of such a matrix is anticipated to be filled with a metal-water suspension, while the inner cavity may be filled either with dry powder or the same suspension. By selecting an appropriate sintering mode that facilitates easy removal of the weakly sintered outer porous part, the final model will resemble a sintered powder devoid of channels from polymer elements, minimizing its contact with external media during sintering.

Conclusions

Therefore, our experiments have validated the feasibility of transforming stereolithographic prototypes into metal or metal-ceramic forms. Through the use of titanium as an exemplary material, we have effectively showcased the genuine potential for such a transformation. By employing the described prototypes, we expand the utility of stereolithography, enhancing its versatility. Notably, the proposed solution does not necessitate any alterations to the photopolymer.

In contrast to additive technologies applied to metals or ceramics, which typically involve the use of significantly more expensive equipment, stereolithography equipment has consistently stood out as one of the most precise and user-friendly types of additive technology.

Additionally, it's noteworthy that the methods we propose facilitate the manufacturing of models with varying degrees of porosity. This aspect holds significance in both technical and medical applications of such models.

References / Список литературы

1. Jacobs P.F. Introduction to rapid prototyping and manufacturing. rapid prototyping and manufacturing: Fundamentals of stereolithography. 1st ed. Dearborn, MI, USA: Society of Manufacturing Engineers, 1992. 434 p
2. Baumers M., Dickens P., Tuck C., Hague R. The cost of additive manufacturing: machine productivity, economies of scale and technology-push. *Technological Forecasting and Social Change*. 2016;102:193–201. https://doi.org/10.1016/j.techfore.2015.02.015
3. Bartolo P.J., Gaspar J. Metal filled resin for stereolithography metal part. *CIRP Annals-Manufacturing Technology*. 2008;57(1):235–238. https://doi.org/10.1016/j.cirp.2008.03.124
4. Colombo P., Mera G., Riedel R., Soraru G.D. Polymer-derived ceramics: 40 years of research and innovation in advanced ceramics. *Journal of the American Ceramic Society*. 2010;93(7):1805–1837. https://doi.org/10.1002/9783527631940.ch57
5. Rice R.W. Ceramic fabrication technology. New York: CRC Press, 2003. 362 p.
6. Gonzalez-Gutierrez J., Cano S., Schuschnigg S., Kukla C., Sapkota J., Holzer C. Additive manufacturing of metallic and ceramic components by the material extrusion of highly-filled poymers: A review and future perspectives. *Materials*. 2018;11(5):840. https://doi.org/10.3390/ma11050840
7. Popovich A., Sufiiarov V. Metal powder additive manufacturing. *New Trends in 3D Printing*. 2016;215–236. https://doi.org/10.5772/63337
8. DebRoy T., Wei H.L., Zubuck J.S., Mukherjee T., Elmer J.W., Milewski J.O., Beese A.M., Wilson-Heid A., Zhang A.W. Additive manufacturing of metallic components – Process, structure and properties. *Progress in Material Science*. 2018;92:112–224. https://doi.org/10.1016/j.pmatsci.2017.10.001
9. Halloran J. W., Griffith M., Chu T-M. Stereolithography resin for rapid prototyping of ceramics and metals: Patent 6117612A (USA).1997.
10. Mireles J., Espalin D., Roberson D., Zinniel B., Medina F., Wicker Fused R. Fused deposition modeling of metals. In: *Proceedings of 23rd Annual International Solid Freeform Fabrication Symposium. An Additive Manufacturing Conference* (Austin Texas, 6–8 August 2012). 2012. P. 836–845.
11. Liu B., Wang Y., Lin Z., Zhang T. Creating metal parts by fused deposition modeling and sintering. *Materials Letters*. 2020;263:127252. https://doi.org/10.1016/j.matlet.2019.127252
12. Giberti H., Strano M., Annoni M. An innovative machine for fused deposition modeling of metals and advanced ceramics. In: *MATEC Web of Conferences (4th International Conference on Nano and Materials Science)*. 2016;43: 1–5. https://doi.org/10.1051/matecconf/20164303003
13. Vnuk V.V., Ippolitov E.V., Kamaev S.V., Markov M.A., Novikov M.M., Cherebylo S.A. Investigation of the pro-

cess of laser photopolymerization of composite materials based on methacrylic oligomers and silicon powder. *Khimicheskaya fizika*. 2020;39(9):88–93. (In Russ.). https://doi.org/10.31857/s0207401x20090137

Внук В.В., Ипполитов Е.В., Камаев С.В., Марков М.А., Новиков М. М., Черебыло С. А. Исследование процесса лазерной фотополимеризации композитных материалов на основе метакриловых олигомеров и порошка кремния. *Химическая физика*. 2020;39(9):88–93. https://doi.org/10.31857/s0207401x20090137

14. Markov M., Vnuk V., Ippolitov E., Kamayev S., Cherebylo S. The prospects for transforming stereolithographic parts from polymer to ceramic by using powder silicium as photocurable resin filler. *The International Journal of Advanced Manufacturing Technology*. 2020;111:1863–1871. https://doi.org/10.1007/s00170-020-06239-0
15. Kiseev V.M. Napominayushchij A.S. Method of obtaining porous titanium: Patent RU2407817 (RF). 2010. (In Russ.).

    Кисеев В.М., Напоминающий А.С. Способ получения пористого титана: Патент RU2407817 (РФ). 2010.
16. Evseev A.V., Lazaryanc V.E., Markov M.A., Mikhlin V.S., Surovtsev M.A., Fershtut E.V. Liquid photopolymerizing composition for laser stereolithography: Patent 2395827 (RF). 2008. (In Russ.).

    Евсеев А.В., Лазарянц В.Э., Марков М.А., Михлин В.С, Суровцев М.А., Ферштут Е.В. Жидкая фотополимеризующаяся композиция для лазерной стереолитографии: Патент 2395827 (РФ). 2008.
17. Gotman I., Gutmans E.Y. Titanium nitride-based coatings on implantable medical devices. *Advanced Biomaterials and Devices in Medicine*. 2014;1:53–73.
18. Shabalin I.L., Roach D.L. Oxidation of titanium carbide-grafite hetero-modulus ceramics with low carbon content: I. Phenomenological modeling of the ridge effect. *Journal of the European Ceramic Society*.2008;28(16):3165–3176. https://doi.org/10.1016/j.jeurceramsoc.2008.04.035
19. Li Y., Zhou X., Wang J., Deng Q., Li M., Du S., Han Y-H., Lee J., Huang Q. Facile preparation of *in situ* coated $Ti_3C_2T_x/Ni_{0.5}Zn_{0.5}Fe_2O_4$ composites and their electromagnetic performance. *RSC Advances*. 2017;7(40): 24698–24708. https://doi.org/10.1039/C7RA03402D
20. Lee J.-Y., Jo W.-K. Control of methyl tertiary-butyl ether via carbon-doped photocatalysists under visible-light irradiation. *Environmental Engineering Research*. 2012;12(4): 179–184. https://doi.org/10.4491/eer.2012.17.4.179
21. Gray B.M., Hector A.L., Jura M., Owen J.R., Whittam J. Effect of oxidative surface treatments on charge storage at titanium nitride surface for super capacitor applications. *Journal of Materials Chemistry: A*. 2017;5(9):4550–4559. https://doi.org/10.1039/C6TA08308K
22. Pambudi A.B., Kurniawati R., Iryani A., Hartanto D. Effect of calcination temperature in the syntesis of carbon doped TiO_2 without external carbon source. In: *The 3rd International Seminar on Chemistry: AIP Conference Proceedings, 2018* (Surabaya, Indonesia, 18–19 July 2018). P. 020074. https://doi.org/10.1063/1.5082479
23. Ishkov A.V., Sagalakov A.M. Electric conductivity of composites containig nonstoichometric titanium compounds. *Technical Physics Letters*. 2006;32(5):377–378. https://doi.org/10.1134/S1063785006050038
24. Ghidiu M., Lukatskaya M.R., Zhao M.-Q., Gogots Y.i, Barsoum M. Conductive two-dimensionsl titanium carbide "clay" with high volumetric capacitance. *Nature*. 2014; 516(7529):78–81. https://doi.org/10.1038/nature13970
25. Andrievskii R.A., Alekseev S.A., Dzodziev G.T., Dzneladze A.Z., Travushkin G.G., Turchin V.N., Chertovich A.F. Physicpmechanical proprties of titanium carbide with titanium nitride additions. *Soviet Powder Mettalurgy and Metal Ceramics*. 1980;19:612–615.
26. Chemical encyclopedia. Vol. 4. Moscow: Bolshaya rossyiskaya encyclopedia, 1995. P. 1176–1178. (In Russ.).

    Химическая энциклопедия. Т. 4. Москва: Большая российская энциклопедия, 1995. С. 1176–1178.
27. Chen C., Liu F., Li S., Wang N., Popov A., Jiao M., Wei T., Li Q., Dunsch L., Yang S. Titanium/yttrium mixed metal nitride clusterfullerene TiY2N@C80: syntesis, isolation, and effect of the group-III metal. *Inorganic Chemistry*. 2012;51:3039–3045. https://doi.org/10.1021/ic202354u
28. Wang X.B., Ding C.F., Wang L.S. Vibratioally resolved photoelectron spectra of TiC_x^- ($x = 2–5$) clusters. *The Journal of Physical Chemistry: A*. 1997;101(42):7699–7701. https://doi.org/10.1021/jp971838k
29. Snyder M.Q., McCool B.A., DiCarlo J., Tripp C.P., DeSisto W. An infrared study of the surface chemistry of titanium nitride atomic layer deposition on silica from $TiCl_4$ and NH_3. Thin Solid Films. 2006;514(1-2):97–102. https://doi.org/10.1016/j.tsf.2006.03.013
30. Leon A., Reuquen P., Garin C., Segura R., Vargas P., Zapata P., Orihuela P. FTIR and Raman characterization of TiO_2 nanoparticles coated with polyethylene glycol as carrier for 2-methoxyestradiol. *Applied Sciences*. 2017;7(49): 1–9. https://doi.org/10.3390/app7010049
31. Foratirad H., Baharvandi H.R., Maragheh M.G. Chemorheological behavior of aqueos titanium carbide suspension and evalution of the gelcasted green body propeties. *Material Research*. 2017;20(1):175–182. https://doi.org/10.1590/1980-5373-MR-2016-0410
32. Schramke K., Qin Y., Held J.T., Mkhoyan K.A., Kortshagen U. Nonthermal plasma synthesis of titanium nitride nanocrystals with plasmon resonances at near-infrared wavelength relevant to photothermal therapy. *ACS Applied Nano Materials*. 2018;1:2869–2876. https://doi.org/10.1021/acsanm.8b00505
33. Spectra base. URL: https://spectrabase.com/spectrum/IKP1d7RLMfa (accessed: 18.05.2023).
34. Kaviyarasu K., Thema F.T., Manikandan E., Maaza M. TiO_2 doped graphene oxide (GO) wrinkle nanosheets by wet-chemical method. *Syntesis and Reactivity in Inorganic, Metal-Organic, and Nano-Metal Chemistry*. 2016;7129:722.
35. Jiao K., Zhang J., Liu Z., Kuang S., Liu Y., Liu F. Dissection investigation of Ti(C,N) behavior in blast furnance hearth during vanadium titano-magnetite smelting. *ISIJ International*. 2017;57(1):48–54. https://doi.org/10.2355/isijinternational.ISIJINT-2016-419
36. Wang B., Matsumaru K., Ishiyama H., Yang J., Ishizaki K., Matsushita J. Low temperatura oxodation of titanium nitride under high pxygen pressure by O_2-HIP. In: *Proc. International Conference on Hot Isostatic Pressing Kobe* (Japan, 12–14 April 2011). *Journal of Materials online*. https://doi.org/10.2240/azojomo0308

Information about the Authors

Mikhail A. Markov – Researcher, National Research Centre "Kurchatov Institute"
ORCID: 0000-0003-1054-2615
E-mail: Lc250@mail.ru

Svetlana A. Cherebylo – Researcher, National Research Centre "Kurchatov Institute"
ORCID: 0000-0003-0502-9681
E-mail: Svetlana.cherebylo@rambler.ru

Evgeniy V. Ippolitov – Researcher, National Research Centre "Kurchatov Institute"
ORCID: 0000-0002-0622-6727
E-mail: ippevg@yandex.ru

Sergey V. Kamaev – Researcher, National Research Centre "Kurchatov Institute"
ORCID: 0000-0001-7423-1264
E-mail: ksv6@rambler.ru

Mikhail M. Novikov – Senior Researcher, National Research Centre "Kurchatov Institute"
ORCID: 0000-0003-0626-793X
E-mail: novikov@rambler.ru

Vyacheslav V. Vnuk – Junior Researcher, National Research Centre "Kurchatov Institute"
ORCID: 0000-0003-2536-6626
E-mail: ren651@mail.ru

Сведения об авторах

Михаил Александрович Марков – науч. сотрудник, Федеральное государственное бюджетное учреждение «Национальный исследовательский центр «Курчатовский институт»
ORCID: 0000-0003-1054-2615
E-mail: Lc250@mail.ru

Светлана Александровна Черебыло – науч. сотрудник, Федеральное государственное бюджетное учреждение «Национальный исследовательский центр «Курчатовский институт»
ORCID: 0000-0003-0502-9681
E-mail: Svetlana.cherebylo@rambler.ru

Евгений Викторович Ипполитов – науч. сотрудник, Федеральное государственное бюджетное учреждение «Национальный исследовательский центр «Курчатовский институт»
ORCID: 0000-0002-0622-6727
E-mail: ippevg@yandex.ru

Сергей Валентинович Камаев – науч. сотрудник, Федеральное государственное бюджетное учреждение «Национальный исследовательский центр «Курчатовский институт»
ORCID: 0000-0001-7423-1264
E-mail: ksv6@rambler.ru

Михаил Михайлович Новиков – ст. науч. сотрудник, Федеральное государственное бюджетное учреждение «Национальный исследовательский центр «Курчатовский институт»
ORCID: 0000-0003-0626-793X
E-mail: novikov@rambler.ru

Вячеслав Владимирович Внук – мл. науч. сотрудник, Федеральное государственное бюджетное учреждение «Национальный исследовательский центр «Курчатовский институт»
ORCID: 0000-0003-2536-6626
E-mail: ren651@mail.ru

Contribution of the Authors

M. A. Markov – contributed to computer model development, participated in conducting experiments, discussions of results, and paper writing.
S. A. Cherebylo – conducted experiments related to the stereolithographic component, contributed to paper writing.
E. V. Ippolitov – conducted experiments involving model preparation and the heat treatment stage, participated in result discussions.

S. V. Kamaev – contributed to result discussions and paper writing.

M. M. Novikov – conducted experiments related to filling models with powder filler, participated in result discussions.

V. V. Vnuk – conducted experiments related to the heat treatment stage and spectroscopy.

Вклад авторов

М. А. Марков – разработка компьютерных моделей, участие в проведении экспериментов, обсуждении результатов и написании статьи.
С. А. Черебыло – проведение экспериментов (стереолитографическая часть), участие в написании статьи.
Е. В. Ипполитов – проведение экспериментов (подготовка моделей и термическая стадия), участие в обсуждении результатов.
С. В. Камаев – участие в обсуждении результатов, написании статьи.
М. М. Новиков – проведение экспериментов (заполнение моделей порошковым наполнителем), участие в обсуждении результатов.
В. В. Внук – проведение экспериментов (термическая стадия, спектроскопия).

Received 06.12.2022
Revised 19.07.2023
Accepted 21.07.2023

Статья поступила 06.12.2022 г.
Доработана 19.07.2023 г.
Принята к публикации 21.07.2023 г.

Зарегистрирован Федеральной службой по надзору
в сфере связи, информационных технологий
и массовых коммуникаций.
Свидетельство о регистрации ПИ № ФС77-79230

Журнал распространяется агентством «Урал-Пресс»
Подписной индекс: 80752 (печатная версия)
05108 (электронная версия)